Contents

Zusammenfassung

Trotz jahrzehntelanger Forschung sind die genauen Mechanismen der Entwicklung und Homöostase der Epidermis noch immer unklar. Die Proliferation der Epidermis wird kontrovers diskutiert und Erkenntnisse wurden größtenteils in Mausstudien gewonnen. Es ist jedoch bekannt, dass sich Maushaut und humane Haut bezüglich Anatomie und vermutlich auch Proliferation stark unterscheiden. Um diese Frage zu untersuchen, wurden die Mitosen in einem humanen Fibroblasten-generierte Matrix-basierten Langzeithautmodell (fdmSE) systematisch erfasst. Die Keratinozyten in dem Hautäquivalent teilen sich auf 4 unterschiedliche Arten: horizontal, perpendikulär oder schräg zur Basalmembran (BM) oder suprabasal. Der größte Anteil wird von den horizontalen Teilungen gestellt (< 80 %). Die zweithäufigste Teilungsart ist die schräge Teilung (< 50 %). Perpendikuläre Mitosen waren in geringer Menge ausschließlich an intermediären Zeitpunkten vorhanden und gänzlich abwesend an frühen und späten Zeitpunkten. Es scheint daher, als seien alle Teilungswinkel in humaner interfollikulärer Epidermis (IFE) vorhanden. Interessanterweise wurde auch ein substanzieller Anteil suprabasaler Mitosen gezählt. Diese Teilung war bisher der Embryogenese, Wundheilung und erkrankter Epidermis vorbehalten. Wir konnten suprabasale Mitosen in normaler Haut *in situ* bestätigen, was darauf hinweist, dass sie tatsächlich ein Teil der epidermalen Homöostase sind. Expression von Keratin 10 zeigte, dass sich diese Zellen in einem frühen Stadium der Differenzierung befanden und gelegentlich noch in Kontakt mit der BM standen.

Ein weiteres Ziel dieser Arbeit war die Untersuchung asymmetrischer Teilung in der IFE. Um die Balance zwischen Selbsterneuerung und Differenzierung aufrechtzuerhalten, müssen Vorläuferzellen sich asymmetrisch teilen. Unterschiedliche Nachkommen können auf zweierlei Arten generiert werden: durch perpendikuläre Orientierung wodurch eine Tochterzelle entfernt von der Stammzellniche platziert wird, oder durch ungleiche Verteilung determinierender Faktoren auf die Tochterzellen. Einige Faktoren sind bekannt, die für die orientierte Mitose verantwortlich sind, darunter der PAR-Komplex, und die Adapterproteine NuMA, Inscuteable und LGN. Hier konnten wir diese Faktoren jedoch mit den verfügbaren Antikörpern nicht nachweisen. Stattdessen haben wir den Notch-Inhibitor Numb als potenziellen Asymmetriemarker in Keratinozyten identifiziert. Numb wurde während einiger Mitosen in 2D Kultur asymmetrisch verteilt. Um seine Funktion zu untersuchen, haben wir einen stabilen CRISPR/Cas9 Knockdown etabliert. Bemerkenswerterweise hatte die Abwesenheit von Numb keine Auswirkung auf die kurzzeitige Proliferation (14 Tage). Dies weist darauf hin, dass Numb keine Rolle in der Mitose *per se* spielt. Ob es stattdessen eine Rolle in der Regulation des Zellschicksales während der epidermalen Regeneration spielt, bleibt eine offene Frage für zukünftige Studien.

Summary

Despite decades of research, the exact regulation of epidermal development and homeostasis remains elusive. Proliferation in the epidermis is controversially discussed and knowledge is mostly derived from studies of mouse skin. However, it is well established that mouse and human skin differ regarding anatomy and likely also proliferative regulation. To address this question, mitoses were systematically assessed in a long-term human fibroblast-derived matrix-based skin equivalent (fdmSE). Keratinocytes in our fdmSE divided in 4 different ways: horizontal, oblique, or perpendicular to the basement membrane (BM) or suprabasally. The largest proportion of divisions occurred in horizontal orientation (< 80 %) at all time points. The second most common division type was oblique division (< 50 %). Perpendicular divisions were found at a low frequency (< 20 %) at intermediate time points only. They were absent at early and late time points. Thus, it appears that in the human interfollicular epidermis (IFE) all types of divisions are active. Importantly, we also observed suprabasal mitoses present at all analysed time points in the SE. Suprabasal division in epidermis has so far been restricted to embryogenesis, wound healing and diseased skin. We could confirm that it is also part of the normal human epidermis *in situ* thus suggesting that this spatial mitotic organisation is part of tissue homeostasis in human epidermis. These cells are in an early stage of differentiation as suggested by their expression of keratin 10 with a connection to the BM still detectable in some cases.

Furthermore, we aimed at investigating asymmetric cell division in the IFE. To maintain the delicate interplay between self-renewal and differentiation, progenitor cells have to divide asymmetrically. Differential daughter cell fate can be established in two ways: oriented division which displaces one daughter cell from the stem cell niche, or asymmetric distribution of cell fate determinants to the daughter cells. Several components of oriented division have been proposed in invertebrate and vertebrate systems including the PAR-complex, or the adaptor proteins NuMA, Inscuteable and LGN. However, antibodies available for those proteins did not allow detecting these markers here. Instead, we identified the Notch inhibitor Numb as a possible marker for asymmetric keratinocyte division. Numb was segregated asymmetrically during some divisions of the human keratinocytes in 2D cultures. To determine its function, we established a protocol to stably knock down Numb in the human keratinocytes using CRISPR/Cas9. Notably, Numb deletion did not affect proliferation in short term culture (14 days), suggesting that it is not essential for mitosis *per se*. Instead, Numb may be important for the regulation of cell fate in epidermal regeneration, a question that needs to be addressed in future studies.

Abbreviations

°C	Degree Celsius
µg	Microgram
µL	Microlitre
µm	Micrometre
AB	Antibody
Asc. a. ph.	Ascorbic acid phosphate
bFGF	Basic fibroblast growth factor
BM	Basement membrane
BrdU	5‘-Brom-2‘-desoxyuridine
BSA	Bovine serum albumin
cDNA	Complementary DNA
cm	Centimetre
CO_2	Carbon dioxide
Cy3	Indocarbocyanine
d	Day(s)
D10	DMEM with 10% FCS
DAPI	4’,6-Diamidino-2-phenylindol
DMEM	Dulbecco`s modified Eagle medium
DNA	Deoxyribonucleic acid
dNTP	Deoxyribonucleotide triphosphates
ECM	Extracellular matrix
EDTA	Ethylenediaminetetraacetic acid
EGF	Epidermal growth factor
et al.	*et alii/aliae*, and others
EtOH	Ethanol
FA	Formaldehyde
FCS	Fetal calf serum
fdm	Fibroblast-derived matrix
Fig	Figure
g	Gram(s)
GAPDH	Glyceraldehyde-3-phosphate-dehydrogenase
h	Hour(s)
H&E	Hematoxylin & Eosin
HaCaT	Human adult Calcium Temperature
HCl	Hydrochloric acid
HRP	Horseradish peroxidase
IdU	5-Iodo-2’-deoxyuridine
IF	Immunofluorescence
IFE	Interfollicular epidermis
IGF	Insulin-like growth factor
KH	Human keratinocyte
Ki67	Nuclear protein associated with proliferation
L	Liter
LRC	Label-retaining cell
Lrp6	Low-density lipoprotein receptor-related protein 6
MeOH	Methanol
mg	Milligram
min	Minute(s)
mL	Millilitre
mm	Millimetre
mRNA	Messenger RNA
ms	Millisecond
NaN_3	Sodium azide
nm	Nanometre
NuMA	Nuclear mitotic apparatus protein
ON	Over night
PAGE	Polyacrylamide gelelectrophoresis
ParD6α	Partitioning defective 6 homolog alpha
PBS-	Phosphate buffered saline
PBS+	Phosphate buffered saline containing Magnesiumchloride and Calciumchloride
PCR	Polymerase Chain Reaction
Pen/Strep	Penicillin / Streptomycin
PFA	Paraformaldehyde
pH	*pondus hydrogenii*
RNA	Ribonucleic acid
rpm	Rounds per minute
RT	Room temperature
SC	Stem cell
SDS	Sodium dodecyl sulfate
SE	skin equivalent
TEMED	N, N, N´, N´-Tetramethyldiamin
TGF-β	Transforming growth factor β
TPX2	Targeting protein for Xklp2
V	Volt
WM	Wholemount

1. Introduction

1.1 The human skin

The human skin, despite being only up to a few millimetres thick, is the largest organ of the body. It provides effective protection against parasites, UV irradiation, dehydration, and mechanical and environmental stress. The skin regulates body temperature and provides tactile sense via nerve cells and receptors. The complex structure of human skin can be divided into three layers: First, the outermost epidermis. It is tightly connected to the second layer, the matrix-rich dermis. The third layer is the underlying subcutis which mainly consists of fat and is in contact with muscles and tendons (Kanitakis, 2002). Several appendages such as hair follicles, sweat and sebaceous glands and nails complete the skin (McGrath et al., 2004; Urmacher, 1990). The stretches between hair follicles are referred to as interfollicular epidermis (IFE).

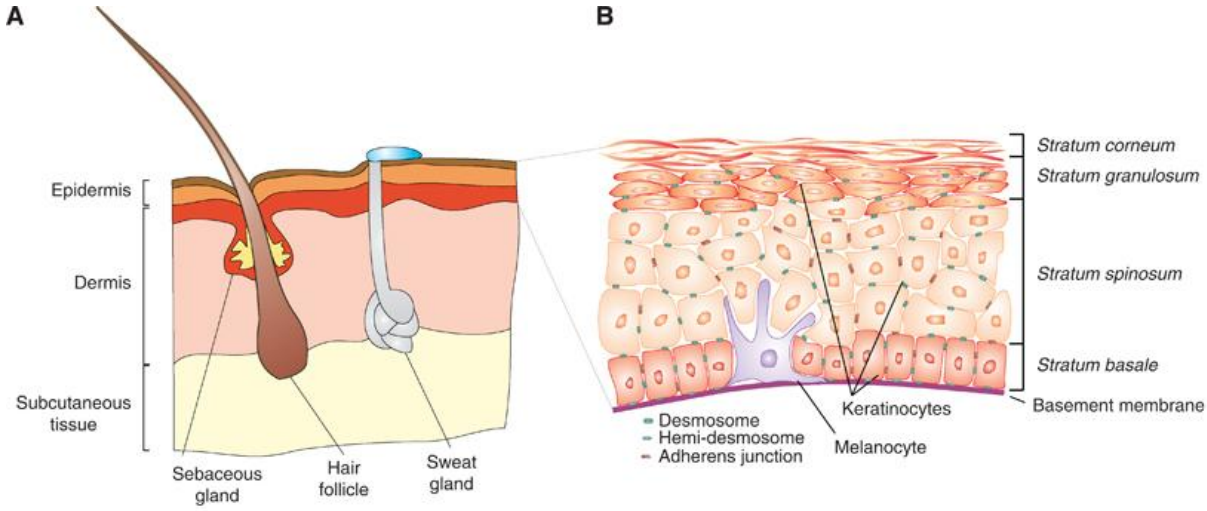

Figure 1.1 Structure of the human skin. (A) The subcutaneous layer, the dermis and the epidermis together make up the human skin. Appendages, including sebaceous glands, sweat glands and hair follicles complete the tissue. (B) The outermost layer, the epidermis, is a tightly regulated stratified epithelium consisting of several layers. Adapted from Kern et al., 2011

1.1.1 The dermis

The dermis is predominantly made up by fibroblasts. They secrete extracellular matrix (ECM) components that form the dense connective tissue of the dermis. Collagen fibres render the skin tear-resistant, whereas elastic fibres provide the elasticity that makes the skin return to its original state after deformation (McGrath et al., 2004). These fibres are surrounded by mucopolysaccharides and proteoglycans, gel-like and interfibril substances, the ground substance that help in retaining water and serve as stem cell niche and provide cell-matrix contact (Wilkes et al., 1973).

In addition to the spindle-shaped fibroblasts, cell types of the immune system can be found in the dermis, including mast cells, macrophages and dendritic cells (Salmon et al., 1994). The upper part of the dermis is rich in nerve endings and blood vessels. The indentations of the dermal papillae with the epidermal rete ridges increase the contact surface of dermis and epidermis and thereby provide improved adhesion and stability (Kanitakis, 2002). Appendages of the skin such as hair follicles and sweat and sebaceous glands are embedded in the dermis. The dense basement membrane, consisting of lamins, proteoglycans and collagens, serves as a separation and connection between dermis and epidermis (Kalluri, 2003; McMillan et al., 2003).

1.1.2 The epidermis

The multilayered, stratified epidermis forms the outermost body surface. It consists mainly of keratinocytes that follow a tightly regulated differentiation program, but also contains melanocytes, Langerhans cells and Merkel cells (Urmacher, 1990).

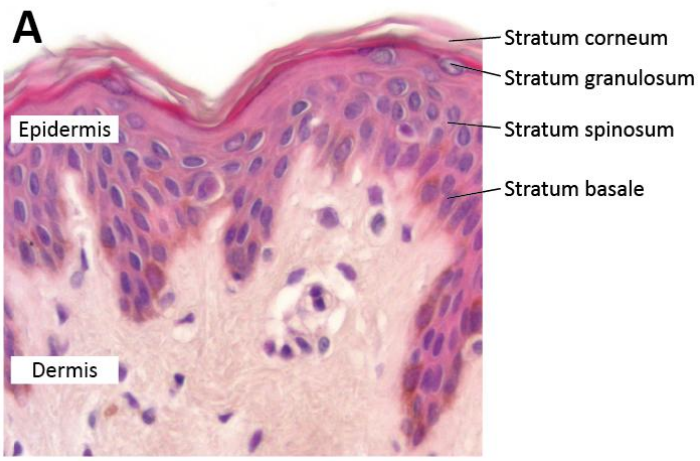

Figure 1.2 Layers of the epidermis. The epidermis consists of four distinct layers of morphologically distinct keratinocytes. Adapted from Löffler et al., 2007

Four morphologically distinct cell layers form the epidermis (Green, 1977; Urmacher, 1990). The columnar basal cells of the *stratum basale* are tightly attached to the underlying basement membrane by adhesion molecules, the hemidesmosomes. This cell layer harbours the stem cell (SC) compartment of the IFE (Cotsarelis et al., 1989; Lavker and Sun, 1983). Above the basal cell layer, several layers of smaller, spinous cells follow. In this *stratum spinosum*, cells start to differentiate and express markers of differentiation such as keratin 1 and 10 (Fuchs, 1993; Watt and Green, 1982). Migrating further toward the outer cell layers, the keratinocytes flatten. Cells of the *stratum granulosum* contain basophilic keratohyalin granules. The nucleus begins to disintegrate and

cytoplasmic organelles are lost. The cells of the outermost *stratum corneum* form a dense, hydrophobic layer at the inner side of the cell membrane, known as the cornified envelope. Finally, horn squames are shed. Roughly every 4 weeks, the entire epidermis is renewed in this way (McGrath et al., 2004; Urmacher, 1990). The homeostasis of human skin is maintained by a complex interplay of differentiation and proliferation, with the epidermal stem cells playing the central role.

1.1.3 Stem cell hypotheses

Recent research has identified several distinct stem cell compartments within the epidermis: the hair follicle bulge, the sebaceous gland and the IFE.

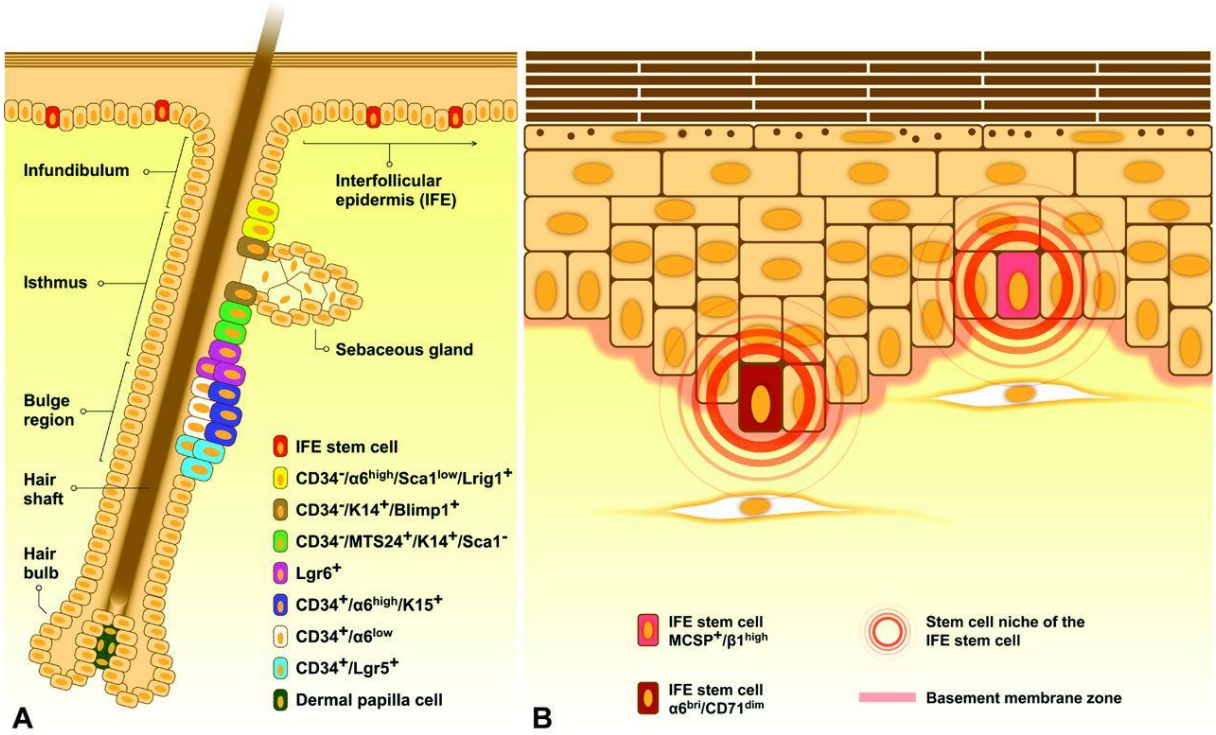

Figure 1.3 Stem cell niches of the skin. Several distinct stem cell niches have been identified in murine and human epidermis. In the murine hair follicle (A), stem cell niches include the bulge region and the isthmus. In the human IFE (B), two distinct stem cell populations have been proposed: one α6 integrin^{high} and CD71^{low}-expressing population and one MCSP^{+}/ β1 integrin^{high} population. Graphic taken from Boehnke et al., 2007.

1.1.3.1 Murine epidermal stem cells

Most of our current knowledge on epidermal stem cells is derived from murine skin. Since mice are covered by a dense fur, the hair follicle (HF) stem cell niches provide the "lion's share" of the epidermal stem cells. Three different CD34^{+} SC populations were characterised in the hair bulge region, expressing different levels of α6-integrin (α6) and Lgr5 (Barker and Clevers, 2010; Blanpain et al., 2004). Further HF stem cell niches include an actively cycling Lgr6^{+} population above the bulge region and a CD34^{-}/MTS24^{+}/K14^{+}/Sca1^{-}expressing population at the isthmus below the sebaceous

gland (SG) (Woo and Oro, 2011). The sebaceous gland harbours its own SC population expressing $CD34^{-}/K14^{+}/BLIMP1^{+}$. Finally, a quiescent SC population characterised by $CD34^{-}/\alpha6^{high}/Sca1^{low}/Lrig1^{+}$ expression was identified between the upper isthmus and the infundibulum (Jensen et al., 2009). Although several studies suggest the presence of a distinct SC population of the murine IFE, it could not be clearly identified so far (Ito et al., 2005; Levy et al., 2005).

1.1.3.2 Human epidermal stem cells

Notably, much of this knowledge about murine stem cells seems not to be transferable to the human epidermis. Much less is known about human skin, which consists mainly of large stretches of interfollicular epidermis and only sparse hair follicles. Therefore, the IFE must play a more significant role in providing a stem cell niche than in mouse skin. Regarding markers of the mouse hair follicle stem cell populations, most of them cannot be applied to human HFs. For instance, $CD34^{+}$ cells are restricted to the hematopoietic lineage in humans (Ohyama, 2005) and Keratin 15 which could be used to isolate murine HF stem cells from the bulge (Morris et al., 2004) is not specific for human bulge SCs (Ohyama, 2007). It is known that HF stem cells contribute to wound healing and can even take over homeostasis of the IFE in situations of need (Ito et al., 2005; Levy et al., 2007; Tumbar et al., 2004). The mouse HF cycle takes about 4 weeks, whereas a human HF can have a cycle time of up to 8 years. It is therefore likely that the HF stem cells are of lesser significance in humans than in mouse, due to the sparse distribution and because of longer cycling times. Two distinct and competing stem cell populations of the human IFE have been proposed in the literature: one α6 $integrin^{high}$ and $CD71^{low}$-expressing population at the base of the rete ridges (Webb et al., 2004) and one population characterised by expression of β1 $integrin^{high}$, melanoma chondroitin sulfate $proteoglycan^{+}$ and the epidermal growth factor receptor (EGFR) antagonist Lrig1+ at the tip of the rete ridges where the dermis is closest to the skin surface (Ghazizadeh and Taichman, 2005; Jensen et al., 2009; Jones and Watt, 1993; Legg et al., 2003). However, our own observations (Muffler et al., 2008) rather suggest a distribution of slow-cycling cells throughout the basal cell layer as was also found in labelling studies by Ghazizadeh and colleagues (Ghazizadeh and Taichman, 2005).

1.1.3.3 Stem cell hypotheses

Maintenance of the epidermis relies on the proliferation of IFE stem cells to balance the constant turnover of differentiated keratinocytes. Several competing theories about stem cell hierarchy in the interfollicular epidermis are being discussed in the literature.

The earliest proposed model involves the arrangement of keratinocytes in columnar stacks called epidermal proliferative units (EPU), with a central stem cell surrounded by 10 – 11 basal cells (Potten, 1974, 1981; Potten and Morris, 1988). In this model, clone sizes are of roughly the same size and

clone numbers are largely invariable during homeostasis. About 10 % of basal cells have stem cell character and give rise to transit amplifying (TA) cells that account for about 60 % of basal cells. In this hierarchical model, TA cells undergo several generations of proliferation before they leave the basal cell layer and migrate upwards while following their terminal differentiation program (Barrandon and Green, 1987; Jones and Watt, 1993).

Recently, a competing model has emerged. In 2007, Clayton and colleagues showed that epidermal clone sizes in mouse tail epidermis increase over time, contradicting the classical stem / transit amplifying cell model involving EPUs. Instead, they proposed a stochastic model where all basal cells possess progenitor character and fate decisions occur stochastically. This population asymmetry, in contrast to the previously discussed invariant asymmetry, leads to a hallmark scaling behaviour of the clone size and distribution. In contrast to the hierarchical EPU model, where clone size and number remains stable over time, clones in the stochastic model become less in number and vary in size. This population asymmetry leads to a characteristic scaling behaviour of the clone size distribution (depicted schematically in figure 1.4).

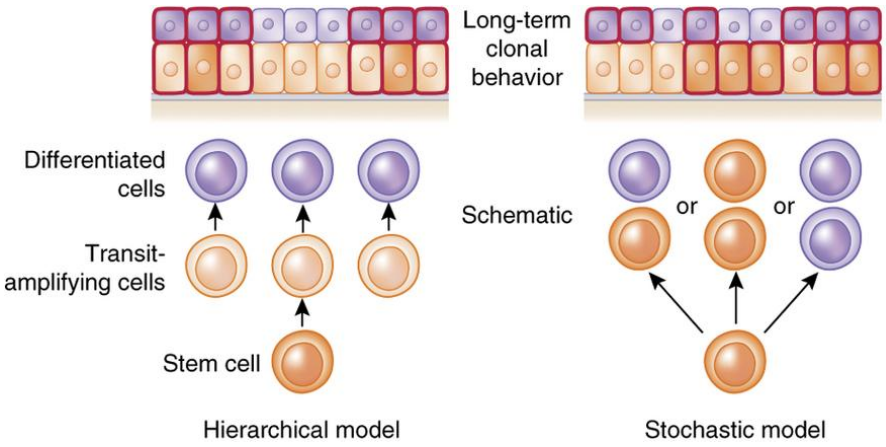

Figure 1.4 Hierarchical vs. stochastic stem cell model. The classical SC model consisting of stem and transit amplifying cells (left panel) would lead to an invariant asymmetry with similar and invariant clone sizes. In contrast, a progenitor population with stochastic fate leads to population asymmetry involving different sized clones over time (right panel). Picture taken from Hsu et al., 2014.

Admittedly, a very slowly cycling population of quiescent stem cells would be undetectable in the applied labelling approach (Clayton et al., 2007). This model was recently confirmed by further lineage tracing experiments in mouse IFE in combination with mathematical modelling (Blanpain and Simons, 2013; Lapouge et al., 2011; Mascré et al., 2012). Here, a quiescent stem cell population with only 4 – 6 divisions per year was proposed. Progenitor cells follow a pattern of balanced stochastic fate, where one in five divisions leads to progenitor cell loss. It was shown before, that stem or progenitor cell populations might be heterogeneous, with cells reversibly assuming different states

of competence (Graf and Stadtfeld, 2008). These fate transitions are unfortunately hard to discern in lineage tracing approaches. It is therefore difficult to conclude which cells are true quiescent stem cells or whether such a population does even exist in the interfollicular epidermis (Blanpain and Simons, 2013).

An overview over the currently discussed hypotheses on stem cell hierarchy in the epidermis is shown in Figure 1.5.

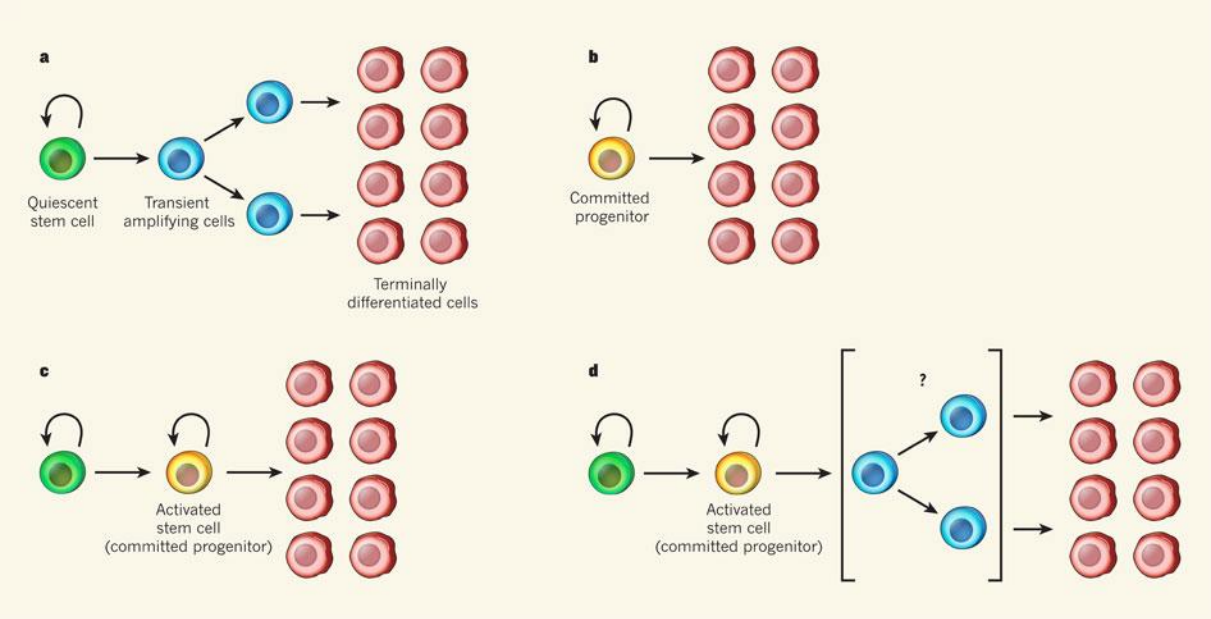

Figure 1.5 Stem cell hypotheses. In addition to the classical model involving a quiescent stem cell and a transit amplifying population (a), recent modelling approaches suggest the existence of committed progenitors with stochastic fate giving rise directly to differentiated cells (b). Further models combine these two theories and include both a quiescent and a committed progenitor population (c) and may or may not include a TA population (d). Image taken from: De Rosa and De Luca, 2012

To determine which of the competing theories holds true, Li and colleagues undertook a long term mathematical simulation of the three hypotheses: (1) the classical SC / TA model following an invariant asymmetry, (2) the population asymmetry model of Clayton and colleagues with a committed progenitor population and (3) the extended population asymmetry model of Mascré and colleagues including a quiescent stem cell population (Li et al., 2013). Applying the same parameters for all three models and modelling the scenarios for a time course of 3 years, they found that the classical model relying on stem and transit amplifying cells with restricted proliferative potential would lead to depletion of stem cells and exhaustion of the epidermis within the 3 years. The second model according to Clayton and colleagues (Clayton et al., 2007) did not involve a quiescent stem cell population and also suggested depletion of proliferating cells over time. Instead, the mathematical model favoured the third hypothesis, a quiescent stem cell population and a committed progenitor

population following a stochastic fate and leading to the hallmark scaling behaviour observed by Mascré and colleagues (Mascré et al., 2012). This model also explains ageing phenomenons like decline of healing capacity, since a slow decrease in SC numbers was observed. The existence of a quiescent stem cell population would also be a reasonable explanation for the accumulation of mutations that can finally lead to malignancies, since stem cells are not as readily eliminated as other cells that acquire mutations. Notably, in all the studies mentioned, mitosis does, as a rule, only occur in the basal cell layer. Presumably, keratinocytes lose their proliferative potential as soon as the leave the basal cell layer. Exceptions are early embryonic development and wounding situations where suprabasal mitoses have been observed (Smart, 1970a; Stojadinovic et al., 2005). As a shortcoming, the modelling approach by Li and colleagues assumes that all basal cell divisions occur asymmetrically, meaning perpendicular to the basement membrane, in the first scenario and in horizontal orientation in the other two, which extremely simplifies the situation. We know from several studies that mitosis in the epidermis can occur in different orientations (Lechler and Fuchs, 2005; Poulson and Lechler, 2010; Smart, 1970a). So, while this model appears to be the most accurate and advanced to date, it does still not entirely resemble human interfollicular epidermal homeostasis.

Again, these studies have been performed in mice and therefore, as mentioned above, have to be carefully considered regarding their applicability to the human skin. Since lineage tracing in vital human skin is impossible, epidermal stem cell research is in need for good *in vitro* model systems that mimic human epidermis as closely as possible.

1.2 Symmetric *versus* asymmetric stem cell division

Stem cells have to fulfil the complex balancing act of self-renewal and differentiation. To do so, they have to be able to divide asymmetrically.

1.2.1 Mechanisms of asymmetry in the human epidermis

Several models of asymmetric stem cell division have been proposed in the literature.

Asymmetry can arise through extrinsic cues when basal cells divide in an apical direction, with the mitotic spindle oriented perpendicularly to the basement membrane and the plane of division parallel to the basement membrane. The resulting basal daughter cell remains in contact with the basement membrane and the stem cell niche, and retains stem cell properties. The apical daughter cell, on the other hand, loses contact with the niche and instead receives signals from overlying differentiated keratinocytes. This daughter cell is likely to terminally differentiate. In this scenario, extrinsic factors (emanating from the niche or differentiated cells) and cell-cell and cell-niche contacts determine the fate of the stem cell progeny. High β1 integrin levels are one proposed

characteristic of epidermal stem cells (Jensen et al., 1999; Jones and Watt, 1993; Jones et al., 1995). The anchorage of basal cells to the basement membrane seems to be important to retain their undifferentiated state. It is known that integrin signalling suppresses differentiation of keratinocytes (Watt, 2002; Watt et al., 1993), and knockout of β1 integrin in basal cells leads to reduced epidermal growth due to impaired keratinocyte differentiation (Brakebusch et al., 2000). These studies show the influence of integrin binding for cell fate. Division with the mitotic spindle perpendicular to the basement membrane was observed in oesophageal epithelium and developing mouse epidermis as well as in mouse back skin but not in adult mouse tail epidermis (Clayton et al., 2007; Koster and Roop, 2005; Lechler and Fuchs, 2005; Seery and Watt, 2000). Controversely, older studies as well as observations in mouse tail skin report parallel mitosis as the main division direction, resulting in two basal daughter cells (Clayton et al., 2007; Smart, 1970a). Still, this kind of division can lead to asymmetry and differential daughter cell fate by asymmetric distribution of factors inside the mother cell. Even though both daughter cells stay in contact with the niche at first, a determining factor will be passed on unequally to the daughter cells and influence their behaviour. While the factors leading to a perpendicular spindle orientation in epidermal keratinocytes are relatively well characterised (Bowman et al., 2006; Du and Macara, 2004; Merdes et al., 2000), intrinsic cues regulating parallel division remain elusive.

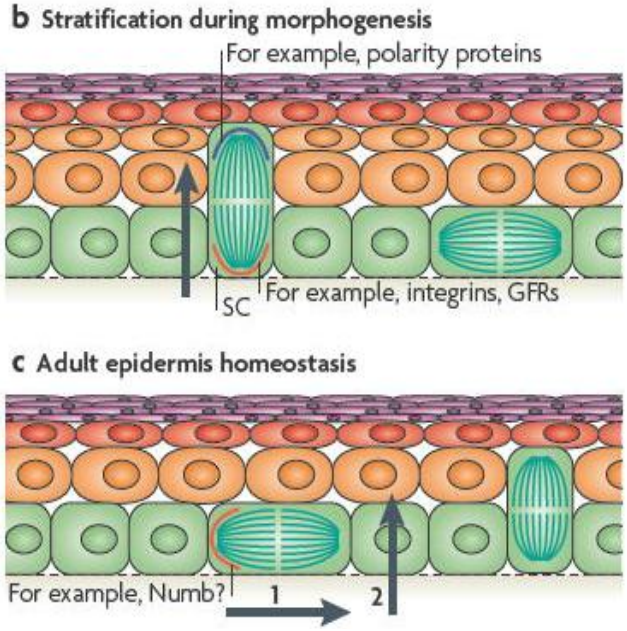

Figure 1.6 Model of asymmetric stem cell division. Asymmetry in the mother cell can arise by (b) perpendicular orientation of the mitotic spindle, thereby creating on basal and one suprabasal daughter cell or by (c) a gradient of proteins within a cell which divides in parallel to the basement membrane. Adapted from Blanpain and Fuchs, 2009

1.2.2 Markers of asymmetry

A number of proteins that could play a role in asymmetric division of stem cells have been proposed. For division vertical to the basement membrane, the cell has to establish cortical polarity and tightly regulate spindle orientation (Lechler and Fuchs, 2005; Poulson and Lechler, 2010; Williams et al., 2011). In mammalian epidermis, an assembly of conserved cortical spindle pole proteins is involved in spindle orientation, including Par6, mammalian Inscuteable (mInsc), Leu-Gly-Asn–enriched protein (LGN), nuclear mitotic apparatus protein (NuMA), Gαi and dynein / dynactin (Du and Macara, 2004; Merdes et al., 2000; Zigman et al., 2005). All of these seem to be essential for correct spindle assembly as was shown in knockout studies (Bowman et al., 2006; Kraut et al., 1996; Schober et al., 1999; Siller et al., 2006; Williams et al., 2011).

A schematic overview of the apical polarity complex is shown in Figure 1.7.

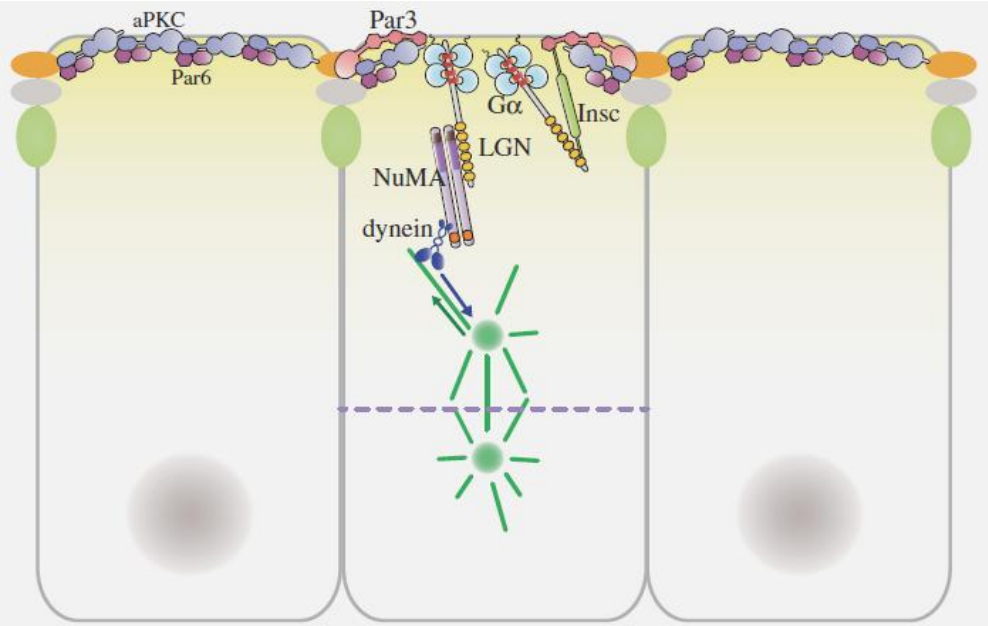

Figure 1.7 Proteins of the polarity complex. A delicate interplay and competition between several proteins provides apical polarity to cells and is essential for correct spindle assembly in perpendicular mitosis. From Mapelli and Gonzalez, 2012

The initial assumption was that these components are all part of one complex. However, recent evidence shows that the assembly of the spindle pole is more complex and involves competitive interactions of mInsc and NuMA with LGN (Culurgioni et al., 2011; Zhu et al., 2011). The exact mechanisms and all of the factors involved in regulating spindle orientation are not entirely clear yet. Some of these factors will be introduced and discussed more extensively below.

1.3 Organotypic culture of human keratinocytes

In our laboratory, a scaffold-based model system to cultivate organotypic skin co-cultures has been established and used for years (Boehnke et al., 2007; Muffler et al., 2008; Stark et al., 2004). Originally based on collagen hydrogels as dermal equivalent (DE) (Stark et al., 1999), the stability and long-term support of an epidermis was greatly improved by the use of scaffolds. Fibroblasts were cultivated in a fibrin gel on top of a defined, fibrous scaffold based on esterified hyaluronic acid (Boehnke et al., 2007; Muffler et al., 2008; Stark et al., 2004). Recently, this model was further developed into a long term organotypic co-culture system comprising a fibroblast-derived matrix dermal equivalent (fdmDE) without scaffold, co-cultured with normal human skin keratinocytes providing a three-dimensional *in vitro* skin model. The model was thoroughly tested for reproducibility under different culture conditions and using a variety of epidermal cells from different donors (Berning et al., 2015). These advanced culture conditions permitted us to cultivate the fibroblasts of the DE without a scaffold. The advantage of a scaffold free model for the present study is the translucent and permeable DE. It allows staining and confocal imaging of the entire SE without peeling off the epidermis as is commonly done for wholemount staining of epidermis. Thereby, the tissue architecture is maintained and cells can be imaged in their 3D context without damaging the tissue.

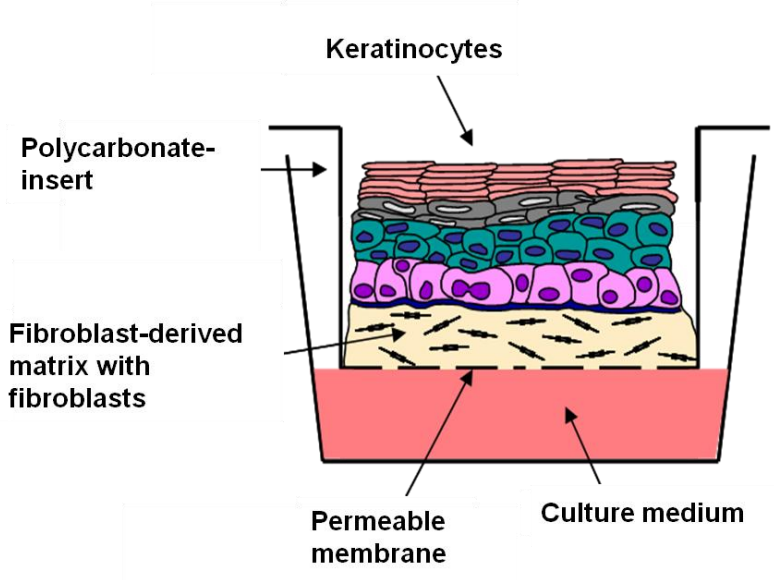

Figure 1.8 Fibroblast-derived matrix-based skin equivalent (fdmSE). The keratinocytes are seeded onto a fibroblast-derived dermal equivalent and cultivated at the air-liquid interface for periods of up to six months.

In these 3D models, keratinocytes differentiate and form a stratified interfollicular epidermis including a microenvironment and a niche for stem cells (Muffler et al., 2008). The stem cells of the epidermis were previously identified by long-term labelling. These label-chase experiments made use

of the fact that stem cells are slow-cycling and thus retain a label (for example, a base analogue like IdU) for up to several weeks, while proliferating cells lose the label quickly. Label-retaining cells (LRC) could be identified in the scaffold SE model, confirming the presence of progenitor or stem cell-like cells in our 3D *in vitro* long-term organotypic culture models (Muffler et al., 2008).

1.4 Project outline and objectives

Despite the fact that the epidermis is a well accessible organ, very little is known about the stem cell hierarchy and its regulation in human interfollicular epidermis. Markers known to date largely refer to the murine hair follicle and cannot be directly transferred to the human IFE. Existing stem cell hypotheses are based on the assumption that stem or progenitor cells of the human IFE must be able to divide asymmetrically, either in response to extrinsic cues or regulated intrinsically. However, several important questions remain elusive:

- Which mechanism of asymmetry occurs at what stage – embryogenesis *versus* tissue homeostasis?
- Which cells in the human IFE are able to proliferate – only basal cells or also suprabasal cells?
- Which are the decisive factors?

Thus, the aim of this thesis was to determine the mechanism of asymmetric cell division in the human epidermis.

First, we wanted to know what types of mitoses are present in human IFE. Second, in a quantitative approach, the proportion of the different types of mitoses was assessed over a time span starting with early, hyperproliferative time points up to late, homeostatic time points our fdmSE model system. To this end, mitotic events were counted in histological sections and in wholemount samples of the SE over a time course of up to 5 months.

In addition, we wanted to discover potential markers of asymmetric cell division. Several markers discussed in the literature were investigated with immunofluorescent staining both in keratinocyte monocultures as well as in the organotypic co-cultures. Promising candidates were further functionally studied in knock-out experiments employing the novel CRISPR/Cas9 technology. In this way, the importance of potential markers regarding cell fate in epidermal homeostasis should be elucidated.

2. Materials and Methods

2.1 Materials

2.1.1 Cell lines and skin samples

2.1.1.1 Normal human keratinocytes (KH) and dermal fibroblasts

Primary keratinocytes and primary fibroblasts were routinely isolated in our laboratory from explant cultures of human skin. In this thesis, keratinocytes from three different donors and fibroblasts from one donor were used. The internal name of the keratinocytes and fibroblasts is the date of isolation (Table 2.1). The skin samples were kindly provided by Dr. Doebler (ATOS Klinik, Heidelberg) and the women's Hospital in Tübingen with the consent of the Ethics Commitee.

Table 2.1 Normal human keratinocytes (KH) and fibroblasts from primary human explants.

Internal name	Age	Gender	Area
Fib1 04.04.07	23 years	female	n/s
KH1 04.04.07	23 years	female	n/s
KH17.04.07	43 years	female	breast
KH19.04.12	49 years	female	breast

2.1.1.2 HEK293 cells

The human embryonic kidney 293 cell line which was used as control cell line for most antibody stainings in this thesis was kindly provided by Dr. S. Diederichs, Department of RNA Biology and Cancer, DKFZ Heidelberg.

2.1.1.3 A431 cells

The human epithelial carcinoma cell line A431 was kindly provided by Prof. Herrmann, Functional Architecture of the cell, DKFZ Heidelberg.

2.1.1.4 Human induced pluripotent stem cells (hiPS)

Human induced pluripotent stem cells were produced and kindly provided by Prof. Utikal, Dermato-oncological co-operation DKFZ and University Mannheim.

2.1.1.5 Schneider 2 cells

The embryonic Drosophila Schneider 2 (S2) cells were obtained from Dr. Weyd, Dep. of Tumour Immunology, DKFZ Heidelberg.

2.1.1.6 Human skin samples

Skin sampling was conducted according to the Declaration of Helsinki Principles. Skin samples were obtained from surgical excisions that were not required for histological diagnostics and kindly provided by Prof. Utikal, University Clinic Mannheim. The patients signed the informed consent in the respective Departments of Dermatology. These were approved by the Institutional Commission of Ethics of the University of Heidelberg (103/2001).

Table 2.2 Human skin samples. Skin samples of healthy skin areas were obtained from donors in the University clinic Mannheim.

Age	Gender	Area
76 years	male	leg
64 years	female	chin
49 years	female	breast
46 years	female	back
26 years	male	axilla

2.1.2 Cell culture supplements and media

Table 2.3 Cell culture supplements and media

Article	Supplier
Adenine	Sigma Aldrich, Steinheim, Germany
Ascorbic acid stock: 50 mg / mL fdmSE medium: 50 µg / mL	Sigma-Aldrich, Taufkirchen, Germany
Choleratoxin	Sigma Aldrich, Steinheim, Germany
DermaLife	LifeLine, CA, USA
DMEM (Dulbecco´s Modified Eagle´s Medium)	Cambrex (Lonza), Verviers, Belgium
EDTA (Ethylenediaminetetraactetate) (0.05% (w/v)) in PBS+ 1 µL / mL phenolred	Serva Electrophoresis GmbH, Heidelberg, Germany
EGF (Epidermal growth factor)	1 ng/ml, Sero-med, Wien, Austria
F12	Cambrex (Lonza), Verviers, Belgium
FCS (Fetal calf serum)	Invitrogen Gibco, Darmstadt, Germany
FGF (Fibroblast growth factor)	Invitrogen Gibco, Darmstadt, Germany
Glycerol	Carl Roth, Karlsruhe, Germany
Hydrocortisone	Sigma Aldrich, Steinheim, Germany
Penicillin / Streptomycin (10U/ml; 10µg/ml)	Biochrom, Berlin, Germany
Penicillin / Streptomycin / Amphotericin	Cambrex (Lonza), Verviers, Belgium
rhInsulin	Sigma Aldrich, Steinheim, Germany
TGF-β1 human recombinant 10 µg / mL dissolved in 4 mM HCl with 1 mg / mL BSA, SE medium: 5 ng / ml	R&D Systems, Minneapolis, USA, 240-B/CF
Thrombin S lyophilized 10 I.E. / mL in PBS + CaCl2 (5,88 mg / mL)	Baxter, Unterschleißheim, Germany
Trypsin 0.1 % in PBS / 1 µL / mL Phenolred	Roche Biochemica, Mannheim, Germany

Table 2.4 Cell culture media

Article	Ingredients
D10	DMEM + 10 % FCS + 1 % Penicillin (10 U / mL) / Streptavidin (10 µg / mL)
FADcomplete	1:1 DMEM / F12, 5 % FCS, 1 % Pen / Strep, 5 mg / L Insulin, 10^{-10} M Choleratoxin, 1 µg / L rhEGF, 24µg / L Adenin, 0.4 µg / mL Hydrocortison
fdmMedium	1:1 DMEM / F12, 10 % FCS, 1 % Pen / Strep / Amph., 200 µg / mL Asc. Acid, 1 µg / mL TGFβ, 2.5 ng / mL EGF, 5 ng / mL FGF, 5 µg / mL rhInsulin
Freezing Medium	DMEM containing 20 % FCS and 10 % (v/v) Glycerol
rFAD	1:1 DMEM / F12, 10 % FCS, 1 % Pen / Strep, 200 µg / mL Asc. Acid, 0.4 µg / mL Hydrocort., 10^{-10} M Choleratoxin
Trypsin / EDTA	0.05 %Trypsin / 0.025 % (w/v) EDTA in PBS with Phenolred

2.1.3 Antibodies and kits

Table 2.5 Primary antibodies

Epitope	Species	Dilution	Supplier / Order no.
Acetylated Tubulin	mouse	1:200	Sigma T6793
GAPDH	mouse	1:50,000 (WB)	Millipore MAB374
H3S10ph	rabbit monoclonal	1:200	Epitomics 1173-1
H3S10ph	mouse monoclonal	1:5000	Millipore 05-806
Inscuteable	goat	1:400	Santa Cruz SC243091
Integrin α6	rat	1:500	Progen 10709
Integrin α6	mouse monoclonal	1:20	Millipore CBL458
K19	mouse monoclonal	1:20	Progen 11417
Keratin 10	mouse monoclonal	1:10	Progen 11414
Ki67	mouse monoclonal	1:20	Dako M724029-2
Ki67	rabbit	1:400	Abcam 15580
LRP6Sp1490	rabbit	1:250	C. Niehrs, DKFZ Heidelberg
LRP6total	rabbit	1:250	
LRP6Tp1479	rabbit	1:250	
Ninein	rabbit	1:250	O. Gruss, ZMBH Heidelberg
Notch1	rabbit	1:100	Abcam 27526
NuMA	rabbit	1:1000	Novus Biologicals NB 500-174
Numb	mouse	1:400 (IF), 1:15,000 (WB)	S. Pece, Milano, Italy
ParD6A	goat	1:500	Santa Cruz 14401
TPX2	rabbit	1:10,000	O. Gruss, ZMBH Heidelberg

Table 2.6 Secondary antibodies

Host species	Reactive species	Conjugation	Dilution	Supplier / Order no.
donkey	rabbit	DyLight488	1:500	Invitrogen A21206
donkey	goat	DyLight488	1:800	Dianova 705-486-147
goat	rabbit	Cy3	1:500	Jackson 111-165-003
goat	mouse	Alexa488	1:500	Invitrogen A11029
goat	mouse	Cy3	1:500	Jackson 115-165-068
goat	rat	Alexa488	1:500	Jackson 112-545-003
goat	guinea pig	DyLight488	1:500	Dianova 106165003
horse	mouse	HRP	1:20,000	Cell Signalling 7076S

Table 2.7 Ready-to-use kits

Kit	Supplier
BCA Assay	Thermo Scientific, Schwerte, Germany
Hematoxylin & Eosin (H&E) staining kit	Morphisto, Frankfurt, Deutschland
Mycoplasma Detection Kit	Sigma-Aldrich, Taufkirchen, Germany
QIAshredder	Qiagen, Hilden, Germany
RNase-free DNase Set	Qiagen, Hilden, Germany
RNeasy Mini kit	Qiagen, Hilden, Germany
Thermo Scientific RevertAid H Minus Strand cDNA synthesis kit	Fermentas, St.Leon-Rot, Germany

2.1.4 Technical equipment

Table 2.8 Technical equipment

Name	Supplier
CASY® cell counter with TTC analysis system	Schärfe System, Reutlingen, Germany
Cell culture incubator HeraCell 240 and 240i	ThermoScientific, Schwerte, Germany
Cell Freezing machine Kryo 10 Series III	Planer, Sunbry-on-thames, UK
Centrifuge 5417 R (for Eppendorf tubes)	Eppendorf, Wesseling-Berzdorf, Germany
Centrifuge Heraeus Laborfuge 400	Thermo Scientific, Fermont, USA
Cryo boxes	Nunc, Wiesbaden, Germany
Cryostat CM3050S Cryotome	Leica, Wetzlar, Germany
Digital Timer, Neolab 2-2002	neoLab, Heidelberg, Germany
Dispensette	Brand, Wertheim, Germany
ELISA Reader Multiskan FC	Thermo Scientific, Schwerte, Germany
Forceps Dumont	Dumont, Montignez, Switzerland
Gammacell 1000 (137Cs)	Atomic Energy of Canada Limited, Ontario, Canada
Gasprofi 1 micro WLD-Tec	neoLab, Heidelberg, Germany
Lab pipettes, Gilson Pipetman, 10-1000 µL	Gilson, Mannheim, Germany
Laboratory Scale Delta Range PC440	Mettler-Toledo, Gießen, Germany
LightCycler® 480 II	Roche, Mannheim, Germany
Liquid nitrogen	KGW Isotherm, Karlsruhe, Germany
Micro scales	Sartorius, Göttingen, Germany

Name	Supplier
Microcentrifuge II, GMC-060	Daihan Labtech, Corea
Microscope AX-70 (fluorescence) F-View II CCD-camera	Olympus, Hamburg, Germany
Microscope BX-51 (Histology) Color-View I camera	Olympus, Hamburg, Germany
Microscope confocal Leica TCS SP5 II	Leica Wetzlar, Germany
Microscope IX-70 (cell culture) AxioCam ERc 5s	Olympus, Hamburg, Germany
Minifuge RF	Heraeus Intruments, Osterode, Germany
NanoDrop 1000	Thermo Scientific, Dreieich, Germany
Nitrogen tank CHRONOS	Messer, Griesheim, Germany
PCR machine DNA Engine Dyad Peltier Thermal Cycler	BioRad, Munich, Germany
pH Meter ph522	WTW, Weinheim, Germany
Pipetboy acu	IBS Integra Biosciences, Zizers, Switzerland
Pipetboy Comfort	IBS Integra Biosciences, Zizers, Switzerland
Pipettes mLine	Biohit, Göttingen, Germany
Serological pipettes Stripette, 10-50mL	Corning, Amsterdam, Netherlands
Shaker KS250 basic	IKA Labortechnik, Staufen, Germany
Sliding microtome Leica SM2010 R	Leica Biosystems, Nussloch, Germany
Sterile tissue culture hood, HeraSafe HS18	Heraeus Instruments, Hanau, Germany
Thermomixer 5436	Eppendorf, Hamburg, Germany
Tissue-Tek TEC Tissue Embedding Console	Sakura Finetek, Zoeterwoude, Netherlands
Tissue-Tek VIP 5 Jr. Vacuum Infiltration Processor	Sakura Finetek, Zoeterwoude, Netherlands
Vacuboy and VACUSAFE system	Integra Biosciences, Fernwald, Germany
Vortexer REAX 200	Heidolph Instruments, Schwabach, Germany
Water bath	Köttermann, Hänigsen, Germany

2.1.5 Consumables, buffers, chemicals, solutions and enzymes

Table 2.9 Enzymes

Enzyme	Supplier
DNA Polymerase I	Invitrogen, Karlsruhe, Germany
DNase	Roche Applied Sciences, Mannheim, Germany
Hot Start Taq Polymerase, Fermentas	St.Leon-Rot, Germany
Reverse transcriptase	Quiagen, Hilden, Germany
RNase	Roche Applied Sciences, Mannheim, Germany

Table 2.10 Consumables

Article	Supplier
12-well deep-well ThinCert-plates (fdmSE)	Greiner Bio-One,Frickenhausen, Germany
12-well ThinCert 0.4 µm, translucent	Greiner Bio-One,Frickenhausen, Germany
6-well Falcon inserts 0.4 µm, translucent, High pore density	BD Biosciences, Heidelberg, Germany
Cell culture dishes and plates, various sizes	BD Biosciences, Heidelberg, Germany
Cell culture tubes CELLSTAR 15 mL - 50 mL	Greiner Bio-One, Frickenhausen, Germany
Cell Strainer 40 and 70 µm	BD Bioscience, Heidelberg, Germany
Cover glasses, various sizes	Menzel, Braunschweig, Germany
Cryo tube TM Vials	Nunc, Wiesbaden, Germany
Cryomold, various sizes	Sakura Tissue-Tek, Zoertewonde, Netherlands
Filter tips, Tip-One, various volumina	Starlab, Hamburg, Germany
Filter tips, various volumina	Nerbe-Plus, Winsen/Luhe, Germany
Immersion Oil Immersol 518N	Zeiss, Jena, Germany
Liquid Blocker Pen	Daido, Sangyo, Tokyo, Japan
Microscope slides (Histobond®)	Marienfeld, Lauda-Königshofen, Germany
Microscope slides (uncoated)	Langenbrinck, Teningen, Germany
Object glasses (76 x 26 mm)	Menzel, Braunschweig, Germany
Paraffin	Vogel, Gießen, Germany
Parafilm M	Bemis Plastic Packaging, Neenah, USA
PCR tube, 0.5 mL	Eppendorf, Hamburg, Germany
Pipette tips, various sizes	Starlab, Hamburg, Germany
quadriPERM dishes	Greiner Bio-One, Frickenhausen, Germany
Safe-Lock tubes, 1.5 mL	Eppendorf, Hamburg, Germany
Superfrost Plus slides	Menzel, Braunschweig, Germany
Syringe Luer Lock tip (5, 10, 30, 50 mL)	Terumo, Leuven, Belgium

Table 2.91 Buffers

Buffer	Ingredients
Blocking buffer	PBS-, 5 % goat serum, 5 % BSA, 5 % donkey serum
Blocking milk	5 % skim milk in PBS-T
FACS buffer	PBS+, 2 % FCS
PBS-T	PBS-, 1 % Tween-20
RIPA lysis buffer	10 mM Tris-HCl, pH 8.0, 150 mM sodium chloride, 1.0 % Igepal CA-630 (NP-40), 0.5 % sodium deoxycholate, 0.1 % SDS, Aprotinin (2 µg / mL), Leupeptin (10 µg /mL), Pepstatin A (1 µg / mL), PMSF (1 mM), Na-Orthovanadate (1 mM)
SDS-PAGE Running buffer	1 x Tris-Glycine, 10 % SDS in H_2O
Separating gel buffer	1.5 M Tris, 14 mM SDS ad 1 L H_2O
Stacking gel buffer	0.5 M Tris, 14 mM SDS ad 1 L H_2O
Tris-Glycine (10x)	330 mM Tris, 1.9 M Glycin ad 0.5 L H_2O
WB transfer buffer	1x Tris-Glycine, 20 % MeOH in H_2O

Table 2.102 Software

Software	Company
Adobe CS5	Adobe Systems Incorporated
AxioVision Version 40V 4.8	Carl Zeiss Micro Imaging, Göttingen, Deutschland
Cell^D, Cell^F	Olympus, Hamburg, Deutschland
FIJI	Wayne Rasband, National Institute of Health, USA
GraphPad Prism V 4.0	Statcon, Witzenhausen, Germany
GraphPad Prism Version 4.0	Statcon, Witzenhausen, Deutschland
ImageJ Version 1.4	Wayne Rasband, National Institute of Health, USA
Microsoft Excel 2010	Microsoft Corp., USA
Microsoft Power Point 2010	Microsoft Corp., USA

Table 2.13 Solutions and chemicals

Solutions and Chemicals	Supplier
2-Propanol	Sigma Aldrich, Steinheim, Germany
Acetone	Sigma Aldrich, Steinheim, Germany
Aquaguard-1 and -2	PromoCell, Heidelberg, Germany
BSA (Bovine serum albumin)	Sigma Aldrich, Steinheim, Germany
CASY® clean	Innovatis AG, Reutlingen, Germany
CASY® ton	Innovatis AG, Reutlingen, Germany
Dako Fluorescent Mounting Medium	DAKO, Glostrup, Denmark
DAPI	Sigma Aldrich, Steinheim, Germany
dNTPs	Fermentas, St. Leon-Rot, Germany
ECL WB detection reagent	Amersham GE, Freiburg, Germany
Ethanol, absolute	Sigma Aldrich, Steinheim, Germany
Ethanol, denaturated	Berkel AHK Alkoholhandel, Berlin, Germany
Eukitt®	O.Kindler, FREIBURG, Germany
Formaldehyde solution wt. 37 %	Sigma Aldrich, Steinheim, Germany
Full range Rainbow™ marker	Sigma Aldrich, Steinheim, Germany
Glycerol	Carl Roth, Karlsruhe, Germany
Hematoxylin/Eosin (H/E)	Carl Roth, Karlsruhe, Germany
Isoosmolar buffer	Eppendorf, Hamburg, Germany
Methanol	Sigma Aldrich, Steinheim, Germany
Normal goat serum	Dianova, Hamburg, Germany
Nuclease free water	Qiagen, Hilden Germany
PBS (Phosphate Buffered Saline)	Serva Electrophoresis, Heidelberg, Germany
PBS+ (PBS with $MgCl_2$, $CaCl_2$)	Serva Electrophoresis, Heidelberg, Germany
Polybrene	Santa Cruz, Heidelberg, Germany
Polyethylenimine	Polysciences, Eppelheim, Germany
Ponceau S	Sigma-Aldrich, Taufkirchen, Germany
Sodium butyrate	Sigma Aldrich, Steinheim, Germany
ß-mercaptoethanol	Sigma Aldrich, Steinheim, Germany
SYBR®Green	Invitrogen, Karlsruhe, Germany
Triton®X-100	Sigma Aldrich, Steinheim, Germany

2.2 Cell culture methods

2.2.1 Maintenance and passaging of fibroblasts

Fibroblasts were routinely cultivated in D10 medium and maintained in a cell culture incubator providing 5 % CO_2, 5 % O_2 and a humidity of 93 % at 37°C. Fresh medium was supplied every 2-3 days. The cells were split every 10 days and 1.25 x 10^6 cells were passaged to a fresh 15 cm dish. First, the cells were briefly rinsed in 0.05 % EDTA, followed by 2-5 minutes of incubation in 0.1 % Trypsin at 37°C. Cells were resuspended with a pipette and the Trypsin was inactivated in FCS-containing medium of at least equal volume as the Trypsin / EDTA solution. Cells were counted with the CASY® Cell Counter and Analyser System Model TCC (Schärfe Systems) according to the manufacturer's instructions. This counting technique is based on resistance measurement of particles.

All cells were routinely tested for Mycoplasma contamination using the Mycoplasma detection kit.

2.2.2 Freezing and thawing of cells

To freeze cells for long term storage in liquid nitrogen, the cells were trypsinised and counted and the desired cell number was centrifuged for 5 minutes at 1000 rpm. The cell pellet was taken up in freezing medium (DMEM containing 20 % FCS and 20 % Glycerol). 2 x 10^6 cells were aliquoted into cryotubes in 1 mL of freezing medium. To allow the glycerol to diffuse into the cells and dehydrate them, the aliquots were left at RT for 30 min. The pellets were then frozen by gradually lowering the temperature to -196° C in a freezing machine and stored in liquid nitrogen.

Frozen cells were thawed as quickly as possible by transferring them from liquid nitrogen directly into a 37° C water bath. The cell pellet was resuspended gently and seeded into a cell culture dish.

2.2.3 Cell pellets for DNA and protein isolation

Cell pellets for DNA or protein isolation were obtained by growing cells in a 10 cm culture dish and, after washing with ice cold PBS, carefully scraping off the cells with a cell scraper. The cells were collected in 1 mL PBS in a 1.5 mL vial. To remove the PBS, the cells were centrifuged for 5 minutes at 2000 rpm at 4° C. The PBS supernatant was aspirated and the pellet was either processed immediately or snap frozen in liquid nitrogen and stored at -80° C.

2.2.4 Generation of fibroblast-derived matrix-based skin equivalents (fdmSE)

To study the mitotic behaviour of epidermal keratinocytes under *in vivo*-like conditions, organotypic co-cultures mimicking human epidermis and dermis were cultivated. Derived from a scaffold-based culture model published in 2007 by our lab (Boehnke et al., 2007), we have recently developed a scaffold-free culture system (Berning et al., 2015). Here, the keratinocytes are seeded onto a cell-derived matrix dermal equivalent.

12-well cell culture plates (665110, Greiner Bio-One ThinCert-Plate) were equipped with cell culture inserts (665640, Greiner Bio-One, ThinCerts, 12 well, 0.4µm, translucent). In the time course of 1 week, three layers of fibroblasts were seeded in each filter insert. Per well and seeding time point, 0.5 x 10^6 fibroblasts were seeded in 0.5 mL medium containing serum and growth factors (see fdm Medium). After the last seed, the cell-derived matrix was allowed to build up over a pre-cultivation period of 4 weeks with medium changes every 2-3 days.

To create a skin equivalent, keratinocytes were thawed from the liquid nitrogen storage and cultivated in DermaLife medium for 5-7 days. Prior to trypsinising the cells in 0.4 % Trypsin / EDTA for 2-3 minutes, the cells were briefly washed in EDTA to remove Calcium. Single cells were counted in the Casy cell counter. Per well, 2.5 x 10^5 keratinocytes were seeded onto the fdmDE in fdmMedium. The fdmSE were cultivated submerged for 1-2 days and then lifted to the air-liquid interface. Medium was changed 3 times per week.

2.3 Processing of tissue

2.3.1 Harvest and processing of cells and fdmSE

The fdmSE were harvested for either histological preparation, for cryosectioning with subsequent immunofluorescence or for wholemount (WM) immunofluorescence.

2.3.2 Histological processing

Structural properties of tissues can be visualised by Hematoxilin / Eosin staining. Hematoxilin attaches to negatively charged phosphate groups of the DNA and thereby stains the cell nuclei blue. Eosin, on the other hand, stains the acidophilic and basic structures red, mainly cytoplasmic proteins and matrix structures.

The tissue was fixed in 3.8 % Formaldehyde for at least 24 hours before embedding in paraffin and cutting. The paraffin sections were freed from paraffin with Xylol for 8 minutes. The sections then underwent an alcohol series of decreasing concentration (96 %, 80 %, 70 %, 60 %, 4 min. each) before incubating for 2 min in ddH_2O. The staining was done in a two-step process. First, the sections were incubated in the Hematoxilin solution for 6 min and washed for 8 min under running tap water, followed by 6 min of staining in a 1 % Eosin solution and washing for 6 min. Finally, the sections were dehydrated by an increasing alcohol series (1 min 80 %, 2 x 2 min 96 % Ethanol), 2 min in Isopropanol and 2 x 5 min in Xylol and embedded with Eukitt®.

2.3.3 Cryosections

To prepare fdmSE sections for immunofluorescent staining, the SE was embedded in Tissue Tek and frozen in the gas phase of liquid nitrogen. The frozen pieces were stored at -80° C until sectioning at the cryotome. Sectioned SE were either frozen at -20° C until further use or processed directly by fixing in 2 % Formaldehyde for 10 minutes, followed by permeabilisation in 0.2 % Triton-X 100 for 5 minutes. The slides were washed in PBS three times and stained with fluorescent antibodies.

2.3.4 Wholemount harvest and fixation

To stain the entire fdmSE without disrupting the tissue, the SE was taken as a whole and fixed in freshly prepared 2 % Formaldehyde for 1-2 hours, depending on the thickness of the epithelium. The wholemount was then stored in PBS with 0.05 % NaN_3 at 4° C or processed immediately. Prior to staining, the sample was permeabilised in 0.2 % Triton-X and washed three times in PBS.

2.3.5 Cells on objective slides

In order to stain keratinocytes cultivated in 2D monoculture, 1 x 10^5 cells were seeded per objective slide in a quadriperm dish and cultivated until the desired cell density was reached. The slides were then fixed in 2 % Formaldehyde for 10 minutes and either stored in PBS with 0.05 % NaN_3 at 4° C or immediately permeabilised in 0.2 % Triton-X and stained.

2.3.6 Cells on cytospins

For small amounts of cells, cytospins were prepared. A cell number up to 10,000 cells per cytospin was taken up in 100 µL of medium and pipetted into the cytospin funnel. The samples were centrifuged at 1,200 rpm for 5 minutes to press the cells through the funnel and onto the slide. The cells were then processed like cells grown on slides.

2.4 Staining methods

2.4.1 Indirect immunofluorescence (IF)

2.4.1.1 Immunofluorescence of cells and cryosections on objective slides

The permeabilised and washed slides were left to air dry before encircling the area to be stained with a pap pen. When the pap circle was completely dry, the cells were briefly rehydrated in PBS and then blocked in 5 % donkey serum / 5 % goat serum / 5 % BSA in PBS+ for 30 minutes. The primary antibody was diluted in the blocking agent and incubated for 30 minutes at 37° C followed by either 1 h at RT or 4° C ON. The cells were washed 3 x in PBS- before incubating with the secondary antibody and DAPI diluted in blocking agent. The secondary AB incubation was also done for 30 minutes at 37°

C followed by 1 h at RT. After washing 3x in PBS- and once in VE water to remove excess salt, the slides were mounted in Dako mounting medium and stored at 4° C in the dark until imaging.

2.4.1.2 Immunofluorescence of wholemounts

The fdmSE was cut into quarters and blocked in 5 % donkey serum / 5 % goat serum / 5 % BSA in PBS+ for 1 h. Primary antibody incubation was done in the blocking agent for 30 minutes at 37° C and subsequently at RT with shaking ON. The next day, the sample was washed 3 x in PBS- for 30 minutes. The secondary antibodies and DAPI were diluted in the blocking agent and centrifuged for 10 minutes at full speed to reduce background staining. Secondary antibodies were incubated at 37° C for 30 min and 2 h at RT. After thorough washing for at least 2 h with several buffer changes, the sample was embedded in Dako mounting medium and stored at 4° C in the dark until imaging. For microscopy, the confocal Leica TCS SP5 II was used. Samples were analysed at 40x magnification. Images of 1024 x 1024 pixel with a pixel size of 0.4 µm were acquired. z-stacks were imaged at intervals of 0.7 µm.

2.5 Molecular biology techniques

2.5.1 RNA isolation (Qiagen Qiashredder + RNeasy Mini Kit + RNase-free DNase Set)

RNA extraction was done using the RNeasy Mini Kit and the RNase-free DNase Set according to the manufacturer's instructions. Eluted RNA was stored at -80°C.

2.5.2 cDNA synthesis (Thermo Scientific RevertAid H Minus First Strand cDNA Synthesis Kit)

RNA was transcribed into cDNA with the Thermo Scientific RevertAid cDNA synthesis kit according to the manufacturer's instructions. The concentration of the eluted cDNA was measured at a NanoDrop. cDNA was stored at -20°C or for longer storage times at -80°C.

2.5.3 Polymerase chain reaction (PCR)

DNA was amplified using specific primers for the gene region of interest. The Master mix was prepared as indicated for one reaction in

Table 2.11.

Table 2.11 PCR Master mix for one reaction. Volumes have to be adjusted for the amount of reactions.

Reagent	Volume [µL]
10 x Buffer	2.5
Primer fwd 10 µM	1
Primer rev. 10 µM	1
cDNA (50 ng / µL)	4
ddH_2O	14.25
10 mM dNTPs	0.5
Hot Start Taq (5 U/ µL)	0.25
$MgCl_2$(25 mM)	1.5
Total	**25**

The PCR cycles are listed below. For amplification of Numb and Numblike, a program of 45 cycles was chosen, for amplification of GAPDH, 23 cycles were sufficient.

Table 2.12 PCR cycle for amplification of Numb, Numblike and GAPDH

Step	Temp. [°C]	Time
1	95	2 min
2	94	30 sec
3	60	30 sec
4	72	30 sec
5	72	10 min

Table 2.13 Primer pairs for GAPDH, Numb and Numblike amplification. Specific complimentary (forward) and antisense (reverse) primer pairs were designed to bind to the cDNA of the gene of interest. GAPDH was used as a housekeeping gene.

Gene	Primer
GAPDH forward	GAG AAG GCT GGG GCT CAT TT
GAPDH reverse	CAG TGG GGA CAC GGA AGG
Numb forward	TGGCTGTCAAGGACACAGG
Numb reverse	TGGTCCGACTAGCATCAAAA
Numblike forward	CAGTTCATCTTTTGCCAGTGC
Numblike	TCACCCCAGGCAGAAGTC

2.6 CRISPR/Cas9 knock down

CRISPR (clustered regularly interspaced short palindromic repeats) are DNA loci found in some bacteria and used there as anti-virus defence (Bhaya et al., 2011; Terns and Terns, 2011; Wiedenheft et al., 2012). The bacteria can incorporate short viral DNA repeats and use them as an acquired immune protection. The short repeats, expressed as crRNA and tracrRNA (CRISPR RNA and trans-activating crRNA), bind complementary intruding DNA and the co-expressed Cas9 endonuclease cuts the DNA. Recently, this system has been adapted for gene editing purposes (reviewed in Mali et al., 2013). The gene of interest is targeted by a gRNA (guideRNA) which mimics and combines the hairpin structure of the crRNA and tracrRNA. Additional binding specificity is provided by the protospacer adjacent motif (PAM), a three nucleotide NGG sequence. The Cas9 nuclease cleaves dsDNA, introducing doublestrand breaks (DSB). DSBs are repaired by non-homologous end joining (NHEJ) which leads to insertions or deletions and thereby disruption of the gene locus.

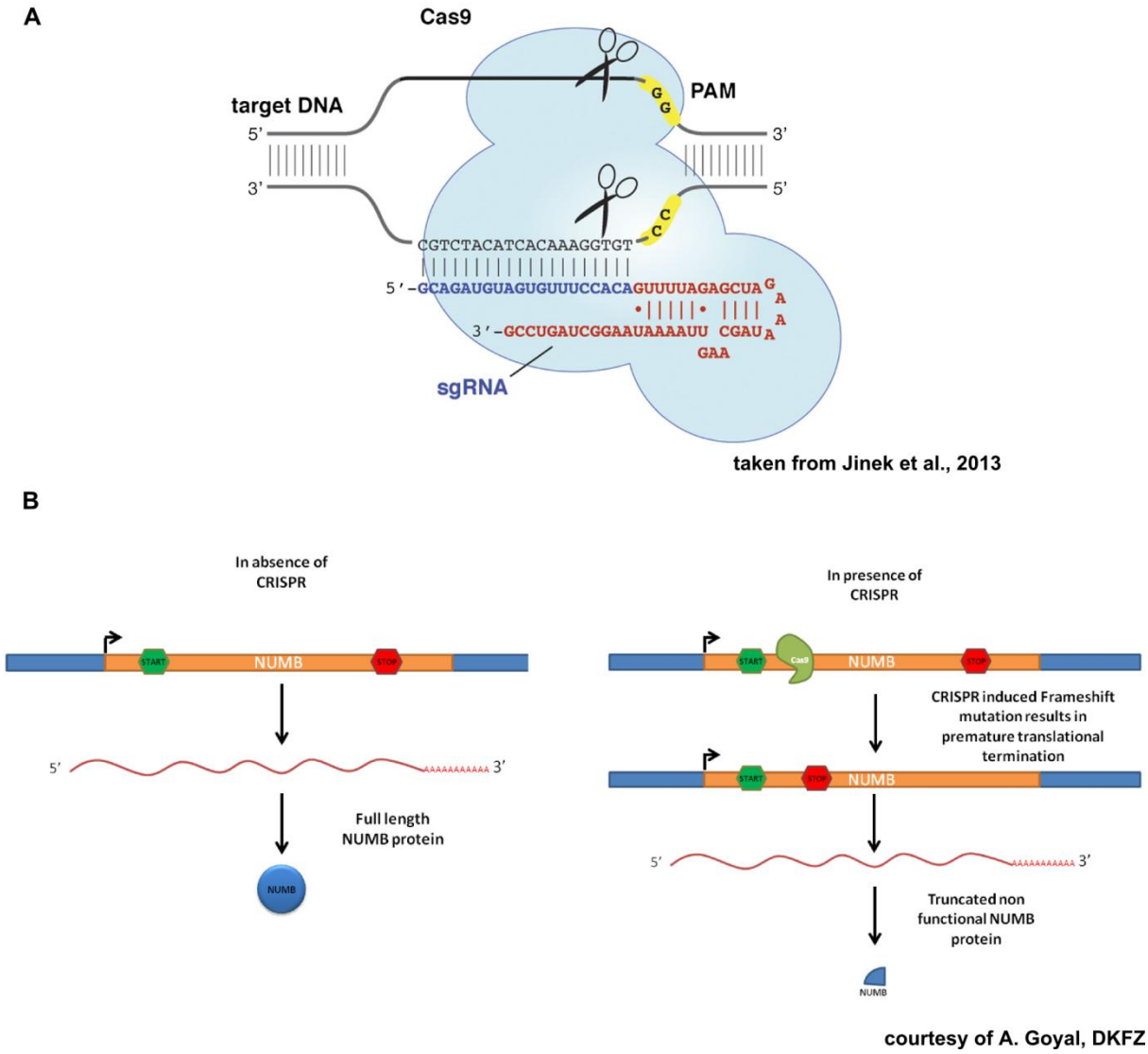

Figure 2.1 CRISPR/Cas9 knock out working principle. To knock out a specific gene, a complementary guide RNA is cloned into a plasmid carrying the Cas9 endonuclease and a selection marker like GFP. After entering

the cell, the guide RNA will bind to the complementary gene sequence and recruit the endonuclease which cleaves the target gene, thereby inducing a double strand break (A). The subsequent frame shift will prevent transcription of a functional protein (B). Upper graphic taken from Jinek et al., 2013.

In collaboration with Ashish Goyal from the division of RNA Biology and Cancer (DKFZ Heidelberg), five different guide RNAs (No. 1, 2, 3, 4 and 8) were designed and cloned into plasmids carrying the Cas9 sequence and a GFP reporter gene. The guide sequences were complimentary to the first exon, shortly after the start codon, and present in all four Numb isoforms found in skin (excluding isoforms 5 and 6 which have only been identified in placenta) but not the Numblike homologue. The knock out should therefore target all Numb isoforms that could be expressed in skin.

2.6.1 CRISPR guide design

The CRISPR/Cas9 plasmids were produced by Ashish Goyal (DKFZ). In brief, the appropriate guide RNA (gRNA) sequences were designed using the software designed by Hsu and colleagues (Hsu et al., 2013), found at http://crispr.mit.edu/. The specific algorithm used by the program is described in the publication. The user enters a 23 – 1000 bp sequence of the target DNA. The program will find all Cas9 target sites within that sequence and display a ranking of the sites according to specificity and off-target sites. We aimed at different sequences covering the start of the transcript of all Numb variants and chose those sequences excluding off-targets with the highest likelihood. Five guide RNA sequences were chosen out of the list and will in the following be labelled #1, #2, #3, #4 and #8.

Table 2.14 CRISPR guide RNA sequences. Five different guide RNAs were designed complimentary to the Numb gene sequence and with minimal off-target binding.

CRISPR gRNA name	gRNA sequence	Spacer sequence
#1	GATGAAGAAGGCGTTCGCACCGG	GATGAAGAAGGCGTTCGCAC
#2	CTGCCACTGATGTGGACGACTGG	CTGCCACTGATGTGGACGAC
#3	TGATGTGGACGACTGGCCTCTGG	TGATGTGGACGACTGGCCTC
#4	AGGCCAGTCGTCCACATCAGTGG	AGGCCAGTCGTCCACATCAG
#8	CACCGGAAAATGTAGCTTCCCGG	CACCGGAAAATGTAGCTTCC

These sequences were cloned into the pSpCas9(BB)-2A-GFP (PX458) plasmid, additionally encoding the Cas9 sequence as well as a GFP protein as transfection marker. pSpCas9(BB)-2A-GFP (PX458) was a gift from Feng Zhang (Addgene plasmid # 48138) (Ran et al., 2013).

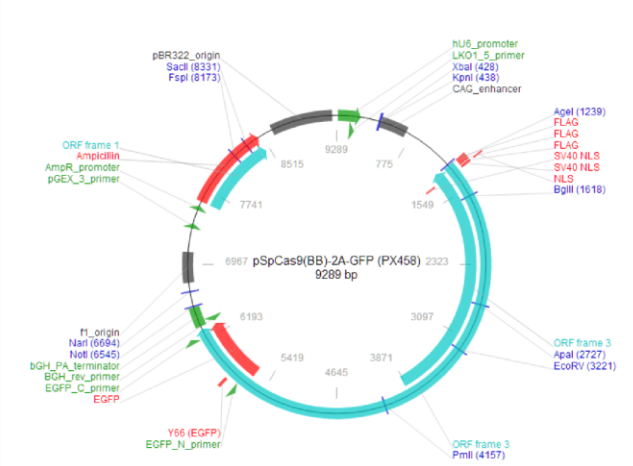

Numb guide sequences designed with http://crispr.mit.edu/

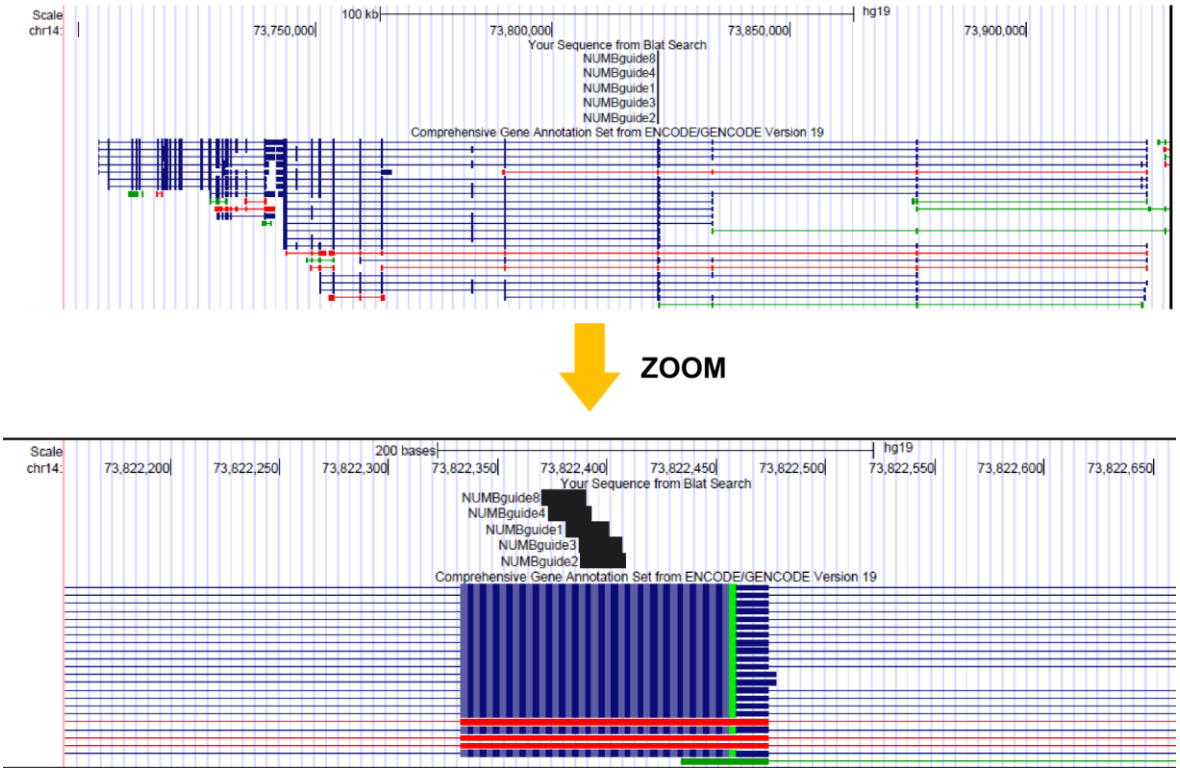

2.2 CRISPR guideRNA design. The gRNA sequences were designed with the software at http://crispr.mit.edu/. Out of the output list, five sequences with the least off-target binding were chosen.

Functionality of the plasmids was checked in HEK293 cultures. A T7 endonuclease test proved efficient gene cleavage. In brief, during the T7 test, the gene region around the DSB is PCR-amplified. The PCR products are heat denatured and reannealed to create heteroduplexes. These are recognised and cut by the T7 endonuclease. As a read out, the fragments are separated on a gel. The highest band indicates the wildtype gene region while two smaller double bands are the cleaved fragments and thereby show effective gene cleavage by Cas9.

2.6.2 Transfection of keratinocytes with electroporation

For transfection of the keratinocytes, the Invitrogen NEON™ electroporation system was used. Freshly thawed keratinocytes were cultivated in DermaLife for 5 days up to a confluency of 70 – 80 %. The cells were trypsinised, counted and taken up in transfection buffer or DermaLife without supplements. Plasmid DNA in an end concentration of 5 or 10 µg / mL was added and 2.5 x 10^5 cells were taken up in 100 µL with the NEON™ transfection pipet and the appropriate transfection tip. After pulsing the cells, they were either incubated on ice for 10 minutes or directly transferred into collagen-coated 6-well plates containing pre-warmed DermaLife. All conditions tested are listed in

Table 2.15.

Table 2.15 Electroporation conditions tested for transfection of KH with the Invitrogen NEON™ kit. Outcome was measured according to two parameters: attachment of the cells after transfection and transfection efficiency as observed by GFP signal. – indicates no attachment or no GFP signal; +, ++, +++ indicate ranking of outcome from + indicating sufficient to +++ very good.

Resusp. medium	Cell no.	DNA [µg]	Voltage [V]	Pulse width [ms]	Pulse no.	Cell attachment	Efficiency
Buffer R (Neon Kit)	1 x 10^6	5	1400	20	2	-	-
	5.6 x 10^5	5	1400	20	2	-	-
	2 x 2.5 x 10^5	5	1200	20	2	+++	-
		5	1200	30	2	++	-
		10	1200	20	2	++	+
		10	1200	30	2	+	++
		5	1300	20	2	+++	++
		5	1300	30	2	+	-
		10	1300	20	2	+++	++
		10	1300	30	2	+++	++
		5	1400	20	2	+++	++
		5	1400	30	2	-	-
		10	1400	20	2	+	+
		10	1400	20	2	+	-
Isoosm. buffer	2 x 2.5 x 10^5	10	800	30	2	++	+
		10	800	40	1	+	+
		10	900	20	3	+	+
		10	1000	20	3	+	+
		10	1000	30	2	+	+
		10	1100	30	2	+	-
		10	1100	40	1	+	+
		10	1200	20	3	+	+
		10	1200	30	2	+	+
		10	1200	40	1	-	-
		10	1200	30	2	+++	+++
		10	1300	30	2	+++	+++
Isoosm. Buff., 10 min. on ice	2 x 2.5 x 10^5	10	1300	20	3	-	-
		10	1300	30	2	-	-
DermaLife w/o suppl., each 10 min. on ice / no ice	2 x 2.5 x 10^5	10	500	20	3	+++	-
		10	500	30	2	+++	-
		10	500	40	1	+++	-
		10	650	20	3	+++	-
		10	650	30	2	+++	-
		10	650	40	1	+++	-
		10	800	20	3	+++	-
		10	800	40	1	+++	-
		10	1000	20	3	+++	-
		10	1000	30	2	++	++
		10	1000	40	1	+++	++
		10	1100	30	2	+++	++
		10	1100	40	1	+++	+++
		10	1200	30	2	+	++
		10	1200	40	1	++	++
		10	1300	20	3	++	+
		10	1300	30	2	+	-
		10	1300	40	1	+	+

2.7 Fluorescence-activated cell sorting (FACS)

To sort GFP-positive transfected cells in a fluorescence-activated cell sorter (FACS), the cells were trypsinised and counted as described above. Approximately 2 x 10^6 cells per 1 mL were taken up in FACS buffer (PBS+ with 5 % FCS) with 1 µL 7AAD or FxCycle for live staining of the cells. Cells were sorted at the DKFZ core facility and collected in 5 mL Falcon tubes containing medium. The collected cells were processed immediately after sorting.

2.8 Western Blot

2.8.1 Protein extraction

Cell pellets were thawed on ice and resuspended in 35 – 75 µL freshly prepared RIPA buffer containing protease inhibitors. The suspension was incubated on ice for 30 minutes with occasional flipping of the tube. The cell debris was pelleted by 30 minutes of centrifugation at 14,000 rpm at 4° C. The supernatant was transferred into a fresh tube and the pellet discarded. The total protein concentration was determined by a BCA assay with a BSA standard curve. In brief, 25 µL of 1:10 dilutions of the samples were incubated with 200 µL of a 50:1 mixture of the BCA reagents for 30 minutes at 37° C. The colorimetric change was read out by a 96-well plate reader at 562 nm.

2.8.2 SDS-Polyacrylamide gel electrophoresis

The proteins of the cell lysates were separated according to their size on a 10 % SDS gel. First, the proteins were denatured by boiling at 95° C with 5x Lämmli buffer containing β-mercaptoethanol which breaks the disulfide bonds. The SDS in the running buffer provides the denatured proteins with a negative charge in proportion to their molecular weight. The proteins therefore travel through the gel toward the cathode if a current of approximately 100 V is applied. For molecular weight reference, the Rainbow molecular weight marker was used.

2.8.3 Protein transfer and detection

The proteins were transferred to a nitrocellulose membrane with the wet blot method using the BioRad apparatus. The gel was placed onto the membrane between Whatman paper and sponges in a blotting cassette. The proteins were blotted onto the membrane for 2.5 h at a current of 48 V. To check for successful protein transfer, the membrane was bathed briefly in Ponceau dye and rinsed in water to visualise total protein bands.

After blocking unspecific binding sites in 5 % skim milk for 1.5 h, the membrane was washed briefly in TBS-T buffer and incubated ON at 4° C with the appropriate antibodies diluted in TBS-T on a rolling shaker. The next day, the membrane was washed 2 x in TBS-T and once in blocking buffer before

incubating for 1 h at RT with the HRP-coupled secondary antibody diluted in blocking milk. After three more wash steps, the membrane was incubated for 1 min with the ECL solution containing the substrate for the HRP. The luminometric reaction was detected on an X-ray film in the dark.

3. Results

3.1 Four different types of mitoses were found in human skin equivalents

To assess in which way the keratinocytes in the fdmSE divide, H & E stained tissue sections were examined. So far, it is described that only basal keratinocytes in adult epidermis possess proliferative potential. Only during embryogenesis and wound healing are suprabasal cells able to divide (Lechler and Fuchs, 2005; Smart, 1970a; Stojadinovic et al., 2005). The mitotic orientation found in homeostatic skin differs according to the tissue. In mouse back skin, it was found that most cells divide perpendicular to the basement membrane (BM) (Lechler and Fuchs, 2005) whereas in mouse tail skin the predominant proportion of divisions occurred in horizontal direction (Clayton et al., 2007).

Unexpectedly, we identified four different types of mitosis. (1) Division in parallel to the BM with both daughter cells remaining in contact with the BM, classically referred to in the literature as “symmetric division”. (2) Division perpendicular to the BM, which places one of the daughter cells in the suprabasal layer. (3) Division at an oblique angle between 0 and 90° degrees to the BM. (4) Suprabasal division where neither the mother cell nor a daughter cell stayed in contact with the BM (figure 3.1).

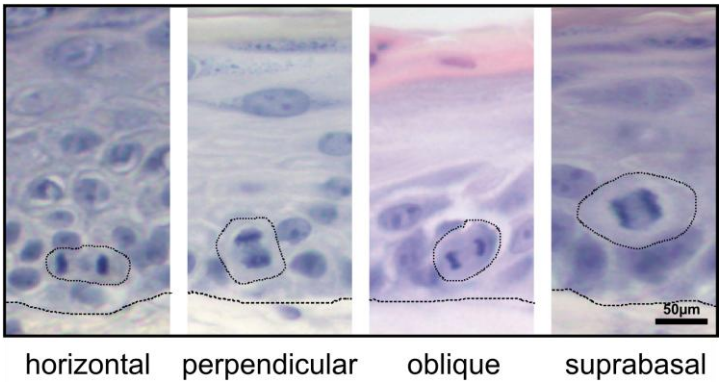

Figure 3.1 Four different types of mitosis were found in the human skin equivalent. In H & E stained sections of the fdmSE, keratinocytes divided in four ways: horizontal to the basement membrane, perpendicular to the basement membrane, at oblique angles or suprabasally.

To find out which types of mitosis play a role during expansion and homeostasis of the epidermis in skin equivalents, I quantitatively assessed the mitotic events in the fdmSE at time points ranging from 4 days to 5 months.

First, mitoses were counted in H & E stained sections of the fdmSE (figure 3.2). The processing and imaging is quick and reproducible. On the other hand, the cutting plane may distort the appearance of the division angle or location. Nevertheless, since these cutting artefacts probably only account for a small proportion of the counted events, the analysis of mitoses found in histological sections is nevertheless a reliable first assessment of the mitotic behaviour of keratinocytes in the fdmSE.

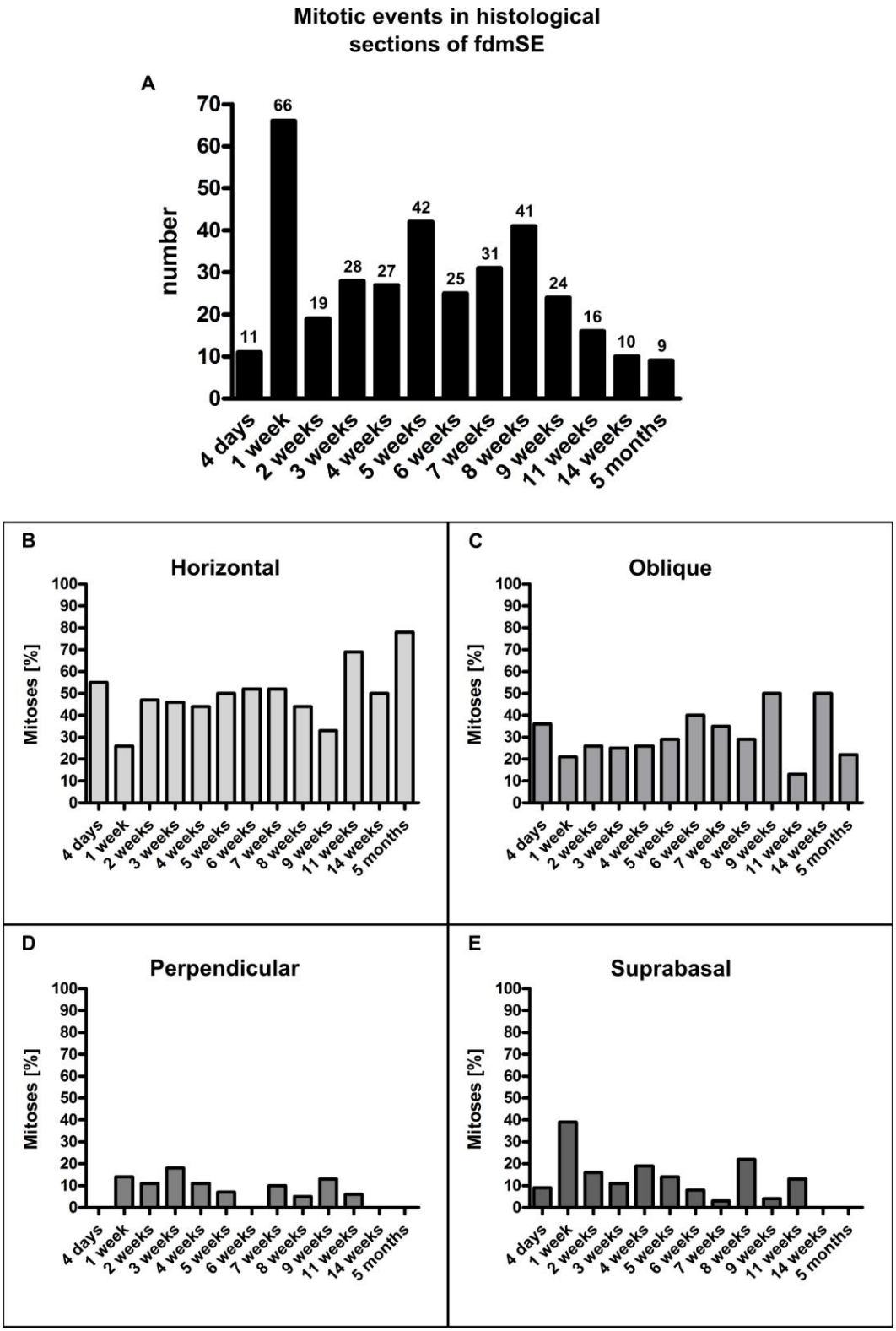

Figure 3.2 Types of mitoses found in histological sections of the fdmSE. In H & E stained histological sections of the skin equivalents, 349 mitotic events were counted over a time span of 5 months (A). About 50 % of mitoses occurred in horizontal orientation (B), 20 – 30 % at oblique angle (C), up to 10 % at perpendicular angle (D) and between 10 and 20 % of cells divided suprabasally (E).

Of 349 counted mitotic events in the fdmSE (figure 3.2 A), horizontal divisions made up the largest proportion at all time points with mostly about 50 % (figure 3.2 B). At one week, only 25 % of cells divided horizontally, which was also the time point with most suprabasal mitoses with almost 40 % (figure 3.2 E). The highest proportion of horizontal divisions occurred at late time points with almost 70 % at week 11 and about 75 % at 5 months. The second most frequent division type was oblique division with a proportion of 20 – 40 % (figure 3.2 C). This distribution was relatively stable over the entire observed time period of 4 days to 5 months of culture with the exception of a drop to 10 % at week 11 and an increase at weeks 9 and 14 weeks. These time points seemed to be in reciprocal correlation with the horizontal divisions, which increased at week 11 and dropped at week 9 and 14. Perpendicular divisions occurred at low frequencies of about 10 % and were entirely absent at week 6 and 14 and 5 months as well as 4 days (figure 3.2 D). We found a substantial amount of suprabasal mitotic events, accounting for 10 – 20 % at most time points (figure 3.2 E). Suprabasal division peaked at two weeks and remained stable except at the very late time points, where no suprabasal division was seen.

In addition to the histological sections, mitotic events were counted in wholemounts of the fdmSE, meaning the entire tissue piece was fixed and stained. Processing and imaging is more laborious than the H & E stained sections. However, the information obtained from the wholemounts is more reliable since we can image larger tissue areas and reconstruct the 3D morphology of the tissue. FdmSE wholemounts (WM) were fixed and stained for the spindle-associated protein TPX2 and Integrin α6, a hemidesmosomal component connecting basal keratinocytes to the basement membrane (BM). Integrins can be used to reliably identify the basal pole of basal keratinocytes connected to the BM which is important in this case to determine angle and location of the mitotic events. The stained tissue specimens could be imaged with a confocal microscope without disrupting or cutting the tissue, thereby maintaining the 3D structure. Following the confocal z-stack, images were processed in order to reconstruct the 3D tissue organisation (example shown in Figure 3.3).

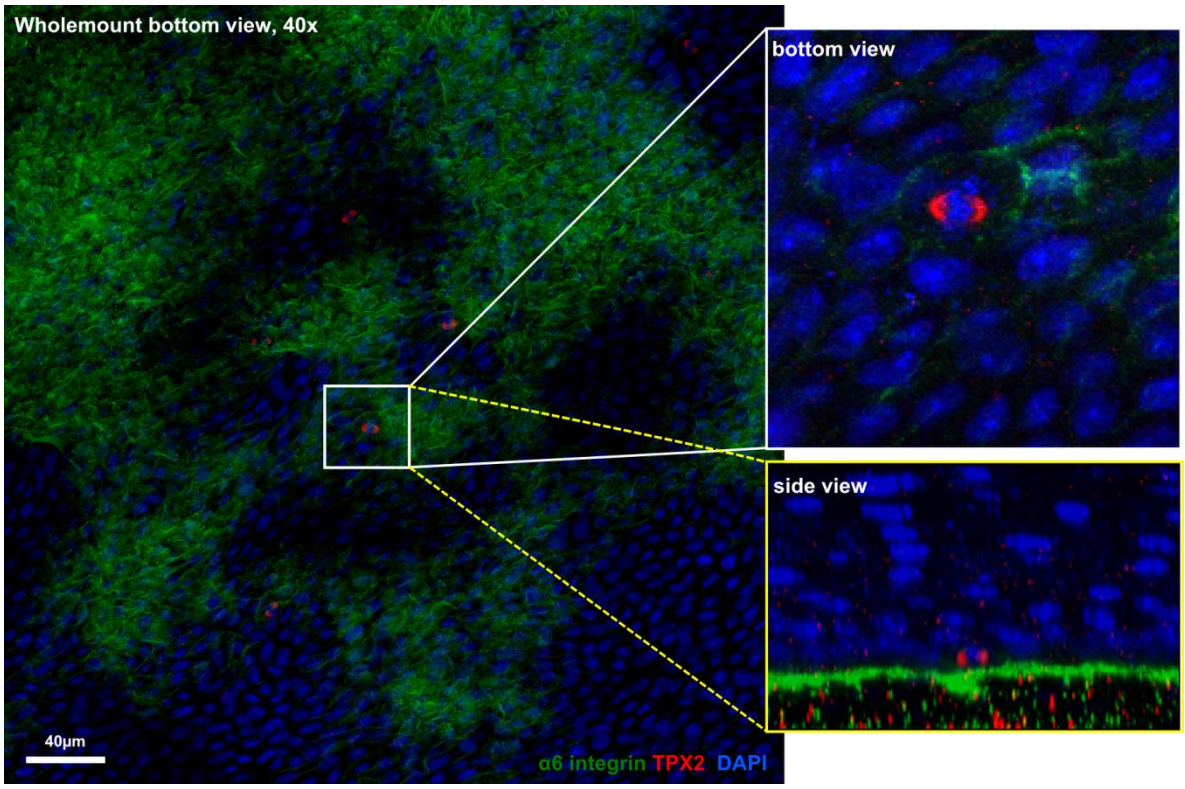

Figure 3.3 3D Reconstruction of whole fdmSE. Whole fdmSE specimen were fixed, stained for Integrin α6 and the spindle-associated protein TPX2 and imaged as z-stacks by a confocal microscope. The staining of the basement membrane appears uneven in the single z-layers due to the naturally uneven basal cell layer. In cross section of the 3D reconstruction, the exact location of mitotic cells and the position of the mitotic spindle relative to the basement membrane was demonstrated.

The uneven staining of Integrin α6 in any one z-layer is a result of the naturally uneven BM. In the 3D reconstruction, however, the entire BM is visible and the exact location and angle of the mitotic events can be determined. Over 600 mitotic events were counted over a culture time from 1 to 10 weeks (figure 3.4 A). The data of three independent experiments for each time point were analysed to ensure reproducibility and reveal the relevance of each division type for each time point (figure 3.4).

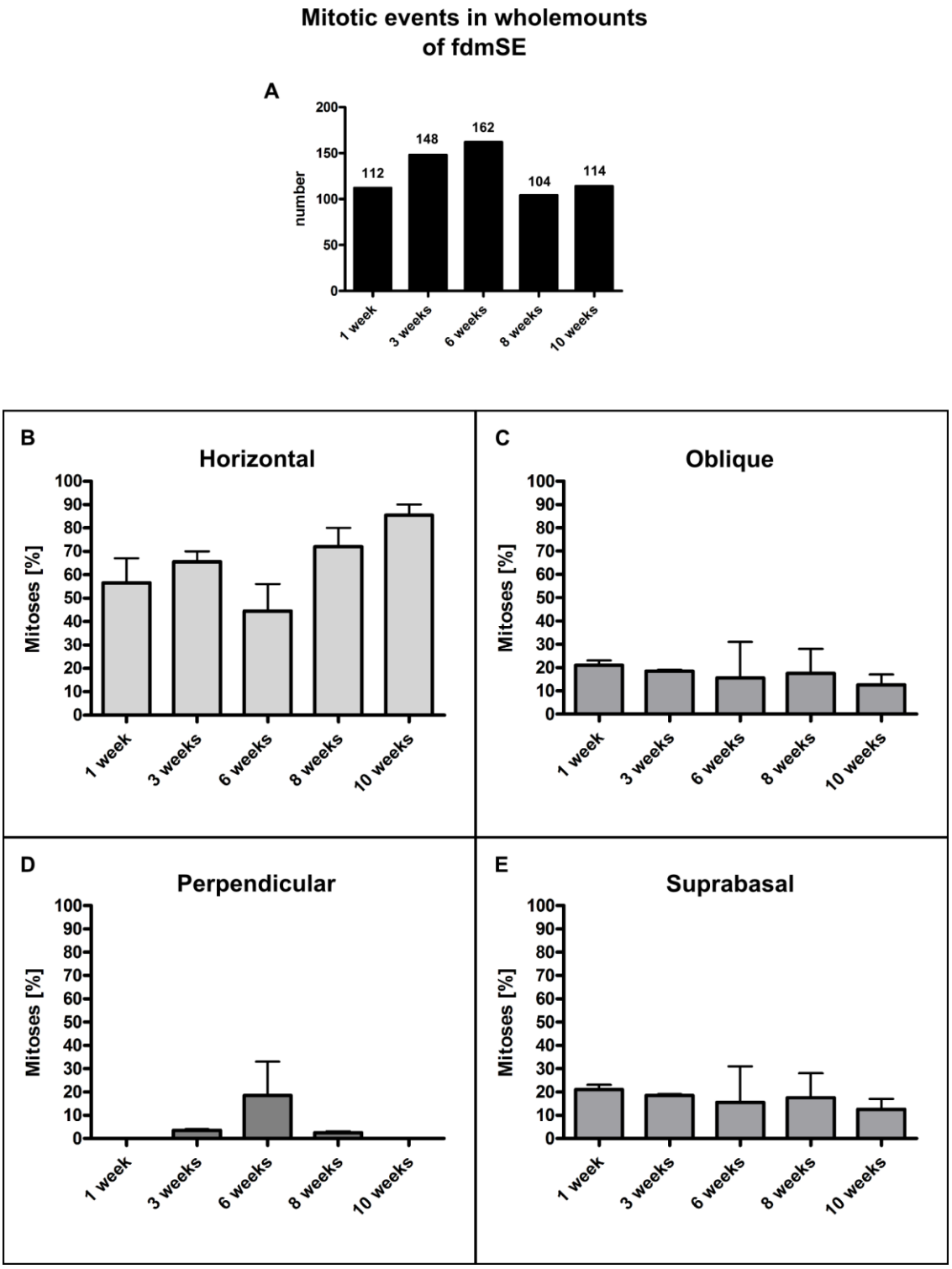

Figure 3.4 Types of mitoses found in wholemounts of the fdmSE. In several independent experiments, over 600 mitotic events were counted in wholemount stainings of the fdmSE over a time span of one to ten weeks (A). Horizontal mitoses accounted for the largest proportion with 40 to 80 % (B). Oblique (C) and suprabasal (E) division each occurred at 10 – 20 % and remained relatively stable over the examined time span. Perpendicular mitosis peaked at 6 weeks with almost 20 % but was rare or absent at the remaining time points (D). Error bars: Standard error of the mean (SEM).

The most prominent division type found here was division horizontal to the BM (figure 3.4 B). Between 40 and 80 % of all divisions occurred horizontally. This distribution was increasing over the entire investigated time span, starting with about 55 % in week 1 and going up to 80 % in week 10, with a drop to 40 % in week 6. Oblique (figure 3.4 C) and suprabasal (figure 3.4 E) divisions were found at similar frequencies of 10 to 20 % at all time points. Reports in the literature concerning division angle are controversial and seem to depend on the investigated tissue and body region. Horizontal division angles were only reported in early mouse embryos (Williams et al., 2011), but not in adult mouse back skin, where about 85 % of homeostatic divisions occur perpendicular to the basement membrane. The proportion of perpendicular divisions found in the human skin equivalent was rather low (0 – 20 %, figure 3.4 D), as was also reported for adult mouse tail epidermis (Clayton et al., 2007). In our study, the number of perpendicular mitoses peaked at week 6 with almost 20 %. In comparison, at the 6 week time point in the H & E stained sections (figure 3.2 D), no perpendicular divisions were detected at all. In the present study, most of the cells divided in horizontal direction, a feature described for developing mouse skin but described to be absent in homeostatic mouse back skin (Lechler and Fuchs, 2005). In addition, a substantial proportion of suprabasal mitoses were found frequently and at all time points (figure 3.4 E), a phenomenon only ascribed to early embryonic stages of skin development and wound or disease situations (Lechler and Fuchs, 2005; Smart, 1970a; Stojadinovic et al., 2005).

3.2 Human keratinocytes frequently divided suprabasally in the fdmSE and in human skin

Since the restriction of mitotic activity to basal epidermal cells is an acknowledged paradigm in the literature, we were intrigued by the repeated occurrence of suprabasally dividing cells in the fdmSE. The fact that they were not only found during the early hyperplastic stages of the fdmSE but were also frequently observed at later time points suggests that suprabasal mitosis might in fact be involved in tissue homeostasis.

Two possible mechanisms could be responsible for these suprabasal mitoses: First, cells detach from the BM during division due to spatial restrictions in the basal cell layer and the daughter cells reinsert into the basal layer after division, as was observed in the branching ureteric bud epithelium (Packard et al., 2013). Second, they may be genuine suprabasal, early differentiating cells. To further investigate this question, keratinocytes in sections of the fdmSE at different time points were stained with a mitotic marker. Since mitotic spindles are frequently destroyed during sectioning, fixing and staining and are hard to discern in the sections, a anti-Phosphohistone antibody was used to label mitotic cells. Phosphorylation of Histone H3 at Serine 11 (H3S10ph) by Aurora kinase B and

subsequent chromosome condensation is a prerequisite for the mitotic onset (Gurley et al., 1973; Hendzel et al., 1997; Paulson and Taylor, 1982). The detection of H3S10ph is, therefore, an established mitotic marker. Cells with phosphorylated H3 were found in cryosections of fdmSE at low frequencies but at all investigated time points (Figure 3.5). Interestingly, the suprabasal cells showing H3S10ph signal were mostly also Keratin 10 (K10) positive, indicating that they already entered the differentiation program.

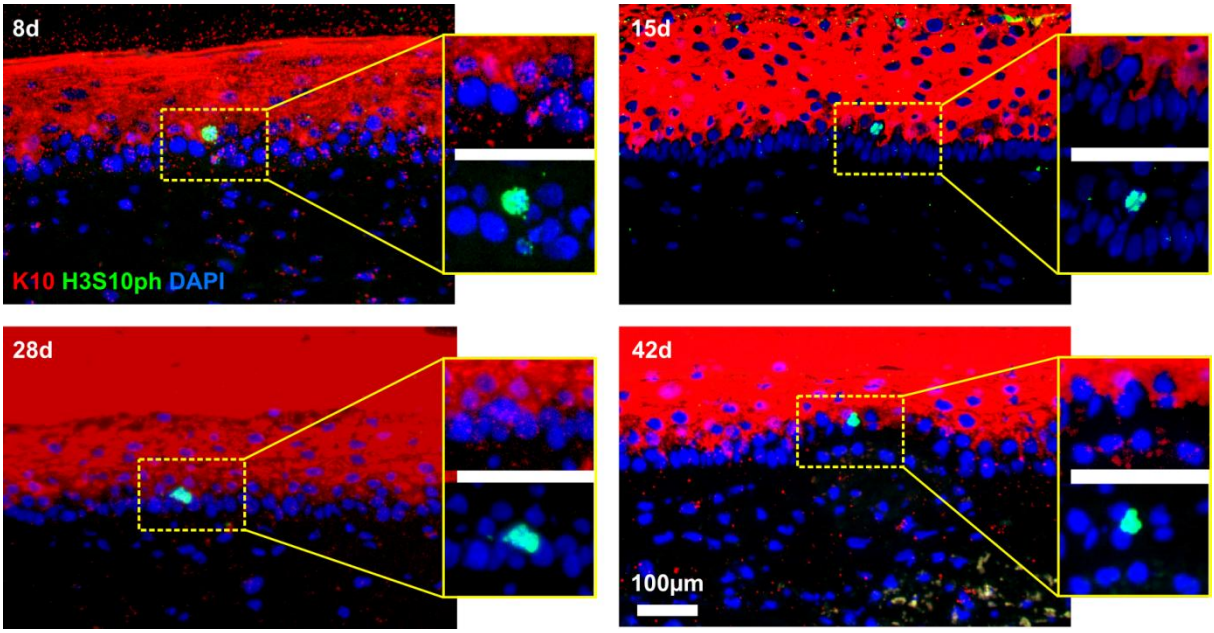

Figure 3.5 Suprabasal mitoses in cryosections of the skin equivalent. In cryosections of the fdmSE, mitotic cells were stained with anti-Phosphohistone (H3S10ph) antibody. Co-staining with Keratin10 (K10) reveals the differentiation state of the suprabasal cells. Mitoses in suprabasal layers were found frequently and even at later time points (42 days).

During the first 3 weeks, the epidermis of the fdmSE is hyperproliferative due to the seeding of single keratinocytes which recapitulates a wound situation. As mentioned before, during wound healing, when the epidermis needs to expand quickly, suprabasal mitosis is frequently observed (Stojadinovic et al., 2005) as is the case in tumourigenic, dysplastic epidermis (Blanton et al., 1992; Meuten, 2008). It would therefore not be surprising to find suprabasal mitoses restricted to early time points of the fdmSE. Notably, suprabasal mitoses did not seem to be a special feature of the wound-like situation that we observe in early fdmSE. On the contrary, suprabasal mitotic activity was also observed in unwounded donor skin. In skin samples of three different donors, suprabasal mitotic cells were found with differing frequencies and apparently independent of the donor age (Figure 3.7). Wholemounts were freshly prepared from donor skin for 3D reconstruction.

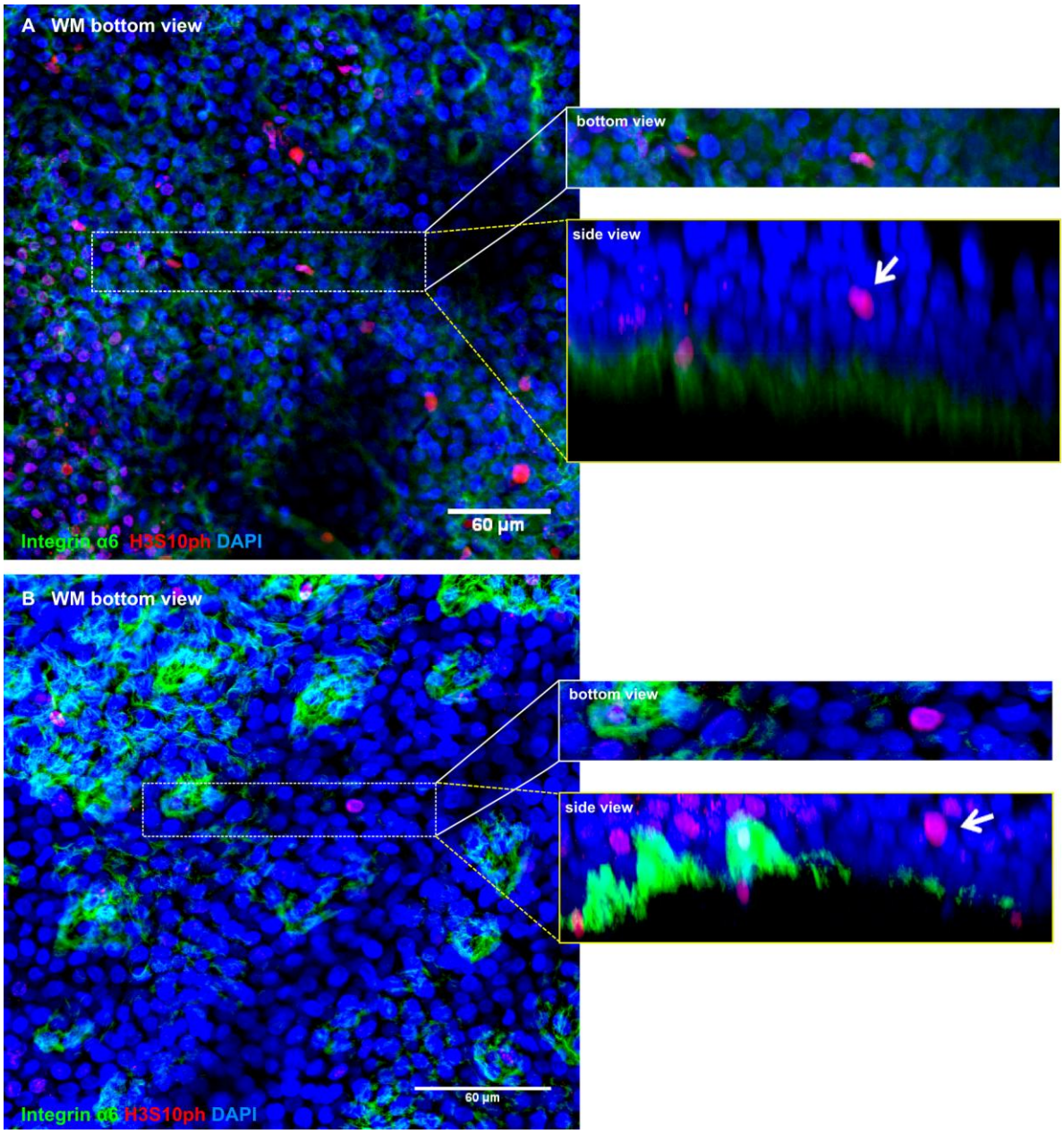

Figure 3.6 Suprabasal mitosis in skin wholemounts. In 3D reconstructions of human skin wholemounts, suprabasal mitotic cells were identified with anti-H3S10ph (red). The BM is identified by Integrin α6 (green). Suprabasally dividing cells were identified frequently in skin of two different donors (white arrows show two examples). A: donor age 76 years, B: donor age 39 years.

Here, instead of K10 as a differentiation marker, Integrin α6 was co-stained with H3S10ph to identify the BM in the z-stack. The 3D reconstruction of the z-stack images revealed that indeed suprabasal mitosis occurs at low but detectable frequencies in healthy skin of two different donors of different age.

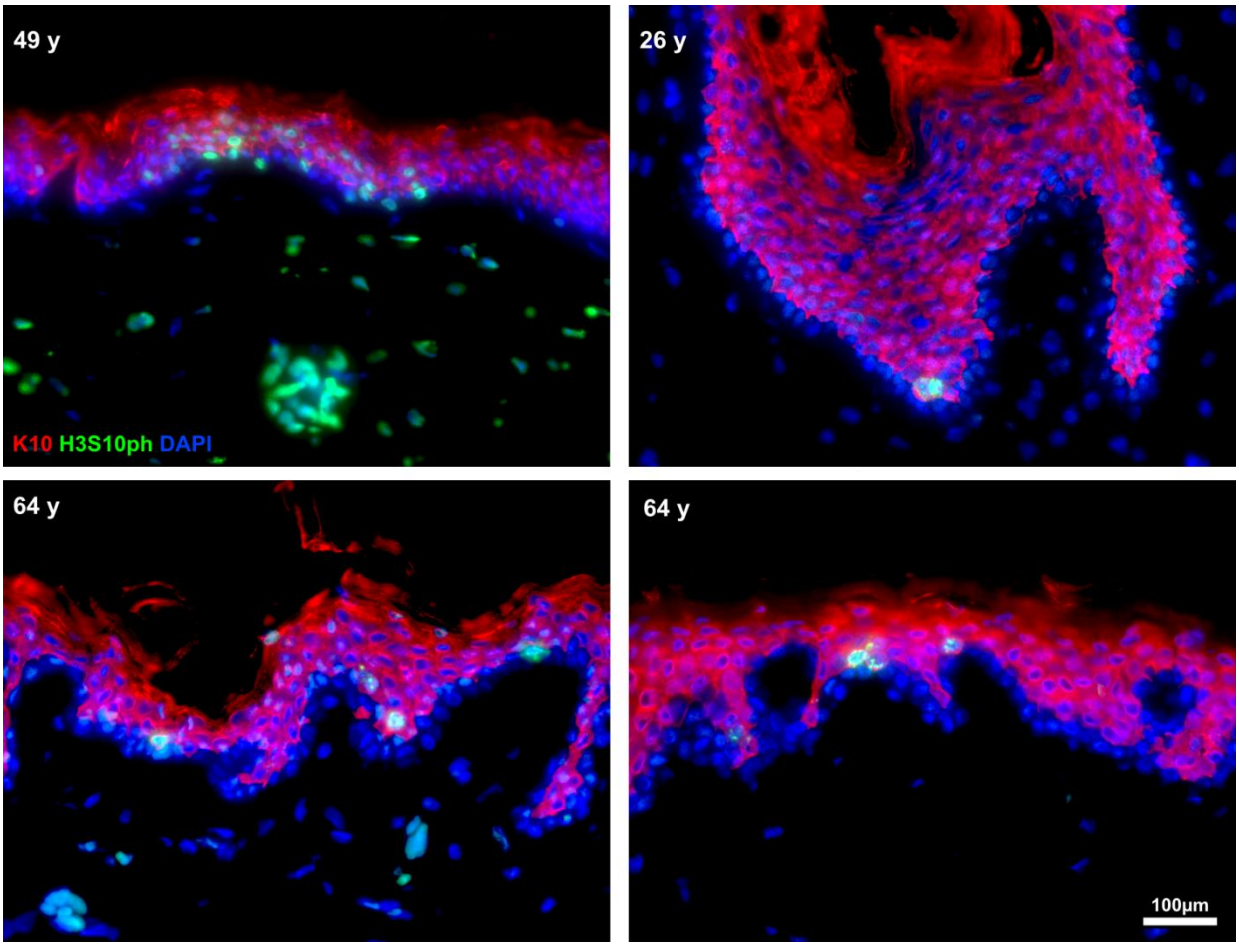

Figure 3.7 Suprabasal mitosis in healthy skin. In cryosections of healthy human skin of three different donors of different age, suprabasal mitotic cells could be identified by staining for H3S10ph (green). Co-staining with Keratin 10 (red) showed that these cells are mostly Keratin-positive, early differentiating cells.

Also in human skin, these suprabasal cells were positive for both the mitotic marker H3S10ph as well as for K10.

Suprabasal mitotic cells appeared to be in an early state of differentiation as indicated by K10 expression. It would be of interest to know whether they might still be in contact with the basement membrane. FdmSE sections were stained with Laminin 5, a component of the BM and Keratin 19, which was proposed as a stem cell marker for epidermal keratinocytes (Michel et al., 1996). Rare events of suprabasal keratinocytes that maintained a connection to the basement membrane were identified (Figure 3.8).

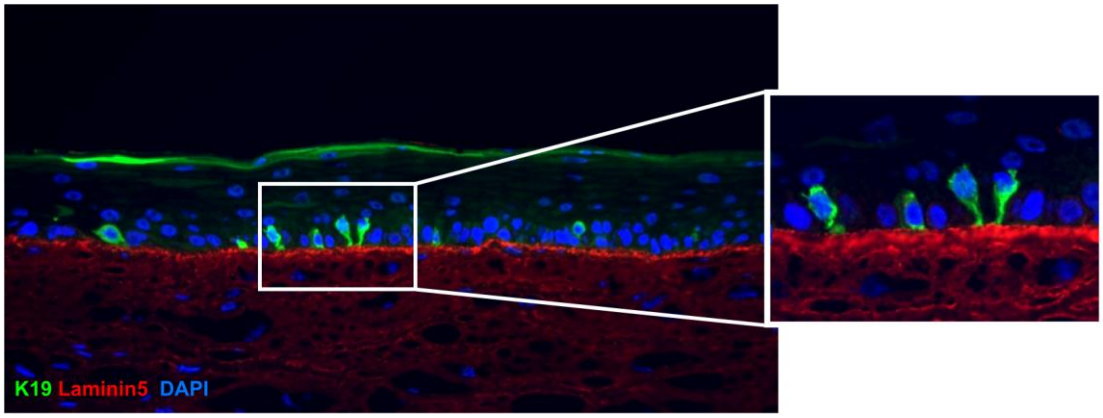

Figure 3.8 Keratin 19 in human skin equivalents. 13 days old fdmSE were stained for Keratin 19 and Laminin 5, a BM component. In rare cases, a cytoplasmic connection of suprabasal cells to the basement membrane was observed in the fdmSE. Images kindly provided by Dr. Hans-Jürgen Stark.

Keratin 19 has long been discussed as a potential skin stem cell marker (Michel et al., 1996). However, definite proof of a stem cell character of K19 expressing cells is still missing. Here we see that in rare cases, suprabasal keratinocytes retain K19 and a cytoplasmic connection with the BM. The rare occurrence of this phenomenon might indicate a previously unknown transitory state of keratinocytes between a basal, proliferative and a suprabasal, post-mitotic character.

Taken together, we found that the occurrence of mitotic types in the human fdmSE was more diverse than previously assumed. In addition to the classical symmetric division in parallel to the BM and a large proportion of mitoses at oblique angles, we frequently find perpendicular basal divisions as well as suprabasal cell division of early differentiating keratinocytes. The suprabasal, early differentiating mitotic cells are not an artefact of our fdmSE model but recapitulate normal human skin homeostasis.

3.3 Potential markers of asymmetric cell division

In addition to assessing the types of mitoses occurring in human skin, this project aimed at better understanding the factors influencing cell fate in the human epidermis. Previous research in different model organisms revealed that a complex interplay of intra- and extracellular molecules of the PAR complex, including PAR3/PAR6/aPKC, LGN, NuMA and Inscuteable, is necessary for proper spindle alignment (reviewed for example in Knoblich, 2008; Panousopoulou and Green, 2014; Williams and Fuchs, 2013). Genetic studies in mice identified the key players NuMA and LGN involved in orienting the mitotic spindle in epidermal keratinocytes and thereby maintaining the balance between self-renewal and differentiation (Poulson and Lechler, 2010). However, as mentioned before, mouse and human skin differ in many respects and therefore caution is needed when trying to transfer these

markers identified in mouse to the human context. In addition, factors involved in asymmetric cell fate known to date are mostly extracellular molecules emanating from the niche. These molecules predominantly accumulate at the apical cell cortex and act as facilitators for apical-basal spindle orientation. This subsequently leads to division perpendicular to the basement membrane. On the other hand, factors that play a role in asymmetric division in parallel to the basement are largely elusive. So far, cell intrinsic cues leading to differential cell fate of the two daughter cells of parallel asymmetric division are lacking.

Some of the factors identified or suggested so far will be introduced in the following chapters and were investigated here regarding their occurrence in the human skin equivalent. In all cases, the markers were stained with specific antibodies in at least three independent experiments. To investigate the occurrence of the marker in question in undifferentiated and early differentiating keratinocytes, 2D keratinocytes cultures maintained in DermaLife medium were used. This serum-free, low-Calcium medium is routinely used to expand keratinocytes without inducing differentiation. These cultures are more likely to expand asymmetrically than cultures maintained in FADcomplete, a calcium-rich medium which promotes keratinocyte differentiation. In addition, sections of fdmSE of week on to three were stained, assuming that at these stages asymmetric division would be most prominent.

3.3.1 LRP6 (low density lipoprotein receptor-related protein 6)

There are some clues about cell extrinsic factors emanating from the ECM and surrounding cells that could influence division direction. For example, in mouse embryonic stem cells it could be shown that a localized Wnt3a signal presented to only one side of the cell orients cell division accordingly (Habib et al., 2013). The phosphorylated Wnt receptor LRP6 was distributed unequally to the daughter cells. LRP6 is essential in transmitting Wnt signalling to the cell interior. It could be shown that LRP6 phosphorylation peaks at G2/M and plays a major role in cell cycle progression and proliferation (Davidson et al., 2009). LRP6 and Frizzled receptor are also required for kinetochore attachment to the mitotic spindle via GSK3, β-catenin, Axin2 (Huang et al., 2007; Kikuchi et al., 2010; Niehrs and Acebron, 2012) and other Wnt pathway components are involved in providing microtubule stability and chromosome segregation (Fodde et al., 2001; Hadjihannas et al., 2006). Still, a direct regulatory role of Wnt could not be demonstrated so far.

To determine the specific location of LRP6 in keratinocytes and to investigate whether asymmetric LRP6 distribution plays a role in KH division, 2D cultures and sections of the fdmSE were stained with LRP6 antibodies. The antibodies were specific for either the total fraction of LRP6 or for LRP6 phosphorylated at either Serine 1490 (LRP6Sp1490) or at Threonine 1479 (LRP6Tp1479) (Davidson et al., 2005). Priming phosphorylation of LRP6 at S1490 followed by the activating phosphorylation at T1479 is required for signalling and therefore indicative of active Wnt pathway.

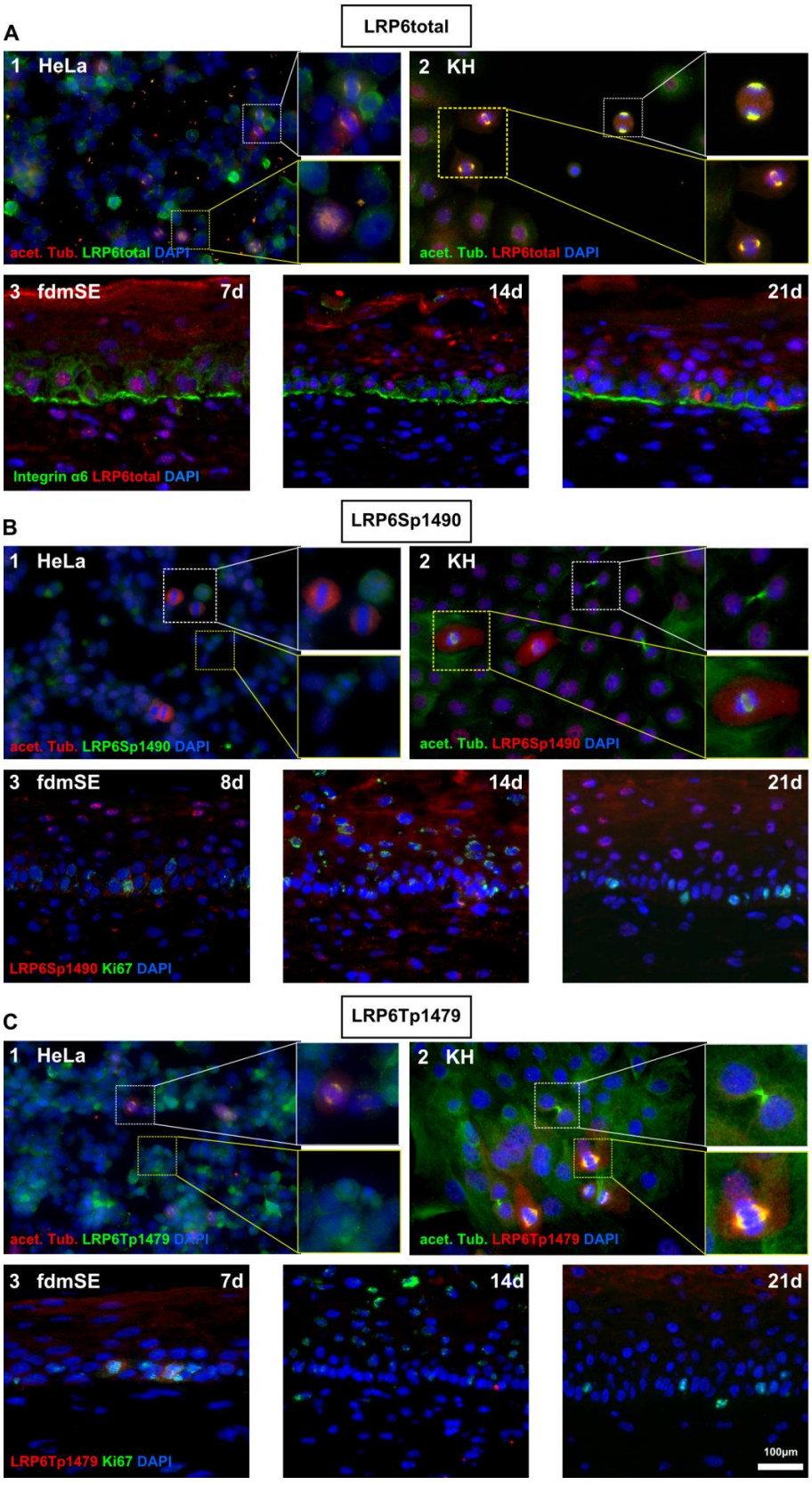

Figure 3.9 LRP6 in KH and fdmSE. The total fraction of LRP6 (A), LRP6 phosphorylated at Serine 1490 (LRP6Sp1490) (B) and at Threonine 1479 (LRP6Tp1479) (C) was co-stained with acetylated Tubulin (acet. Tub.) or the proliferation marker Ki67. HeLa 2D cultures were used as positive control. In the 2D cultures, the different LRP forms were detected at the mitotic spindles and in the cytoplasm (A2, B2, C2). In cryosections of the fdmSE, LRP6 was found in the nuclei of single cells in the basal cell layer (A3, B3, C3).

Signal for the total fraction of LRP6 was detected diffusely in and around some cell nuclei in both dividing and non-dividing HeLa cells and keratinocyte 2D cultures (figure 3.9 A1 and 2). In keratinocytes, LRP6 seemed to accumulate at the mitotic spindle whereas in HeLa this was only the case in some divisions. In the sections of fdmSE of weeks 1 to 3 (C3), LRP6total was found diffusely distributed in some cell nuclei as well as in the intercellular space of the stratum corneum.

As for the phosphorylated receptor molecules, both phosphorylation sites were detected in HeLa and KH 2D cultures (B1 and 2, C1 and 2). These were distributed around the nuclei and co-localised at the mitotic spindles. Similarly, both antibodies stained positive at early time points of the fdmSE sections (B3 and C3). The phosphorylated LRP6 was confined to single cells in the basal cell layer, possibly indicative of G2 / early M phase of these cells. However, asymmetric distribution of LRP6 total or of the phosphorylated molecule was not observed. In plantar mouse skin, Wnt/β-catenin signalling is required for stem cell self-renewal (Lim et al., 2013). In other tissues, localised Wnt signalling on one side of the cell was demonstrated and presenting Wnt3a to only one side of the cell was followed by asymmetric LRP6 partitioning to the cell surface (Habib et al., 2013). However, a localised Wnt signal in epidermis was not observed so far and could also not be observed in this study. Thus, our data suggest that Wnt signalling through LRP6 may not play a role in asymmetric cell fate of human epidermal keratinocytes.

3.3.2 ParD6 (par-6 family cell polarity regulator)

As a member of the cortical polarity complex (PAR), Par6 (or ParD6a) confers polarity to cells (Mapelli and Gonzalez, 2012).

It was shown that the polarity complex containing Par6 / Par3 / PKCzeta or Par6 / Par3 / atypical protein kinase C (aPKC), respectively, plays a role in epithelial cell polarity (Jan and Jan, 2001; Kemphues, 2000; Liu et al., 2004; Ohno, 2001). In *Drosophila* sensory organ precursors, asymmetric cell fate depends on apical localisation of the PAR complex including Par6. As one of the major components, this complex contains Par6 and thus this protein might be a suitable indicator of basal cell polarity and asymmetry in dividing keratinocyte stem cells.

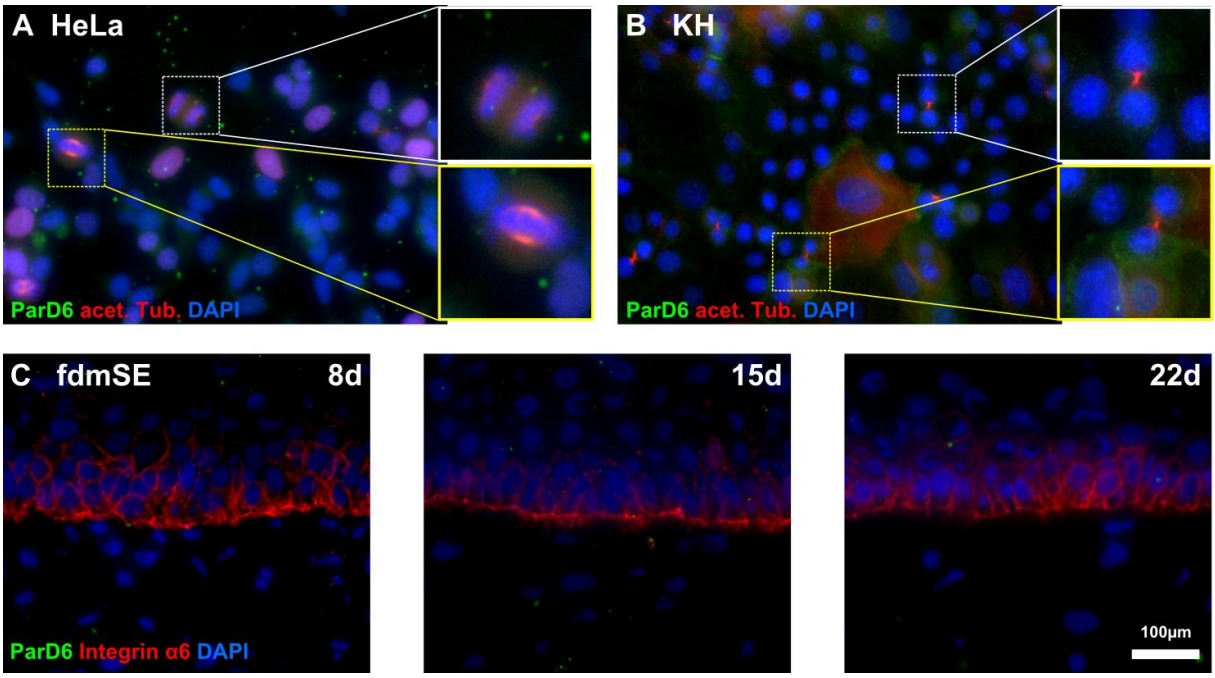

Figure 3.10 Par6 in KH and fdmSE. ParD6a (or Par6), a member of the polarity complex, was stained in KH (B) and fdmSE cryosections of up to three weeks culture age. HeLa cells were used as positive control. The 2D KH and HeLa cultures were co-stained with acetylated Tubulin (acet. Tub., green) or Integrin α6 (green). Weak and diffuse Par6 signal was detected in HeLa (A) and KH (B) but no Par6 was detected in fdmSE sections (C).

In HeLa and keratinocyte 2D cultures, a weak and diffuse signal of Par6 was detected in the cytoplasm (Figure 3.10 A and B). In fdmSE sections, Par6 could not be detected (Figure 3.10 C). According to The Human Protein Atlas (http://www.proteinatlas.org/ENSG00000102981-PARD6A/tissue/skin), expression of Par6 in skin is medium to high. Unfortunately, this could not be confirmed with our study. In epidermis, Par6 was found basally, but also at cell junctions in the granular layer where it plays a role in barrier formation (Helfrich et al., 2006). It seems that the Par proteins have several overlapping but also independent functions in skin and take part in different complex cellular processes (Thiery and Huang, 2005; Wang et al., 2013b). Par6 is required to maintain apicobasal cell polarity in the developing *Xenopus* epidermis (Wang et al., 2013b). However, a clear indication of Par6 as an asymmetry marker or regulator in human keratinocyte division was not apparent. We therefore decided to not further investigate Par6 in human epidermis.

3.3.3 NuMA (Nuclear mitotic apparatus protein 1) and Inscuteable

As another member of the spindle orientation regulatory complex, NuMA is crucial for proper spindle alignment (Bowman et al., 2006; Du et al., 2001; Izumi et al., 2006; Siller et al., 2006; Srinivasan et al., 2003). During mitosis in the *Drosophila* neuroblast, LGN recruits NuMA to the cell cortex (Du and Macara, 2004). The adaptor protein Inscuteable (Insc) recruits NuMA / LGN / Gαi to the apical cell cortex (Mapelli and Gonzalez, 2012). NuMA and Insc bind to LGN exclusively and competitively

(Culurgioni et al., 2011; Zhu et al., 2011). In mouse skin, NuMA co-localised both with mammalian Inscuteable (mInsc) (Poulson and Lechler, 2010) as well as with LGN (Williams et al., 2011) during asymmetrical (perpendicular) basal cell division. Short-term overexpression of mInsc in mouse epidermis caused misalignment of mitotic spindles, an effect that was reversed during long-term overexpression of Insc. This shows that a delicate interplay between NuMA and Insc during mitosis is necessary for proper spindle orientation and asymmetric distribution of one or both proteins may be indicative of differential cell fate of the daughter cells.

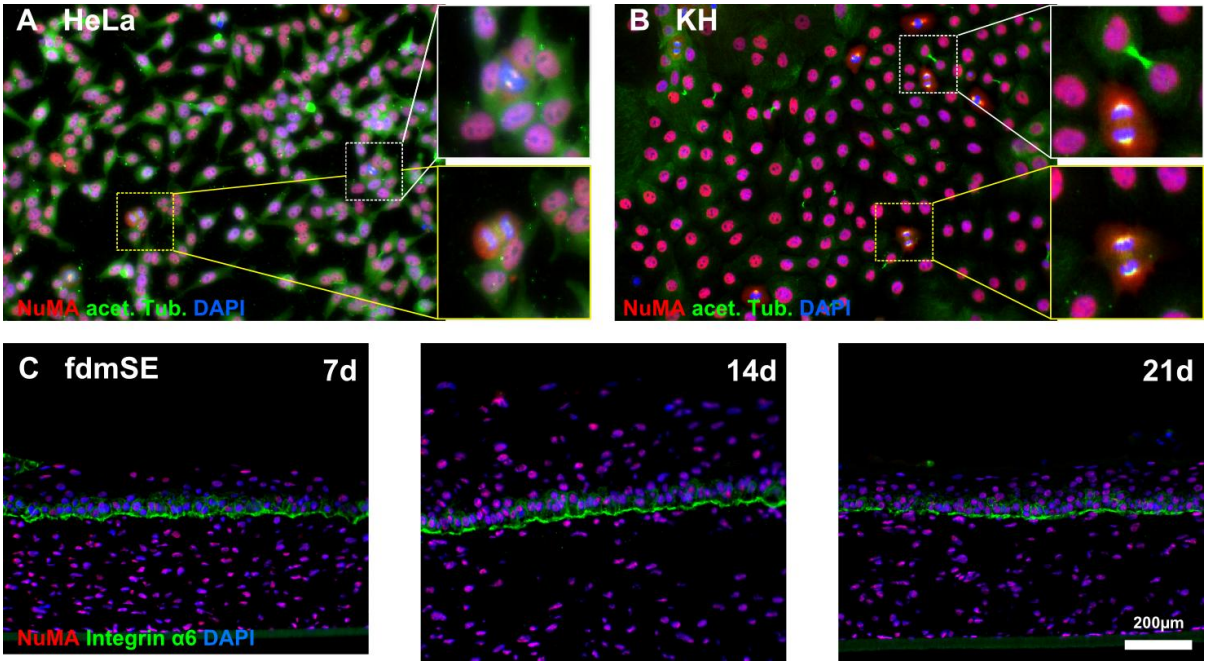

Figure 3.11 NuMA in KH and fdmSE. The Nuclear mitotic apparatus protein 1 (NuMA, red) was detected in nuclei and at mitotic spindles in HeLa (A) and KH (B). Cryosections of the fdmSE of time points up to three weeks were co-stained with Integrin α6 (C). NuMA was expressed strongly in interphase nuclei of all cultures and co-localised to the mitotic spindle in HeLa (A) and KH (B).

In the 2D cultures of HeLa and keratinocytes, a strong NuMA-signal was detected in almost all nuclei (Figure 3.11 A and B). During telophase, NuMA was shown to localise to the nucleus where it remains until the next mitotic cycle (Merdes and Cleveland, 1998). We found that in both HeLa cells and keratinocytes, NuMA was localised at mitotic spindles and in the cytoplasm around the DNA of both daughter cells during anaphase. During telophase and throughout interphase, NuMA resided in the nucleus. Neither in HeLa nor in keratinocyte cultures did we observe asymmetric NuMA localisation at only one spindle pole or in only one emerging daughter cell. In the fdmSE, NuMA was difficult to detect but could be discerned in most of the nuclei of all cell layers (Figure 3.11 C). Apical or otherwise asymmetric localisation of NuMA was not found in the sections of fdmSE up to week 3 of culture.

For stainings of Inscuteable, *Drosophila* Schneider (S2) cells were used as controls, since Inscuteable is an established marker of asymmetry in the *Drosophila* neuroblast (Kraut et al., 1996; Schober et al., 1999). Human homologues of Inscuteable (mammalian Inscuteable, mInsc) were discovered recently (Izaki et al., 2006) and asymmetric polarisation of mInsc at the apical spindle pole seems to play a role in embryonic distal lung epithelium (El-Hashash and Warburton, 2011). Thus, we wanted to determine whether Insc is asymmetrically distributed in human epidermal keratinocytes and has an influence on cell fate.

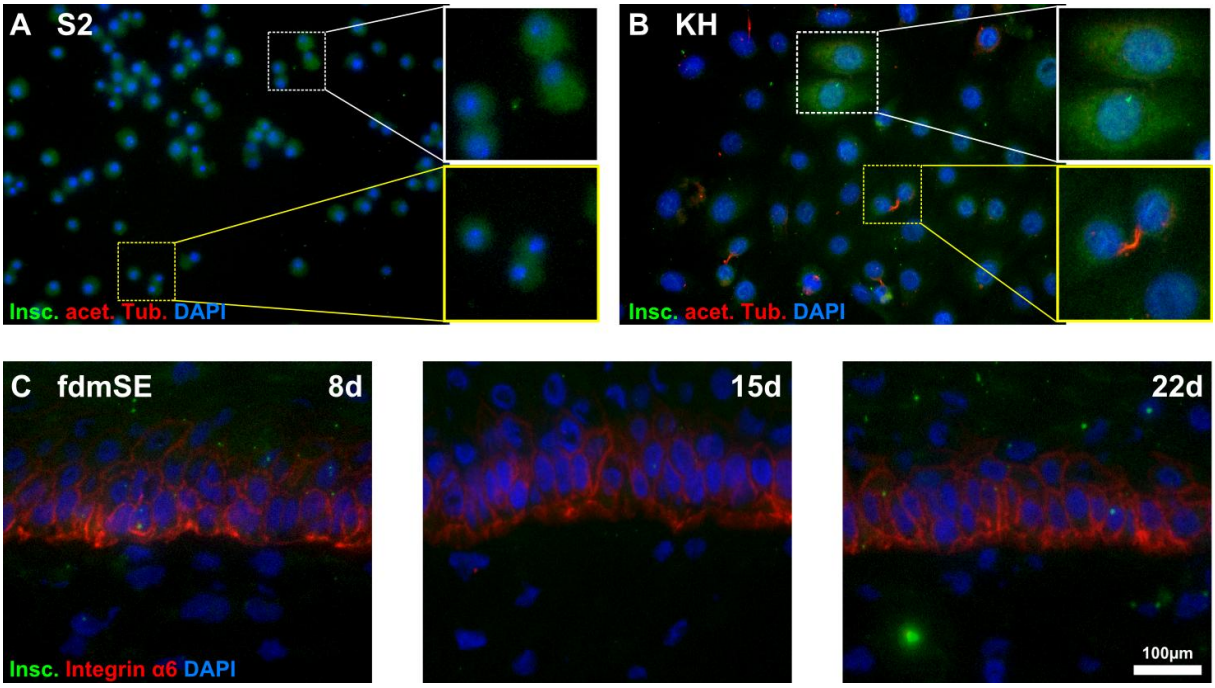

Figure 3.12 Inscuteable in KH and fdmSE. The NuMA-competitor Inscuteable (Insc., green) was stained in KH (B) and, as positive control, in *Drosophila* Schneider cells (S2, A). In addition, cryosections of the fdmSE were stained for Inscuteable. In S2 cells, the protein was detected in the cytoplasm of most cells (A), while in KH, expression was weaker and not detectable in all cells (B). In the fdmSE sections of 8, 15 and 22 days, no Inscuteable could be detected (C).

While the anti-Inscuteable antibody was raised against the human homologue, according to the data sheet it should also detect Insc of other species. Indeed, Inscuteable was found abundantly in the cytoplasm of S2 cells (Figure 3.12 A). In a previous study, mInsc was exogenously overexpressed in mouse where it co-localised with the Par complex at mitotic spindle poles (Lechler and Fuchs, 2005) but expression of endogenous Insc protein in human skin has not been confirmed before. Here, we find that in keratinocytes the signal was weaker than in the S2 cells and was more pronounced in larger cells (Figure 3.12 B). Although Inscuteable co-localisation with the Par complex at mitotic spindle poles is reported for all investigated tissues, it could not be observed here. In cryosections of fdmSE, no specific Inscuteable signal above background level was detectable at all.

Even though in mouse back skin NuMA and Inscuteable were found at the apical spindle cortex in perpendicular divisions (Lechler and Fuchs, 2005), a similar pattern could not be discerned here. This might be due to the fact that in the cryosections mitotic events can rarely be observed. In addition, mInsc was exogenously overexpressed by Lechler and Fuchs to study its function while the endogenous expression and function in epidermis remains unclear. Thus, it presently remains open whether the level of mInsc is too low to be detected or whether mInsc is not endogenously expressed in our human skin equivalent.

3.3.4 Ninein

Ninein and the Ninein-like protein (Nlp) are centrosomal proteins involved in microtubule organisation in interphase cells (Casenghi et al., 2005). Ninein accumulates at the appendages of the mother centriole and at the slow-growing microtubule minus ends which anchor the microtubule to the centrosome (Mogensen et al., 2000). This mother centriole serves as a template for the replication of the daughter centriole during mitosis and also nucleates the primary cilium. Inheritance of the mother centriole was proposed to be characteristic for the retainment of stem cell character in the daughter cell (Pelletier and Yamashita, 2012; Wang et al., 2009; Yamashita et al., 2007). The presence of Ninein during early mitosis might therefore be indicative of asymmetric cell fate of the two daughter cells.

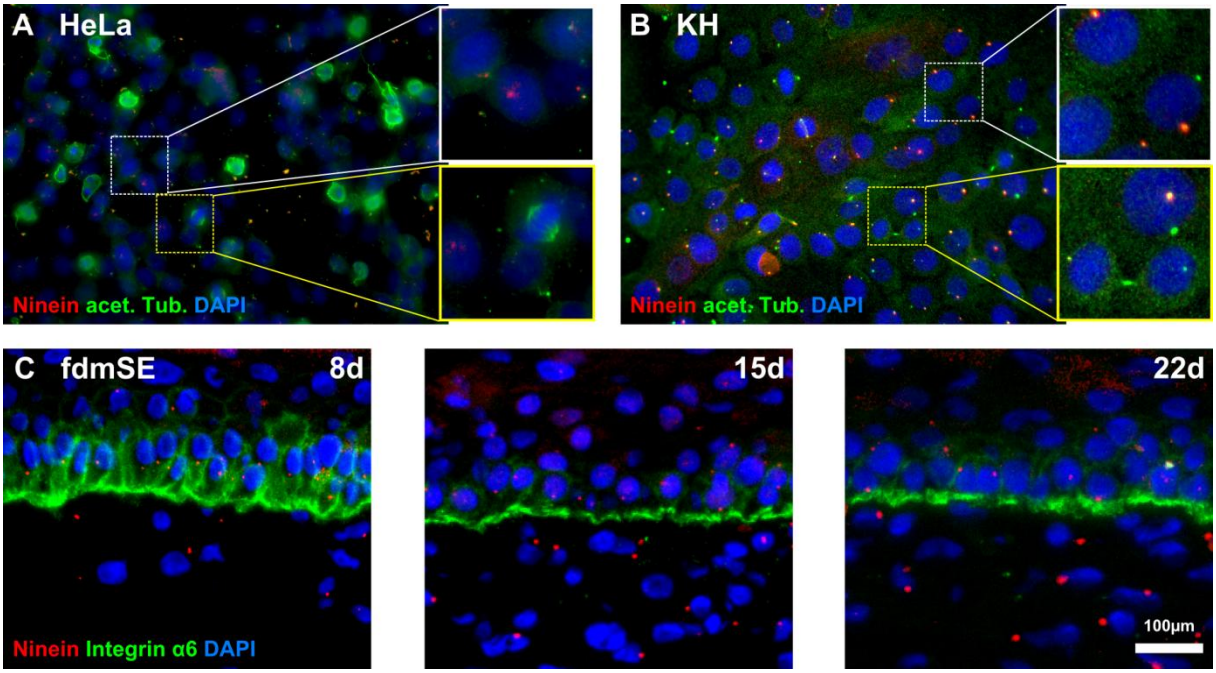

Figure 3.13 Ninein in KH and fdmSE. The centriolar protein Ninein (red) was co-stained with the spindle protein acetylated Tubulin (green) in KH and HeLa control cultures and with Integrin α6 in tissue sections of fdmSE. Centrioles could be detected in HeLa (A), KH (B) and fdmSE sections of week one to three (C).

The anti-Ninein antibody detected centrioles both in HeLa and in keratinocyte 2D cultures (Figure 3.13 A and B). However, in dividing cells, we always found two or no centrioles and no asymmetric signal of Ninein in only one daughter cell. During mitosis, it was shown that Ninein declines from the centrosome and reappears at the end of mitosis (Chen et al., 2003). This observation correlates to our findings (see anaphase HeLa cell in figure 3.13 A and telophase keratinocyte in figure 3.13 B). In the cryosections of fdmSE up to week 3, the centriole location in basal cells did not appear to follow a specific pattern (Figure 3.13 C). In some cases, the mother centriole was located at the basal side of basal keratinocytes. However, more detailed analysis and co-staining with differentiation markers or label-retention markers would be required to draw conclusions about Ninein as a cell fate determinant in human keratinocytes.

3.3.5 Numb

The evolutionary conserved cell fate determinant Numb is a known inhibitor of the Notch1 pathway. Notch1 functions as a key driver of epidermal differentiation (Blanpain et al., 2006; Moriyama et al., 2008; Rangarajan et al., 2001; Watt et al., 2008). Numb influences cell fate by downregulating Notch1 through polarized receptor-mediated endocytosis and degradation of the Notch1 intracellular domain (NICD) (McGill and McGlade, 2003).

Numb plays a decisive role during mouse cortical neurogenesis where it is asymmetrically distributed (Zhong et al., 1996), and during division of the sensory organ precursor cell in *Drosophila* (Rhyu et al., 1994). An involvement in epidermal fate decisions has been proposed (Blanpain and Fuchs, 2009), however, a second study did not find a clear correlation between asymmetric Numb distribution and fate outcome in developing epidermis (Williams et al., 2011). Still, given the importance of Notch1 at the proliferation-to-differentiation switch in epidermal homeostasis and the major influence of Numb on Notch1 regulation, it is likely that Numb is involved in epidermal fate decisions.

In vertebrates, two Numb homologues are described: Numb and Numblike (Nbl). Both are highly conserved homologues of the *Drosophila* Numb protein. In mouse, they play redundant but critical roles in cortical development and the maintenance of neural progenitor cells (Petersen et al., 2002). However, the expression of Numb and Numblike differs. While Numb is a known asymmetry marker in neuronal development, asymmetric distribution of Numblike has not been observed so far (Zhong et al., 1997). Information about Numb and Numblike expression in skin is sparse. Numb was shown to be expressed in Melanocytes (Fukunaga-Kalabis et al., 2015) and mouse keratinocytes (Williams et al., 2011), but information about Numblike expression in human keratinocytes is lacking. Expression of both homologues in normal human epidermal keratinocytes was validated by PCR with primers designed specifically for Numb and its homologue Numblike. RNA was extracted from cell pellets and

transcribed into cDNA. For comparison of the expression level, HEK293 cells were used and brain and placenta lysates functioned as positive controls.

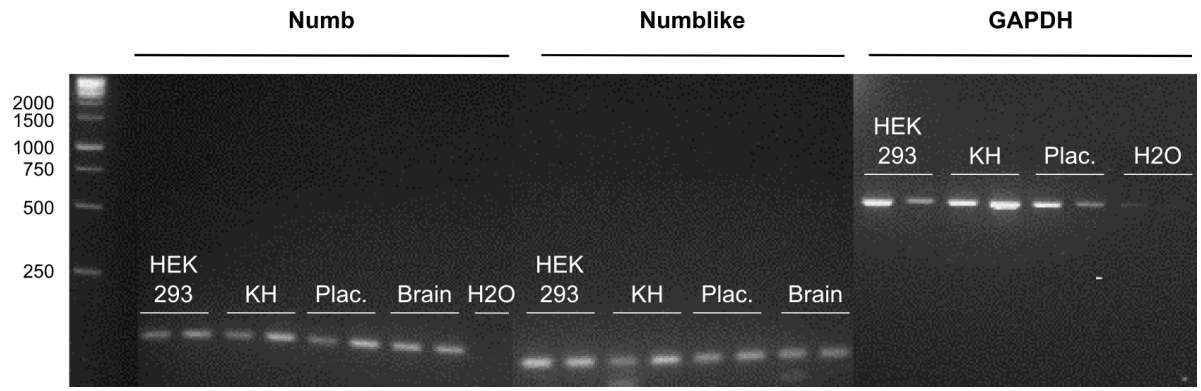

Figure 3.14 Expression of Numb and Numblike in human keratinocytes. Numb and its homologue Numblike were both expressed in normal human keratinocytes (KH). All samples were tested in duplicate. For comparison, HEK 293 cells were tested. Positive ctrls: Placenta (Plac.) and brain lysates.

Both homologues were expressed in HEK293, keratinocytes, placenta and brain lysates (Figure 3.14) in similar amounts. Still, this gene expression on mRNA level does not necessarily resemble the amount of protein transcribed and active in the tissue.

Six mammalian isoforms of Numb have been described so far, all produced from the same transcript by alternative splicing (Dho et al., 1999; Karaczyn et al., 2010; Verdi et al., 1996, 1999). The antibody used for Numb detection in this work is a courtesy of Salvatore Pece, Milan, Italy, and was produced against amino acids 537-551, a sequence common to all Numb isoforms but not the Numblike homologue (Colaluca et al., 2008). The antibody used in all subsequent stainings should therefore exclusively recognise Numb but not Numblike.

First, we assessed Numb distribution in 2D cultures of keratinocytes in DermaLife, the generally used keratinocyte medium. As control cells, we used HeLa and A431, a human epithelial carcinoma cell line. As further control to assess Numb in undifferentiated cells, we stained hiPSCs (human induced pluripotent stem cells, kindly provided by J. Utikal, DKFZ Heidelberg). As a comparison to undifferentiated keratinocytes maintained in DermaLife, we also looked at keratinocytes grown for several days in FADcomplete medium. In contrast to the low-Calcium (0.15 mM), serum-free DermaLife, FADcomplete contains 1.05 mM Calcium and 10 % serum and allows for keratinocyte differentiation. Thus, we can observe and compare keratinocyte cultures in different states of differentiation.

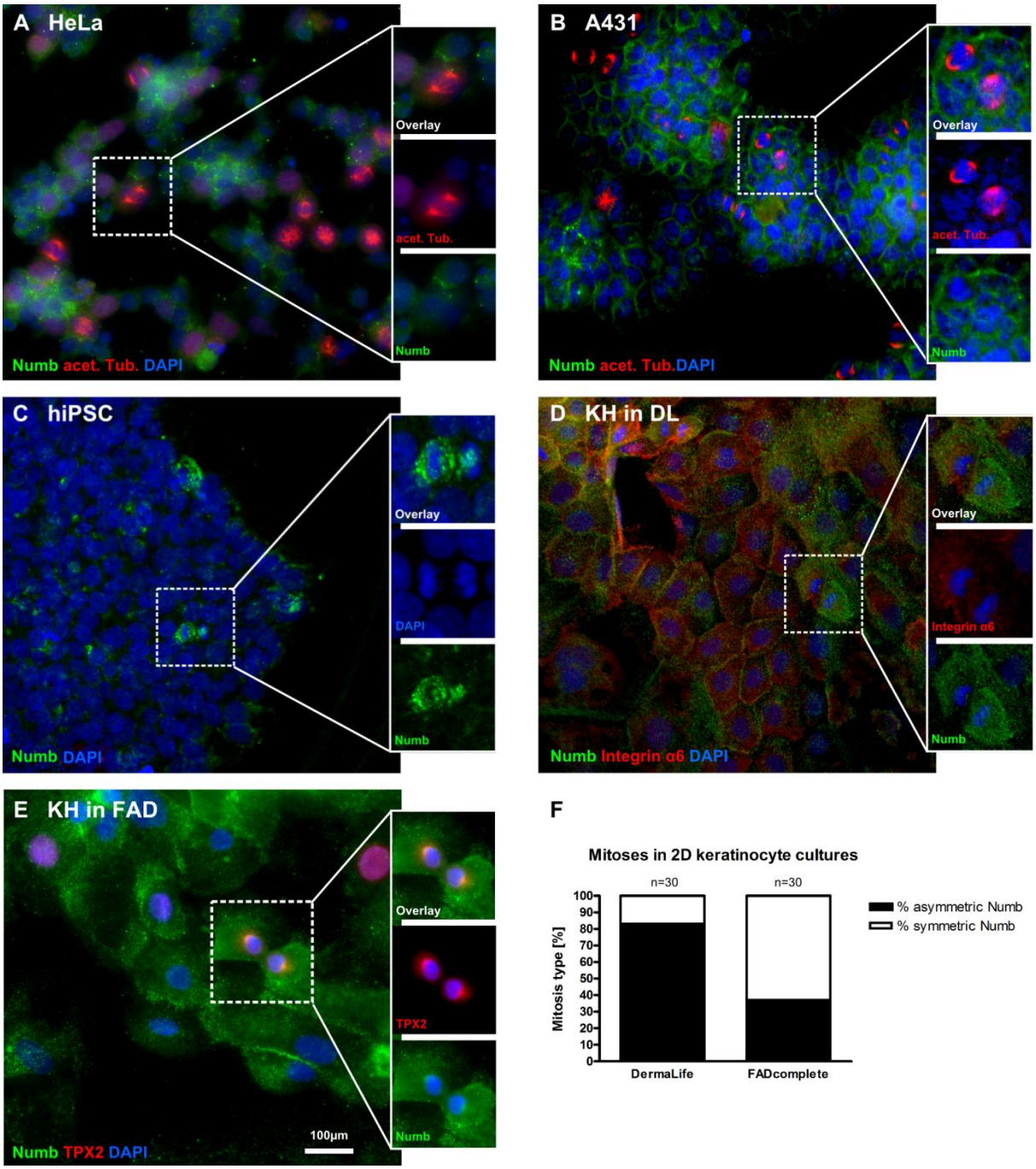

Figure 3.15 Numb in 2D cultures of keratinocytes, hiPSC, HeLa and A431. The cell fate determinant Numb was stained in KH either grown in DermaLife (DL) (D) to maintain an undifferentiated state or in FADcomplete to induce differentiation (E). As positive controls, HeLa (A), the human epithelial carcinoma cell line A431 (B) and undifferentiated human induced pluripotent stem cells (hiPSC) (C) were used. In the keratinocyte cultures, 30 dividing cells each were counted and examined regarding Numb distribution to the daughter cells (F). A larger proportion of KH in DL divided up Numb unequally to daughter cells than keratinocytes grown in FADcomplete (83 % *versus* 37 %).

Numb expression was detected in all samples. The protein was found in a characteristic dotted pattern throughout the cytoplasm which coincides with the staining pattern described for different tissues (Clayton et al., 2007; Schmit et al., 2012; Williams et al., 2011). Both keratinocyte cultures

expressed high levels of Numb protein (figure 3.16 D and E). Keratinocytes retained in an undifferentiated state in DermaLife medium frequently showed asymmetric distribution of Numb to daughter cells in mitosis (figure 3.16 D). In the reprogrammed hiPSC, Numb was expressed only in few cells (Figure 3.15 C). The protein was repeatedly found asymmetrically distributed to the daughter cells, where it accumulated around the nuclei of one of the nascent daughter cells. In HeLa and A431 cultures on the other hand, asymmetric Numb distribution was not observed. In HeLa cells, the protein seemed to be less abundant in some cells and highly abundant in others (figure 3.16 A). In A431 which was chosen as an additional epithelial control cell line, the protein was found rather at the cell borders instead of throughout the cytoplasm.

It seems that Numb shows two different patterns: either distributed throughout the cytoplasm and around the nucleus during mitosis as seen in HeLa, KH and hiPSC (figure 3.16 A, C, D, E); and at the cell membrane as seen strongly in A431 (figure 3.16 B) and less pronounced in HeLa and KH in DermaLife medium (figure 3.16 B and D).

Interestingly, only the undifferentiated cultures, i. e. keratinocytes grown in DermaLife medium and hiPSC, showed asymmetric distribution of Numb during mitosis (Figure 3.15 C and D). While Numb was abundantly present in the differentiated KH cultures grown in the high Calcium FAD medium (Figure 3.15 E), asymmetric Numb distribution to the daughter cells was much less frequent. In randomly counted mitotic events in both keratinocyte growth conditions, the ratio of asymmetric *versus* symmetric Numb distribution was determined. In the DermaLife cultures, the ratio of asymmetric to symmetric Numb distribution was 83 to 17 %, but only 37 to 63 % in the FAD cultures (Figure 3.15 E). This might hint toward a Calcium-dependent expression of Numb.

Next, we assessed Numb distribution in sections of the fdmSE, starting with early time points of 1 up to 10 weeks after keratinocyte seeding.

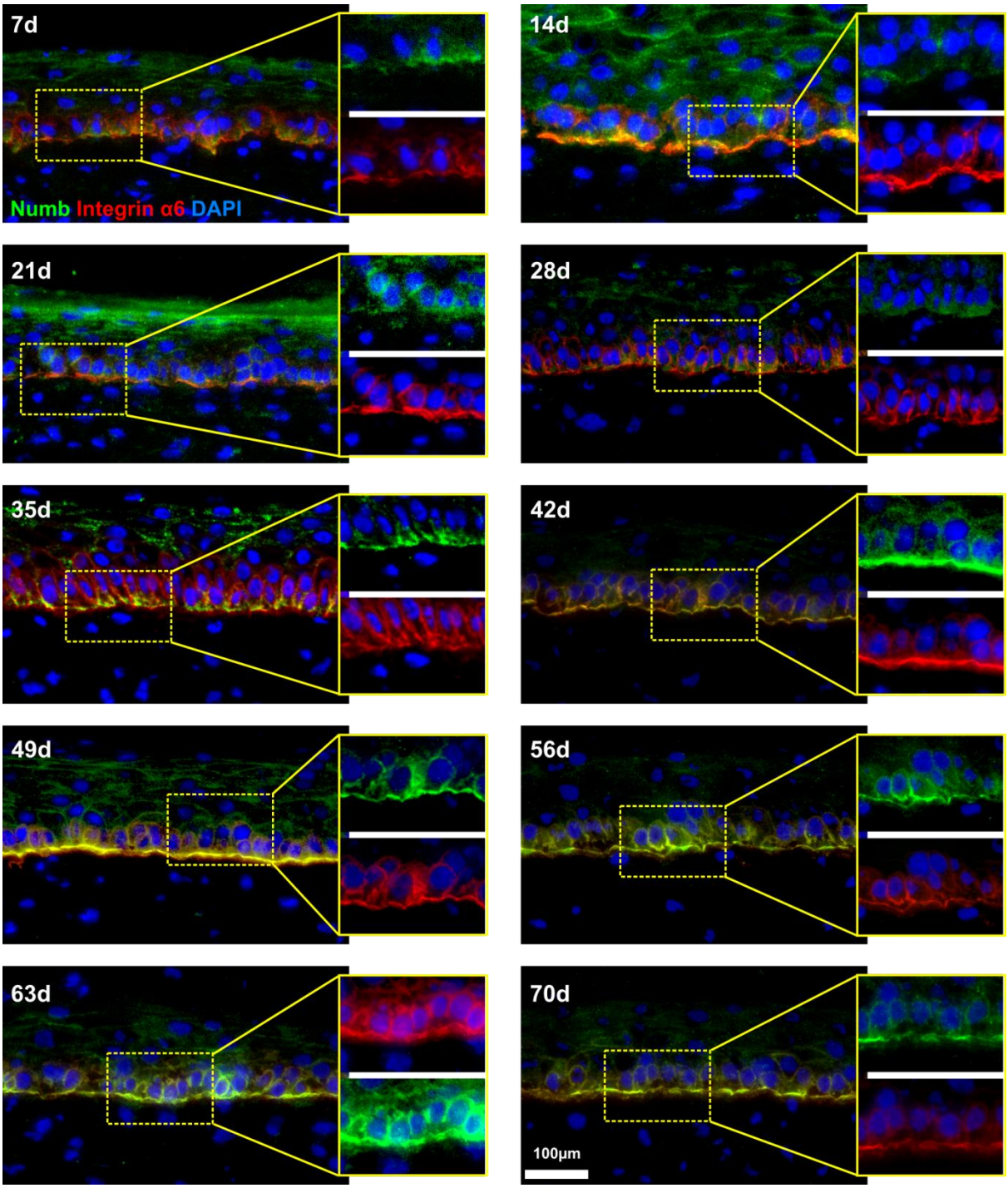

Figure 3.16 Numb and Integrin α6 in cryosections of the fdmSE. Sections of the fdmSE of culture age from 7 days to 70 days were stained with anti-Numb (green) and anti-Integrin α6 (red). Both proteins are mainly localised around the basal cell rim at the basement membrane in a similar pattern. Numb was also found at the cell membranes of suprabasal cells. The protein distribution was comparable at all time points.

Both Integrin α6 and Numb showed a distinctive and specific accumulation around the basal cell rim of basal cells, sometimes engulfing the cells and reaching up into the first suprabasal layer. However, while Integrin α6 was rather evenly distributed throughout the sections of all time points, Numb was detected more strongly in some regions than in others. Overall, the expression of Numb was

comparable at all time points spanning week one to ten. Furthermore, it seemed as if two distinct Numb locations exist in the skin equivalent: one in the basal cell layer, most prominently around the basal cell rim; and another one in the upper granular layers around the cell membrane. Both signals seem to be specific and coincide with the cellular staining patterns observed in the 2D cultures of keratinocytes in DermaLife and A431 (figure 3.16 B and D).

In our laboratory, we repeatedly observed that proliferating epidermal cells are found in clusters instead of individual cells interspersed throughout the culture, a finding also reported by another study (Ghazizadeh and Taichman, 2005). To find out if the clustered occurrence of Numb in the basal cell layer coincides with proliferation, we co-stained Numb with the proliferation marker Ki67 in fdmSE sections.

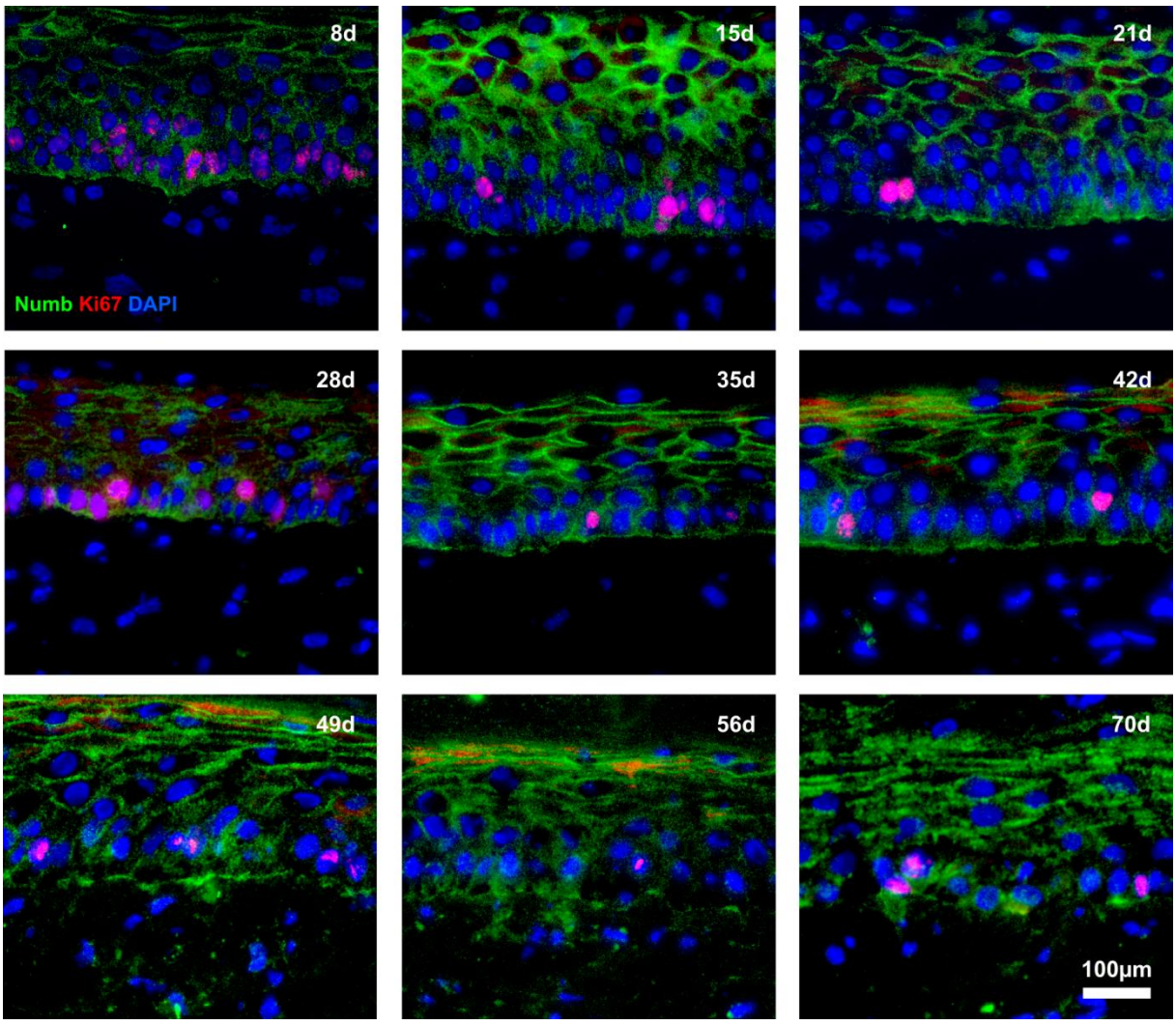

Figure 3.17 Numb and Ki67 in cryosections of the fdmSE. In cryosections of the skin equivalent, Ki67 (red) was frequently found in basal cells. The frequency of proliferating cells decreased with culture age, while Numb (green) was found at comparable levels at all time points. The protein was expressed at the basal rim of basal cells and at the cell membrane of suprabasal cells.

As expected, overall proliferation as seen by Ki67 staining decreased with culture age (Figure 3.17). While many cells of the basal layer and the first suprabasal layer were Ki67-positive in the first week, only few positive cells were found at late time points. Numb, again, was found irregularly accumulating in some regions. Intriguingly, Numb expression in the basal layer was the strongest at intermediate time points (week 3 to 9) and less pronounced at very early and late culture time points (weeks 1 – 2 and 8 – 10). A correlation of Numb expression and proliferation did not become apparent. Like in the sections co-stained with Integrin α6 (Figure 3.16), we again find Numb in two different epidermal compartments: in the basal cell layer and at the cell membranes of granular and cornified cells.

In order to validate Numb expression in human skin, we prepared sections of healthy skin samples from donors of different sex and ages.

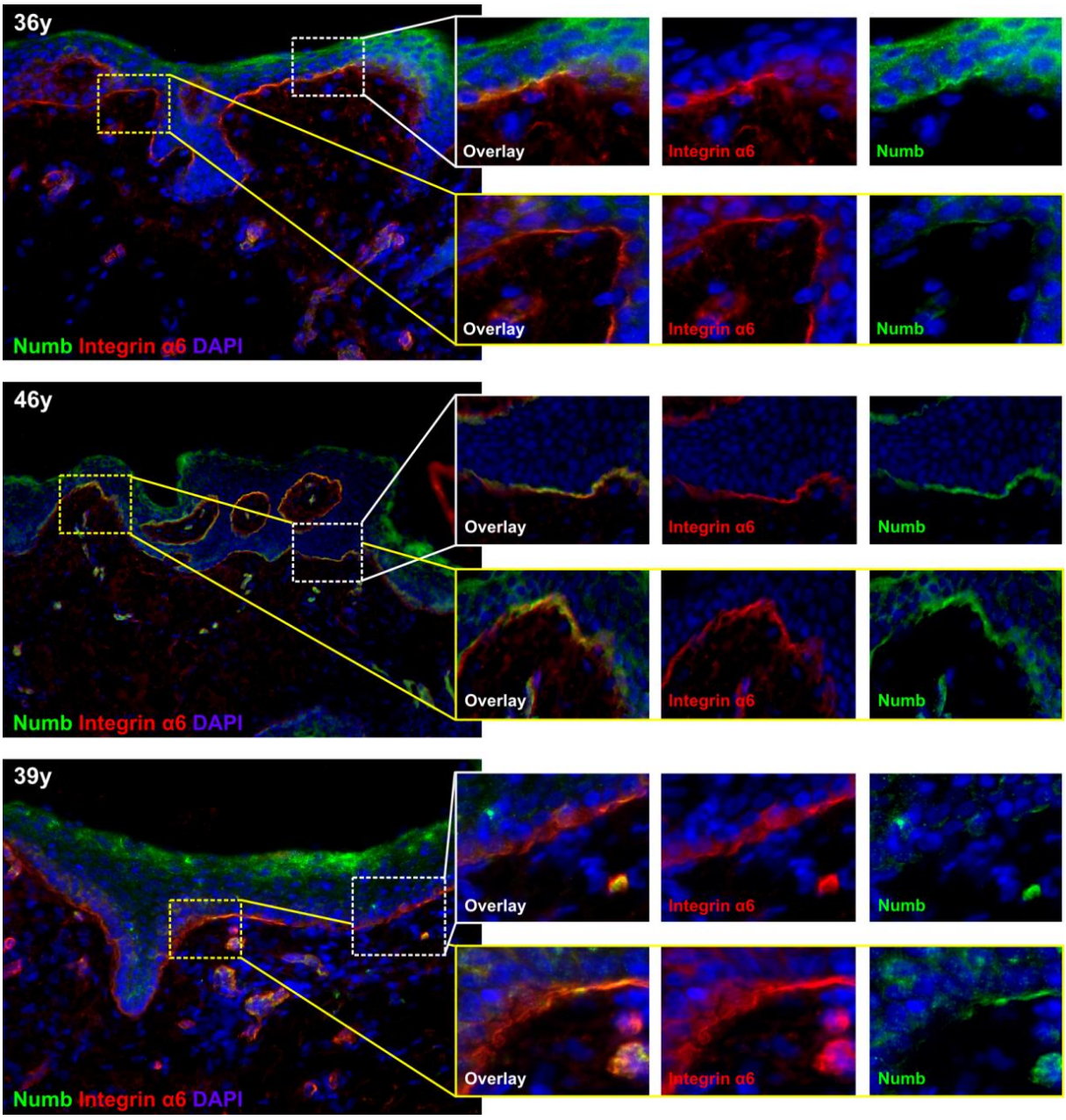

Figure 3.18 Numb and Integrin α6 in cryosections of healthy skin. In sections prepared from the skin of three different donors, Numb (green) was identified in a similar pattern as in the fdmSE. Independent of the donor age (indicated in the upper left corner of each panel), Numb was found irregularly spread throughout the basal sides of basal cells and in the suprabasal layers.

Indeed, the pattern of Numb signal in the skin samples was comparable to the one found in the fdmSE. Numb was found on the basal side of basal cells and distributed unevenly throughout the skin. Some regions seemed to contain more Numb than others, however, a correlation with either rete ridges or appendages was not found. The hemidesmosomal component Integrin α6, on the other hand, was regularly distributed along the basement membrane.

Since Numb, besides its many other functions, is a known Notch inhibitor and Notch plays a well-defined role in the keratinocyte switch to differentiation (Rangarajan et al., 2001), we were interested in the occurrence of Notch in the skin equivalents and its possible relationship to Numb. However, antibody detection of Notch1 in the fdmSE was challenging.

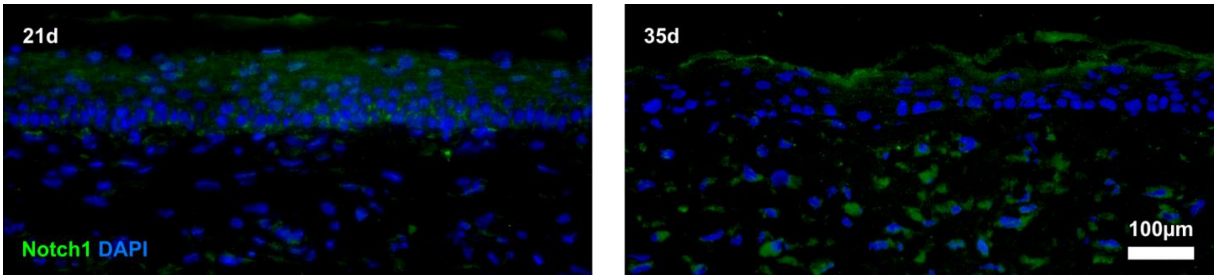

Figure 3.19 Notch1 in cryosections of the fdmSE. Immunofluorescence of Notch1 (green) in cryosections of the fdmSE did not show conclusive and specific signal.

Even with different anti-Notch1 antibodies, different fixation and staining protocols and in different experiments and at various time points, Notch1 staining was weak and not reproducible. Since the results of the stainings were inconclusive and inconsistent between experiments, we did not follow up on Notch1 expression in the fdmSE.

3.3.5.1 Knock down of Numb in human keratinocytes

The specific effect of a protein on a cellular process like differentiation can best be examined by eliminating the protein. The novel CRISPR/Cas9 method makes use of a simple and direct principle to cut the gene of interest and thereby disrupt protein transcription. The method is described in detail in the Materials and Methods section (Figure 2.1 and figure 2.2).

In collaboration with the Department of RNA Biology and Cancer, DKFZ, we designed five different guide RNAs. These are in the following labelled as #1, #2, #3, #4, #8. The guideRNA sequences were cloned into a plasmid containing the Cas9 sequence as well as a GFP reporter protein sequence.

To assess the functionality of each of the guides, HEK293 cells were transfected and harvested after 72 hours. A T7 test of the cell lysates proved the efficacy of the guides (Figure 3.20). In this test, the region around the cut site of the target gene is PCR-amplified and heteroduplexes are created which are recognised and cleaved by the T7 enzyme. The resulting cleavage products can be separated on an agarose gel. Cleavage products shorter than the amplified gene region indicate successful cleavage of the target gene by Cas9.

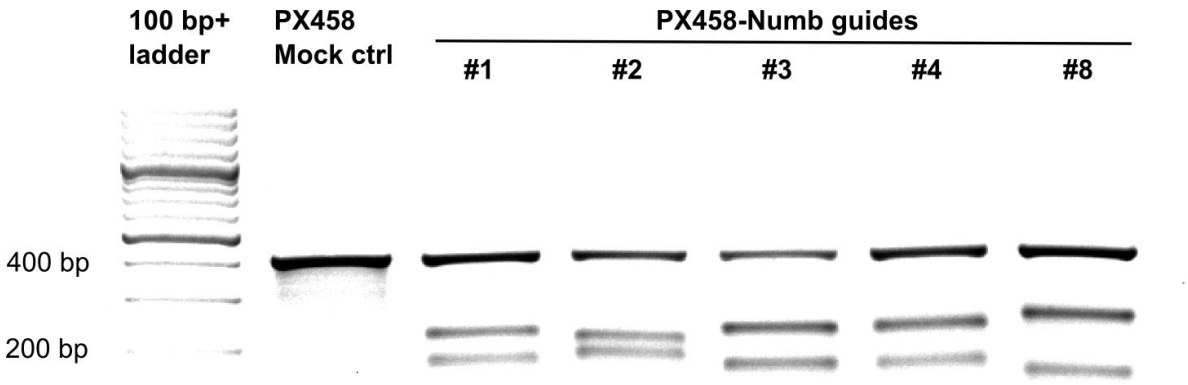

Figure 3.20 HEK293 cells transfected with CRISPR/Cas9 plasmids show Numb cleavage on DNA level. A T7 test in transfected HEK293 cells provides the proof-of-principle for the designed guide plasmids. The upper band at around 400 bp indicates the uncleaved PCR product. The double band at around 200 bp indicates cleavage of the PCR product by the T7 endonuclease and therefore proves successful gene cleavage by Cas9. All guide plasmids induced gene cleavage in HEK293 cells. PX458: CRISPR/Cas9 plasmid. Experiment performed in collaboration with A. Goyal (DKFZ).

We found that all designed CRISPR guide RNAs induced gene disruption in HEK293 cells and concluded that all of the guides could be used in keratinocyte knock out experiments.

The bands at 400 bp indicate the full length PCR-amplified Numb fragment (Figure 3.20). The two double bands at about 200 bp are the cleaved fragments indicating successful gene cleavage. Due to the fact that the gRNA sequences span different gene regions and induce DSB at different sites, the PCR fragment is cleaved at different sites for each of the guides. This results in cleavage products of different sizes.

An electroporation transfection protocol was established for normal human keratinocytes to introduce the CRISPR/Cas9 plasmids to the cells. The original Invitrogen NEON™ protocol (Kim et al., 2008) was optimised regarding pulse times and voltage (detailed description in Materials and Methods). The cells are subjected to a short electric pulse which will temporarily break down the plasma membrane and make it permeable to the plasmid DNA. The cells were then seeded in 6-well plates and left to express the DNA for 48 hours before sorting them in a fluorescent activated cell sorter (FACS). The transfection is transient, meaning the plasmid is not stably integrated. Therefore, the GFP-expression is also transient and only detectable for a few days. However, the gene disruption and subsequent protein knock out caused by the Cas9 endonuclease is passed on to the cell progeny.

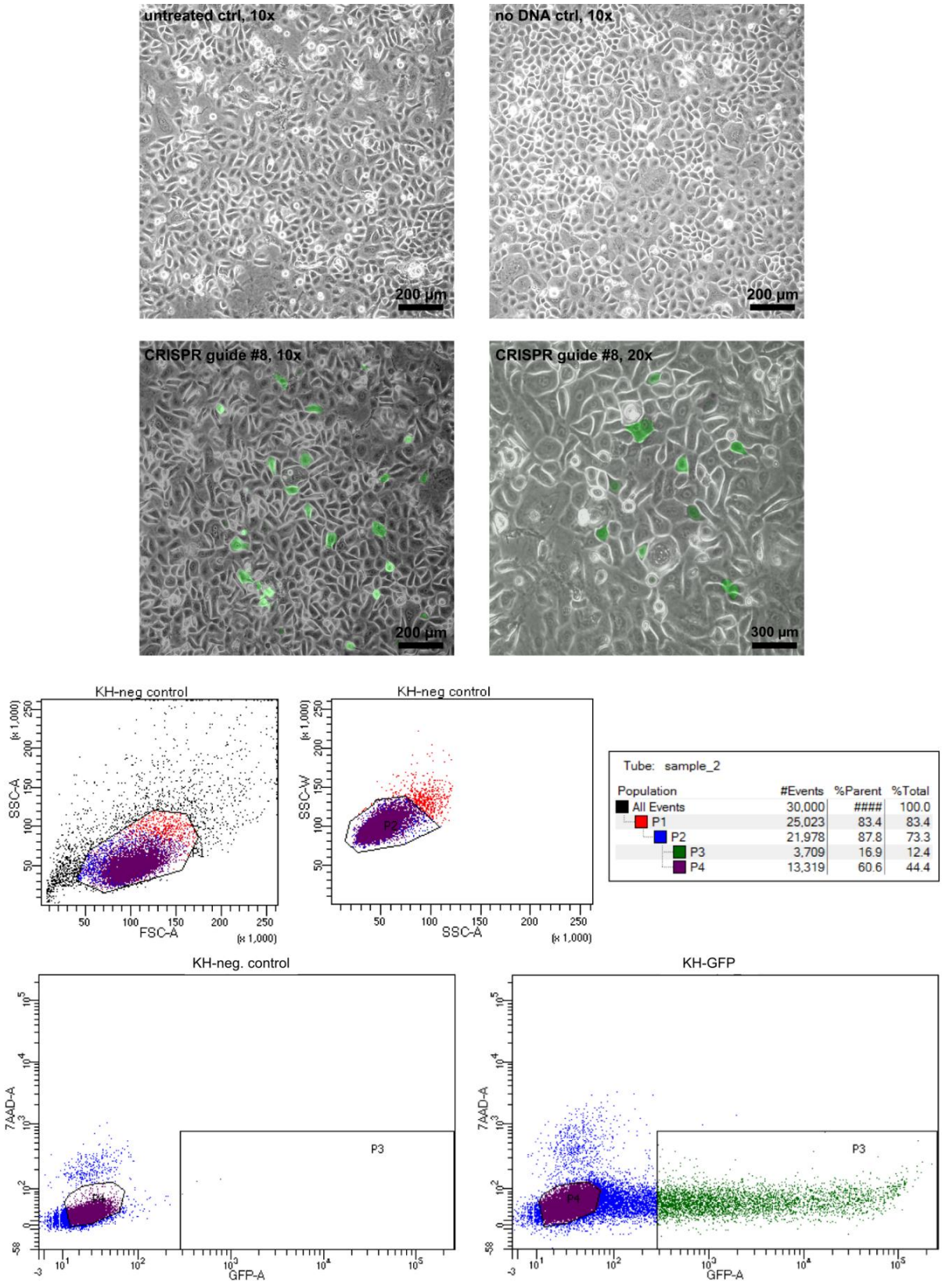

Figure 3.21 Transfected cells and FACS readout. Keratinocytes were transfected with CRISPR/Cas9 plasmid and cultivated for two days in DermaLife medium. Control cells were either left untreated (upper left), transfected without DNA (upper right) or transfected with mock plasmid (not shown). Cells successfully transfected with CRISPR/Cas9 plasmid were positive for the reporter GFP. In a fluorescent activated cell sorter (FACS), the GFP-positive cells were collected for further analysis.

In five independent experiments, the transfection efficiency was between 12 and 25 %. Transfected cells looked healthy, morphology and proliferation was comparable to the untreated control cells.

The FACS settings were adjusted to collect all GFP-positive cells, including dim cells. The GFP-negative fraction was collected as a control population.
Since successful transfection as indicated by GFP expression does not necessarily lead to protein knock down, the presence of Numb protein has to be checked before continuing with functional follow-up experiments. One way to check for proteins in single cells is cytospins. Stainings of cytospins of the transfected cells confirmed protein knock down in the GFP-positive fraction in all five experiments. Figure 3.22 shows representative cytospins of two independent experiments.

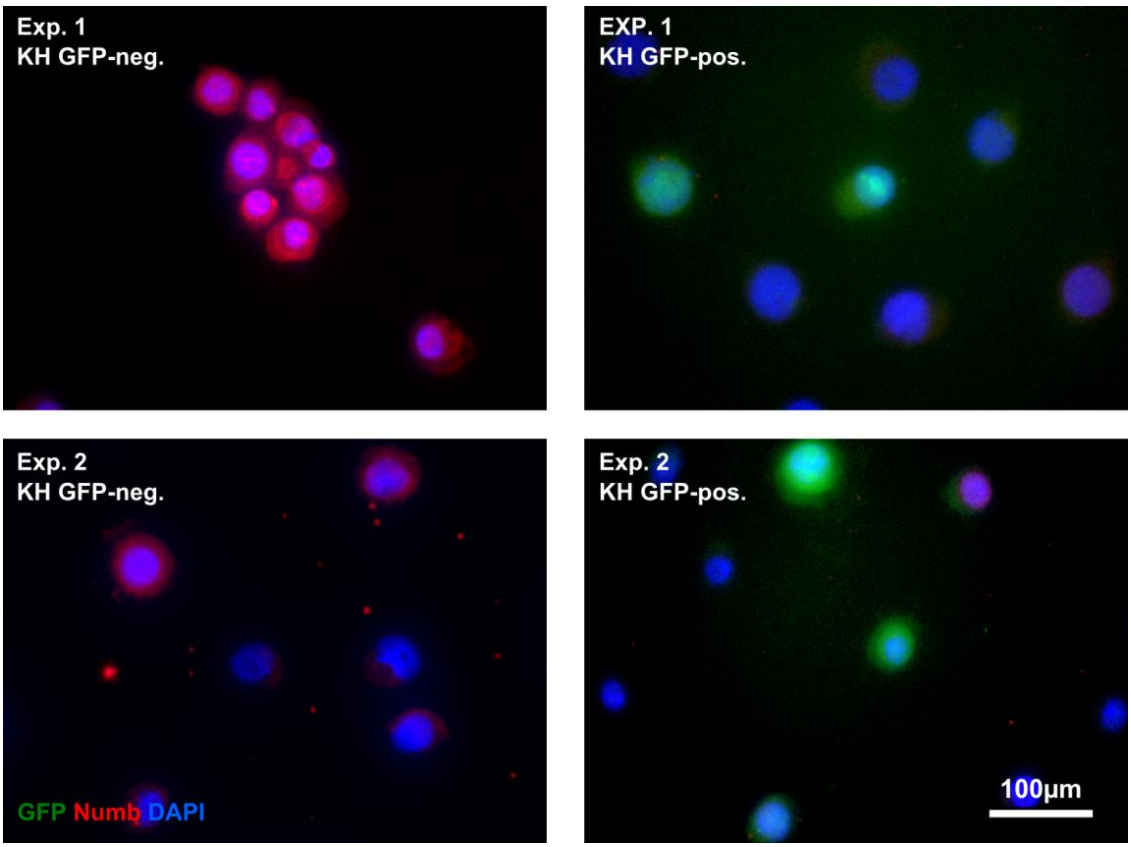

Figure 3.22 Validation of Numb knock down in KH by CRISPR/Cas9. Transfected keratinocytes collected by FACS in two independent experiments were immediately spun onto glass slides in a cytospin and stained immunofluorescently. The collected GFP-negative population was positive for Numb. In GFP-positive keratinocytes, Numb was not detected.

In the GFP-negative fraction, Numb was abundantly detected with antibodies. In the GFP-positive fraction, on the other hand, Numb staining, if present, was only very dim, indicating an efficient knock down.

In addition, protein analysis was performed by Western Blot (Figure 3.23). We found that in five independent experiments, using different guide plasmids or even a combination of two plasmids, the presence of Numb was significantly reduced in the transfected and FAC-sorted GFP-positive cells.

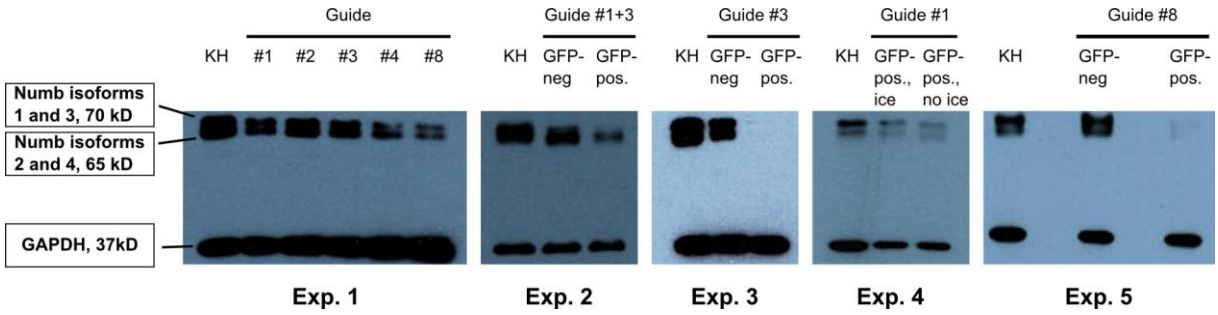

Figure 3.23 Knock down of Numb in human keratinocytes. Western blots of cell lysates of the FACS collected keratinocytes revealed efficient protein knock down in five independent experiments and using different guides. All four Numb isoforms present in human keratinocytes were knocked down by CRISPR/Cas9. Untransfected KH were used as controls. Incubating the cells on ice for ten minutes after the electroporation (Exp. 4) did not seem to improve knock down efficiency.

A reduction of protein was detected in all of the experiments to a varying degree. In experiment 1, the knock down seemed most efficient with guide #8, whereas the other guide sequences did not result in significant protein reduction. In experiment 2, a combination of guide #1 and 3 was used and caused significant reduction in expressed Numb. Guide #3 alone caused a complete elimination of Numb in experiment 3. In experiment 4, guide #1 was used and the cells were either incubated 10 minutes on ice after the pulse or directly suspended in medium, as in the other experiments. The ice treatment did not seem to affect the knock down efficiency. In both cases, the protein is diminished; however, also the GAPDH expression is slightly weaker in the treated cells compared to the KH control. In experiment 5, guide #8 caused efficient knock down of Numb.

As demonstrated in figure 3.23, faint bands of Numb protein were detected in the GFP-positive fraction. This could have several reasons: First, the cells might have taken up the plasmid and expressed the GFP reporter but not the Cas9 endonuclease and therefore no protein knock out occurred in these cells. Second, the endonuclease might be expressed but gene cleavage at both alleles was not 100 % efficient in all cells. Even though biallelic targeting was reported to be high with CRISPR/Cas9 (Jao et al., 2013; Wang et al., 2013a; Yasue et al., 2014), both of these latter scenarios are likely to affect a certain percentage of cells.

In theory, the CRISPR knock down should lead to a gene frame shift that will be passed on to the daughter cells and therefore cause permanent protein deletion. Due to the low transfection efficiency, the collected number of cells was a limiting factor for direct follow up experiments. Therefore, cells were seeded in 96-well plates and cultivated for two weeks after sorting.

First, we stained for Numb to determine if the knock down was stable after two weeks and several rounds of division (figure 3.24 A). In addition, we assessed the proliferation capacity of transfected and sorted GFP-positive cells in a crystal violet cell viability assay. The cell numbers of transfected and untreated control cells were compared after two weeks (figure 3.24 B).

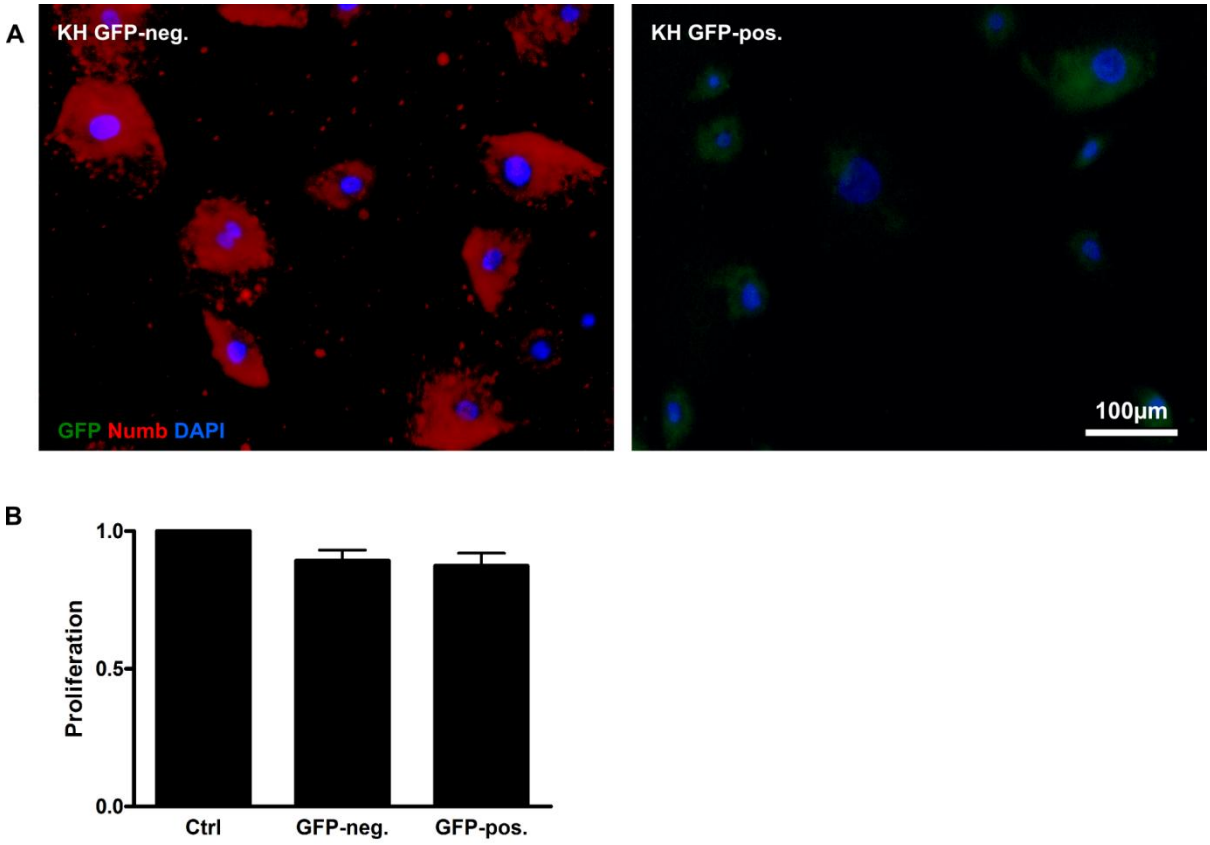

Figure 3.24 Transfected keratinocytes showed stable Numb knock down. The cells transfected with CRISPR/Cas9 plasmid DNA were sorted and GFP-positive and GFP-negative cells were collected, reseeded and cultivated for two weeks. Numb can only be detected immunofluorescently in the GFP-negative cells but not the knock out cells (A). Proliferation, measured in a crystal violet assay, did not differ markedly between transfected and untreated cells (B).

The cells of two independent transfection experiments were reseeded after FACS and analysed with crystal violet and anti-Numb staining after two weeks. There was no significant difference in the proliferation capacity of either GFP-positive or GFP-negative KH compared to the untreated control (figure 3.24 A). Both populations attached well and proliferated. Numb was detected in the cytoplasm of almost all cells in the GFP-negative population but not in the GFP-positive sorted cells (figure 3.24 B). GFP was weakly distributed throughout the cytoplasm of the GFP-positive sorted fraction. Since the plasmid DNA is not stably integrated into the genome, GFP is not continuously transcribed and will be diluted with each cell division.

Taken together, we identified Numb as a novel marker for asymmetric cell division in normal human keratinocytes. The protein is asymmetrically distributed in the majority of cell divisions in cells of undifferentiated character in a 2D context. The observed pattern of Numb distribution in the skin equivalent matched that of normal healthy human skin. Furthermore, we established a protocol to knock down Numb in human keratinocytes using the novel CRISPR/Cas9 technology. We could demonstrate that Numb knock down is not abrogating proliferation and thus is not essential for general mitosis.

4. Discussion

Despite decades of skin research, surprisingly little is known about the exact mechanisms governing the delicate interplay of epidermal stem cell maintenance and differentiation and subsequently the factors regulating homeostasis. This is on the one hand due to the striking discrepancies between human skin and the skin of the mouse which is commonly used as a model organism. Furthermore, even in mouse interfollicular epidermis (IFE) the true stem cell population remains elusive, despite significant efforts to identify reliable markers. This lack of knowledge combined combined led to the development of a variety of differing and competing theories regarding stem cell hierarchy and, on the single cell level, to discordance about potential stem cell populations and their character. The aim of this thesis was therefore to use an advanced human skin equivalent to shed light on the mitotic behaviour of the human keratinocytes maintaining the skin, starting at early, hyperproliferative stages up to late, homeostatic time points. In addition, the question of factors involved in asymmetric cell fate was tackled. The insights gained from our fdmSE were verified by using skin samples from healthy donors to demonstrate the relevance of the 3D human culture model used.

4.1 The fdmSE as a model to study human epidermis

The organotypic co-culture system used in this study was recently developed in our laboratory (Berning et al., 2015). In contrast to the previously published skin equivalent (Stark et al., 2004), the new version of the model does not use a scaffold or fibrin gel. Instead, normal human fibroblasts derived from healthy donors are pre-cultivated on a filter in a special medium to promote the secretion of factors needed to build the extracellular matrix (ECM) of the dermis. In the course of four weeks, a fibroblast-derived dermal equivalent (fdmDE) forms which mimics human dermis and supports a stratified epidermis for six months in a stable and highly reproducible way.

One important advantage for this study is the absence of a scaffold in the fdmSE. The ECM itself is translucent and permeable and thereby allows for microscopic analysis from below without disrupting the tissue. The resulting wholemount images acquired with confocal microscopy reveal the native state of the cells in their 3D context.

However, staining of the tissue *in toto* requires long-term antibody diffusion through the matrix-rich DE and the cell-rich epidermis, thus increasing the probability for high background staining.

4.2 Four types of mitosis maintain normal human epidermis

In the present study, the types of mitoses occurring in the skin equivalent were systematically assessed and counted over culture time points spanning the early, hyperproliferative stages of epidermal development up to late, homeostatic culture conditions, allowing for a long-term regenerating epidermis. A similar study in the mouse ear was described in the landmark publication by Smart (Smart, 1970a). Here, "mitotic figures" were counted in mouse from embryonic state to postnatal day 32. The author found that during embryogenesis, in the single cell layer 75 – 85 % of mitoses occurred in parallel to the basement membrane. After the onset of stratification, the spindle orientation shifted to a perpendicular direction in 75 – 85 % of divisions and suprabasal mitoses were observed frequently. However, from the three-layered stadium up to day 32 which terminated the study, suprabasal mitotic events became less frequent and spindle orientation returned to parallel orientation again. In a different study, Smart found that in oesophageal epithelium, suprabasal mitosis occurred for longer times during development and in higher numbers, but here, too, suprabasal division ceased altogether after stratification (Smart, 1970b). The lower incidence of suprabasal division in the mouse ear might be explained by the extremely thin epidermis of the ear with only few suprabasal layers. Thus, suprabasal mitosis is only reported for a short time window during development and supposedly accounts for the increased need of cell progeny during periods of rapid tissue expansion but is not believed to take part in tissue homeostasis (Smart, 1970a, 1970b).

Newer studies argue controversially about the predominant type of division in the epidermis. Lechler and Fuchs found that, in accordance with the Smart study of 1970, most divisions in the single cell layer stadium of embryonic skin occurred horizontally and shifted to a perpendicular orientation during stratification (Lechler and Fuchs, 2005). However, diverging from Smart, they report a persistence of perpendicular divisions throughout adulthood, even with a prevalence of 85 %. The difference between the two studies is the site of skin used. While Smart investigated ear skin, Lechler and Fuchs studied mouse back skin. Since the epidermis of the two sites already differs in their organisation it is not surprising to also see differences in the mitotic regulation. While that study was performed in mouse back skin, interestingly, studies in mouse tail skin showed the opposite. Here, only 3 % of divisions took place in perpendicular orientation (Clayton et al., 2007).

In our model, we found that most divisions occur in horizontal orientation at all time points (figure 2 and 4), as was reported for mouse ear, oesophagus and tail skin (Clayton et al., 2007; Smart, 1970a, 1970b). Perpendicular mitosis occurred at low frequencies of up to 20 % at week 6 in the 3D wholemount analysis but was absent entirely at early and late time points. Diverging from the published findings, we frequently found suprabasal mitotic events. Thus, the prevalence of the different mitotic types may be different depending on the species and tissue site.

4.3 Suprabasal mitosis as a part of epidermal homeostasis

Independent of the body site, all studies agreed that suprabasal divisions are restricted to embryonic development and wound situations (Stojadinovic et al., 2005).

The work presented here challenges the established paradigm that suprabasal cells in healthy adult epidermis are mitotically inactive. We find suprabasal mitotic events not only during the early stages of the skin equivalents but they are present throughout all time points. During the first 3 – 4 weeks of co-culture, the epidermis of the SE exhibits a wound-like character. This hyperproliferative state can be compared to the rapid expansion during embryogenesis. It is therefore not surprising that we find suprabasal mitosis during these time points. However, in contrast to the findings in mouse skin, suprabasal division persists throughout all culture time points (figures 3.2 E and figure 3.4 E). More importantly, we find suprabasal proliferation in native human skin (figure 3.6).

A first characterisation of these suprabasal mitotic cells revealed that they were in an early stage of differentiation as indicated by Keratin 10 expression. Keratin 10 is a marker characterising the switch from undifferentiated basal to differentiated suprabasal localisation. It is commonly assumed that keratinocytes need a connection to the basement membrane and basal signals to undergo mitosis. So the question was whether the suprabasal mitotic events observed here remain in contact with the BM or whether they are completely detached from the BM. Indeed, we occasionally find Keratin 19 positive cells with supposed stem cell character in the suprabasal layer that retain a cytoplasmic connection to the basement membrane (figure 3.8). Similarly, Keratin 10-positive intrusions can be detected frequently in the human epidermis (see figure 3.7). A connection like this could ensure signalling from the basal compartment to suprabasally located cells.

Furthermore, other studies suggest that there might in fact exist an intermediate state of keratinocyte differentiation. In mouse embryos and hair follicles it was shown that a Keratin 16 expressing population of keratinocytes displayed properties both of mitotic, undifferentiated as well as terminally differentiating cells (Bernot et al., 2002). Similarly, K16 was found expressed in keratinocytes of palmoplantar skin where these cells also showed intermediate properties (Swensson et al., 1998). Cells in the basal cell layer are smaller and more flexible, properties that go hand in hand with frequently dividing cells. Suprabasal cells, on the other hand, become larger and more rigid which makes them less prone to divide. The authors of both studies suggest that this intermediate state, marked by Keratin 16 expression, might be an adaptation to body regions of great physical stress (like the palms) or other situations that require a higher flexibility of the tissue to respond to a demand in cellular expansion (e g embryogenesis or wound healing). However, in the present study we find suprabasal mitoses in different donor skin samples of healthy, adult donors and of different body sites. These findings might be a hint that an intermediate state of early differentiation, with keratinocytes still being proliferatively active, could in fact be part of normal

epidermal homeostasis. We cannot exclude that these suprabasally dividing cells are still connected to the BM and reinsert into the basal cell layer after division, although this seems unlikely since the cells have already entered the differentiation program as indicated by K10 expression. However, at this point it cannot be excluded either, that also “true” suprabasal cells can still divide. Further characterisation of these cells is needed to draw conclusions about their exact role during homeostasis of the skin.

4.4 Asymmetry markers in the epidermis

Many factors are discussed in the context of asymmetric cell division. For invertebrates like *Drosophila* and *Caenorhabditis elegans*, the players involved in orienting the mitotic spindle are relatively well defined (Gönczy, 2008; Jan and Jan, 2001; Rose and Gönczy, 2014). These include factors such as Par3 (Baz in *Drosophila*), Par6 and aPKC, as well as the spindle orientation complex consisting of Gαi, LGN/AGS-3 (Pins) and NuMA (Mud) and the adaptor protein Inscuteable which have also been identified in some vertebrate systems (Du et al., 2001; Vorhagen and Niessen, 2014; Zigman et al., 2005). However, the mechanisms at work in mammalian asymmetric cell division seem to be different, and may even be tissue-specific. For example, the key player LGN is apically located and promotes perpendicular divisions in the mouse embryonic epidermis and mouse embryonic lung bud (El-Hashash et al., 2011; Lechler and Fuchs, 2005; Williams et al., 2011) while in the neocortex LGN is excluded from the apical complex and together with NuMA promotes lateral mitosis (Konno et al., 2008; Peyre et al., 2011; Shitamukai et al., 2011). Inscuteable, which is well described for its role in asymmetric cell division in the *Drosophila* neuroblast (Kraut et al., 1996; Schober et al., 1999), was so far not observed endogenously in vertebrate epidermis. Nevertheless, overexpression studies with tagged Inscuteable suggest that it does have a role in epidermal cell division (Poulson and Lechler, 2010). Taken together, it seems that the mechanisms of asymmetric cell division in vertebrates may be more complex than in invertebrates and are only in part identified to date.

Furthermore, it is important to differentiate between oriented and asymmetric division. In stratified epithelia the term “asymmetric” cell division is commonly used to describe divisions with spindle orientation perpendicular to the basement membrane. However, accurately, this would simply be an oriented division. For a division to be “asymmetric”, cellular factors have to be asymmetrically distributed to the daughter cells. This could happen in either orientation of division.

Asymmetric cell fate of perpendicularly dividing daughter cells is probably influenced by the different locations of the daughter cells, placing one suprabasally while the other one remains in contact with the BM (Seery and Watt, 2000), or could simply be a consequence of division mechanics themselves. Different pulling forces create bigger suprabasal daughter cells. As mentioned before, postmitotic, differentiating cells in the epidermis are bigger (Rowden, 1975). As shown by Lechler and Fuchs, a

subunit of the motor protein complex dynactin (p150glued) co-localises apically with NuMA in perpendicular divisions (Lechler and Fuchs, 2005). Possibly, these different pulling mechanisms at the spindle poles lead to off-centred positioning of the mitotic spindle, resulting in bigger apical daughter cells which are prone to differentiate. However, whether any of the reported factors of perpendicular division actually cause asymmetry or just localise asymmetrically as a consequence of other effectors, remains unanswered.

Regarding upstream regulators of the factors orienting the mitotic spindle, not much is known to date. In p63-null embryos, the epidermis does not stratify and perpendicular division did not occur (Lechler and Fuchs, 2005). P63 has a known regulatory function in the keratinocyte commitment switch to stratification (Koster et al., 2004). During development, it induces stratification while in adult epidermis p63 is required for maintenance of proliferative potential of basal cells. Even though, a direct link between any of the apical polarity factors and p63 is lacking. In the same study, Lechler and Fuchs demonstrated an influence of β1-integrin or α-catenin knockout on LGN/mInsc crescent which is essential for proper spindle orientation in perpendicular mitosis (Lechler and Fuchs, 2005). But again, the molecular mechanism of this connection is still elusive.

Therefore, to truly talk about asymmetric cell division in the epidermis, factors need to be identified that are asymmetrically distributed to the daughter cells.

4.5 Numb as a marker of asymmetric keratinocyte division

From a number of proposed factors that may be involved in asymmetric division, only Numb could be identified as a marker being asymmetrically distributed during mitosis of keratinocytes. In several independent experiments, an uneven distribution of Numb protein to daughter cells was observed in some divisions, notably more so in cultures maintained without Calcium. Keratinocytes are commonly cultivated in a low-Calcium, serum-free medium to suppress differentiation of the cells. In contrast, if keratinocytes are cultivated on feeder in high-Calcium medium, supplemented with 10 % serum, the cells start to differentiate within a few days. Interestingly, Numb is more strongly expressed under these high Calcium conditions (figure 3.15). Furthermore, a distinct Numb signal was found in the suprabasal layers of the fdmSE. In the skin equivalents, two different Numb localisations were detected: at the basal cortex of basal cells and at the cell membrane of suprabasal cells. Since mitosis is a rare event and only takes a few hours, the detection of mitotic events in sections is difficult. Unfortunately, despite extensive efforts, a reliable and reproducible staining of Numb in the fdmSE wholemounts could not be established. We therefore have no proof of asymmetric Numb segregation in a 3D context. Nevertheless, since Numb is an established asymmetry marker in several invertebrate and mammalian systems (Kechad et al., 2012; Shen et al.,

2002; Verdi et al., 1996) and expression of Numb was confirmed in our SE as well as in human skin, the likelihood of Numb being important also for human keratinocytes is incontestable.

4.5.1 Numb regulates cell fate in different species

Numb's function as a cell fate regulator in *Drosophila* has been well described. In the fly, asymmetric partitioning of Numb during mitosis infers asymmetric cell fate to the daughter cells, probably through its inhibition of the Notch intracellular domain (NICD) (Couturier et al., 2013; Uemura et al., 1989). Even though the exact mechanism of Numb-Notch interaction is to date unknown, studies found that Numb plays a role in endocytosis as shown by its interaction with several endocytic proteins and by its localisation to endocytic organelles (Santolini et al., 2000). The widespread expression of Numb suggests that it plays a general role in endocytosis that may or may not be linked to its role as a cell fate determinant.

In mouse neurogenesis of the cortex, Numb was found as a membrane-associated protein segregating asymmetrically to the apical daughter cell which remains a progenitor cell (Zhong et al., 2000). The importance of Numb for cortical development was further demonstrated by several knockout studies (Li et al., 2003; Shen et al., 2002; Zhong et al., 2000; Zilian et al., 2001). In mouse epidermis, on the other hand, Numb was identified but dismissed as a cell fate determinant since asymmetric Numb distribution could not be correlated with LGN localisation in perpendicular division (Williams et al., 2011). Still, overexpressing Numb in embryonic mouse epidermis led to a slight decrease in epidermal thickness which might reflect its role as Notch inhibitor (Williams et al., 2011).

Numb functions as an inhibitor of Notch which in turn plays a key role in the commitment switch of keratinocytes from basal, proliferative to suprabasal, differentiating cells (Rangarajan et al., 2001). Notch expression increases as cells migrate upwards from the basal cell layer and drives differentiation and stratification (Rangarajan et al., 2001). Numb antagonizes Notch function in one of two ways: 1) by ubiquitination of the membrane-bound Notch1 receptor (McGill and McGlade, 2003); and 2) by binding the Notch intracellular domain (NICD) and α-adaptin, a clathrin vesicle adaptor, and thereby facilitating NICD endocytosis (Berdnik et al., 2002). Thus, in its function as a Notch inhibitor, Numb can be either membrane-associated or cytoplasmic, which correlates with our findings in the immunofluorescent stainings (figures 3.17 and 3.18). However, we cannot exclude that Numb plays additional roles in the keratinocytes that are unrelated to Notch signalling.

4.5.2 Stable CRISPR/Cas9 knock down of Numb in human keratinocytes

To investigate the role of Numb in human keratinocytes, we established a protocol to stably knock down Numb by using the CRISPR/Cas9 method.

CRISPR is a relatively new gene editing method that was developed in 2012 (Cong et al., 2013; Hsu et al., 2013; Ran et al., 2013). Adapted from a well-described bacterial innate immune system, CRISPR/Cas9 offers the possibility to edit the genomes of cells or whole organisms in an easy, highly efficient and economic way (Ran et al., 2013). In contrast to other RNA-based systems like RNA interference (RNAi), CRISPR can cause not only knock down but complete knock out of a gene of interest. Compared to ZNF nucleases and TALENs, two other DNA-based editing tools (Christian et al., 2010; Miller et al., 2007; Wood et al., 2011), CRISPR/Cas9 plasmids are substantially easier to generate, as it only requires the creation of a pair of oligos encoding the 20 nt guide sequence.

Five different guideRNA sequences were designed that were all complementary to sequences lying within the first exon of the gene. Since all known isoforms include the first exon, the CRISPR guides should target all of them, if present in the keratinocytes.

In our Western Blot analysis we found two bands at 70 kD and 65 kD (figure 3.25). These account for isoforms 1 and 3 (70 kD) and 2 and 4 (65 kD). Isoforms 5 and 6 would run at 55 kD but could not be detected here and therefore may not be expressed in human keratinocytes. These two isoforms were so far identified in amniotic fluid cells, glioblastoma and metastatic tumour cells (Karaczyn et al., 2010).

After sorting and collecting the CRISPR-transfected keratinocytes, we saw a significant reduction of Numb on protein level in the GFP-positive transfected cells compared to GFP-negative and untransfected control cells (see Cytospins in figure 3.24 and Western Blot in figure 3.25). After two weeks, we still did not detect Numb protein in the GFP-positive fraction (figure 3.26), whereas GFP-negative sorted control cells continued to stain positive for Numb.

Within the two weeks after sorting and reseeding of the transfected cells, no effect on proliferation became apparent in the GFP-positive Numb-negative cells. In two independent experiments, the cells attached well and proliferated comparable to the control. Thus, a direct effect of Numb deletion on proliferation of the keratinocytes can largely be ruled out. A recent publication defined a role for Numb in symmetric mitosis (Schmit et al., 2012). In human melanoma cells, deletion of Numb caused mitotic arrest in G2 / M phase due to a destabilisation of the Plk1 kinase which is required for proper spindle alignment. A role for Numb in symmetric cell division would be one explanation for the high Numb abundance in differentiated keratinocytes. In our Numb knock down study, we did not see an immediate effect on proliferation. However, we cannot rule out that other factors take over Numb functions and thereby rescue the knock down effect in human keratinocytes.

4.5.3 Numb and Numblike

Numb has a homologue called Numblike. Both are homologues of the *Drosophila* NUMB gene and highly conserved in several species, among them human, mouse, rat and zebrafish (see the NCBI

gene data base, gene IDs 8650 and 9253). In mouse, the sequence homology at the N-terminus which contains the active phosphotyrosine binding domain (PTB) is 76 % while homology of the C-terminus of both protein sequences is only about 46.7 % (Zhong et al., 1997). Numblike is only found in the cytoplasm and is not distributed asymmetrically during mitosis in *Drosophila* neural precursors (Zhong et al., 1997). While the different localisation as well as differential expression of Numb and Numblike during mouse cortical neurogenesis suggests distinct roles of the two proteins, there is also evidence for redundant functions of Numb and Numblike (Petersen et al., 2002). For example, both Numb and Numblike can bind the Notch intracellular domain (NICD) (Zhong et al., 1997) and inactivate Notch signalling. Conversely, high levels of Notch lead to a decrease in Numb and Numblike protein in cultured cells and chick neural tubes, probably through PEST-domain mediated proteasomal degradation (Chapman et al., 2006). While the exact mechanisms regulating the relationship of Numb, Numblike and Notch remain to be discovered, the emerging picture reveals a complex and reciprocal interplay of the three proteins. But even though Numblike seems to be involved in similar molecular pathways as Numb, it is unlikely that it would be able to substitute fully in case of Numb loss as demonstrated by lethality of homozygous loss-of-function of Numb in mice (Shen et al., 2002). Therefore, we can conclude that our CRISPR/Cas9 knock down of Numb might in part but not fully be rescued by endogenous Numblike. Since the NICD has a high turnover rate of only about 180 minutes (Fryer et al., 2004), an effect of Numb deletion would be effective within a short time after gene disruption. As we can only exclude an immediate effect on proliferation at this point, further studies are needed to determine the effect of Numb knock down on Notch signalling and subsequent consequences for the differentiation of the keratinocytes.

4.5.4 Upstream regulation of Numb

Not much is known about the upstream regulation of Numb. Interestingly, it was recently shown that Numb is a target of the atypical Protein Kinase C (aPKC) which is a component of the previously discussed polarity complex. Phosphorylation of Numb apparently influences aPKC localisation to the basolateral cell membrane and thereby causes asymmetric distribution of aPKC to daughter cells (Smith et al., 2007). In our staining approach we find Numb at the basolateral side of basal cells but also at the basal cell membrane (figures 3.17 and 3.18). Even though we did not find the polarity complex members Par6, NuMA or Inscuteable here, we did not yet stain for aPKC and can therefore not rule out its influence on Numb in epidermal keratinocytes.

In a recent study, Numb was proposed as a mediator between the Wnt and the Notch pathway (Fukunaga-Kalabis et al., 2015). In human neural crest stem cell (NCSC)-like cells, a UV-induced Wnt7a signal produced by keratinocytes triggered the maturation of NCSC-like cells into melanocytes. This signalling cascade involved the upregulation of Numb and thereby downregulation

of Notch in NCSC-like cells. Upregulation of Numb was due to a post-transcriptional stabilisation of the protein, but a direct connection between Numb and any upstream regulator was not demonstrated. Furthermore, the Wnt7a signal produced by the keratinocytes in the study of Fukunaga et al. was not so far recapitulated by studies in our laboratory. We can therefore not make any statement at this point about the influence of Wnt signalling on Numb protein expression in the human keratinocytes.

4.5.5 The role of Numb in keratinocyte differentiation

The accumulation of Numb at the basal membrane of basal keratinocytes would explain its asymmetric segregation to apical and basal daughter cells in perpendicular division and thereby inhibition of Notch signalling by Numb only in the basal daughter cells. Suprabasal daughter cells would inherit less Numb and therefore be subjected to increased Notch signalling which induces keratinocyte differentiation. Migrating upwards, cells express more Notch which in turn inhibits Numb and Numblike (Chapman et al., 2006; Rangarajan et al., 2001). However, Numb's function as an endocytic protein might be independent from the Notch pathway and explain the high Numb prevalence at the cell membranes of suprabasal cells in the skin equivalent. Still, the most prominent division type in our skin equivalent was the horizontal division in parallel to the basement membrane. As described above, Numb was not evenly distributed throughout the basal cell layer. Protein expression was more pronounced in some regions of the epidermis than others. Thus, Numb could still be asymmetrically segregated to cells dividing in parallel to the basement membrane. The resulting reduced Notch inhibition and induced differentiation in one of the daughter cells might be a trigger for this cell to detach from the basement membrane and migrate upwards. However, this hypothesis has still to be proven in our skin equivalent.

4.6 Conclusion

In this study we could for the first time identify suprabasal mitosis as a part of normal human epidermal homeostasis. So far, suprabasal cells were assumed to be mitotically inactive with the exception of embryogenesis and wound healing or certain disease phenotypes. Here, we show that suprabasal mitotic events occur at a constant rate at all stages of our culture system (figures 3.2 and 3.4) as well as in healthy skin (figure 3.6). These suprabasally dividing cells have entered the differentiation program, as indicated by Keratin 10 expression, but are still proliferative and might therefore be indicative of an intermediate state of keratinocyte development.

Furthermore, by quantifying the occurrence of mitotic types in the epidermis of our *in vitro* skin model mimicking human epidermis, our finding – that 4 types of mitosis are present with most cells dividing in parallel to the BM – is a valuable addition to the presently controversial findings in mouse

skin. The prevalent division type in mouse epidermis seems to depend on the tissue site (mostly perpendicular in back skin *versus* mostly horizontal in tail skin). Since the mouse is covered by a fur and has a hair follicle-dense skin, the hair follicle stem cells play a more important role in maintaining epidermal regeneration than in humans. It could be that the mouse interfollicular epidermis (IFE), at least in fur-dense regions, is maintained mostly by HF stem cells. The density of hair follicles might be one factor influencing the division regulation in the IFE. This argument is supported by the correlation of hairless tail skin to the hairless human skin equivalent regarding the prominence of horizontal divisions. Furthermore, a distinct stem cell population of the mouse IFE has not been clearly identified as of yet. Most studies in mouse refer to HF stem cells, while in our study, the IFE was investigated. In addition, the mouse IFE is much thinner than that of humans (Boury-Jamot et al., 2006; Han et al., 2012) which will probably also influence how homeostasis is maintained. Therefore, our study is an addition to the existing knowledge about IFE tissue homeostasis but cannot be directly compared to findings in mouse epidermis.

The asymmetry markers described in the literature as regulating mouse epidermal cell division are mostly markers of oriented but not necessarily asymmetric division. In this study, we investigated some of the discussed proteins, namely LRP6, Par6, NuMA, Inscuteable and Ninein, but were not able to recapitulate the literature findings in our skin equivalent with the tools used here. Perpendicularly oriented division which would rely on the polarity proteins was not found at high rates and in fact was not found at all at some time points. From the data described here, we would like to propose that these markers might not play the same role in human epidermis as they do in mouse skin. Rather, we propose that the predominant type of asymmetric division that balances self-renewal and differentiation in the human epidermis relies on asymmetric segregation of markers in horizontal division. As one possible marker, we identified Numb. Interestingly, knock down of Numb did not abrogate mitosis in short-term cultures. However, it has to remain open whether stem cell division is impaired by Numb deletion. Thus, further studies need to determine whether Numb plays a specific role in asymmetric division and investigate the mechanism how Numb is involved in this regulation.

References

Barker, N., and Clevers, H. (2010). Leucine-Rich Repeat-Containing G-Protein-Coupled Receptors as Markers of Adult Stem Cells. Gastroenterology *138*, 1681–1696.

Barrandon, Y., and Green, H. (1987). Three clonal types of keratinocyte with different capacities for multiplication. Proc. Natl. Acad. Sci. U. S. A. *84*, 2302–2306.

Berdnik, D., Török, T., González-Gaitán, M., and Knoblich, J.A. (2002). The endocytic protein alpha-Adaptin is required for numb-mediated asymmetric cell division in Drosophila. Dev. Cell *3*, 221–231.

Berning, M., Prätzel-Wunder, S., Bickenbach, J.R., and Boukamp, P. (2015). Three-dimensional in vitro skin and skin cancer models based on human fibroblast-derived matrix. Tissue Eng. Part C Methods.

Bernot, K.M., Coulombe, P.A., and McGowan, K.M. (2002). Keratin 16 expression defines a subset of epithelial cells during skin morphogenesis and the hair cycle. J. Invest. Dermatol. *119*, 1137–1149.

Bhaya, D., Davison, M., and Barrangou, R. (2011). CRISPR-Cas systems in bacteria and archaea: versatile small RNAs for adaptive defense and regulation. Annu. Rev. Genet. *45*, 273–297.

Blanpain, C., and Fuchs, E. (2009). Epidermal homeostasis: a balancing act of stem cells in the skin. Nat. Rev. Mol. Cell Biol. *10*, 207–217.

Blanpain, C., and Simons, B.D. (2013). Unravelling stem cell dynamics by lineage tracing. Nat. Rev. Mol. Cell Biol. *14*, 489–502.

Blanpain, C., Lowry, W.E., Geoghegan, A., Polak, L., and Fuchs, E. (2004). Self-Renewal, Multipotency, and the Existence of Two Cell Populations within an Epithelial Stem Cell Niche. Cell *118*, 635–648.

Blanpain, C., Lowry, W.E., Pasolli, H.A., and Fuchs, E. (2006). Canonical notch signaling functions as a commitment switch in the epidermal lineage. Genes Dev. *20*, 3022–3035.

Blanton, R.A., Coltrera, M.D., Gown, A.M., Halbert, C.L., and McDougall, J.K. (1992). Expression of the HPV16 E7 gene generates proliferation in stratified squamous cell cultures which is independent of endogenous p53 levels. Cell Growth Differ. Mol. Biol. J. Am. Assoc. Cancer Res. *3*, 791–802.

Boehnke, K., Mirancea, N., Pavesio, A., Fusenig, N.E., Boukamp, P., and Stark, H.-J. (2007). Effects of fibroblasts and microenvironment on epidermal regeneration and tissue function in long-term skin equivalents. Eur. J. Cell Biol. *86*, 731–746.

Boury-Jamot, M., Sougrat, R., Tailhardat, M., Varlet, B.L., Bonté, F., Dumas, M., and Verbavatz, J.-M. (2006). Expression and function of aquaporins in human skin: Is aquaporin-3 just a glycerol transporter? Biochim. Biophys. Acta BBA - Biomembr. *1758*, 1034–1042.

Bowman, S.K., Neumüller, R.A., Novatchkova, M., Du, Q., and Knoblich, J.A. (2006). The Drosophila NuMA Homolog Mud regulates spindle orientation in asymmetric cell division. Dev. Cell *10*, 731–742.

Brakebusch, C., Grose, R., Quondamatteo, F., Ramirez, A., Jorcano, J.L., Pirro, A., Svensson, M., Herken, R., Sasaki, T., Timpl, R., et al. (2000). Skin and hair follicle integrity is crucially dependent on beta 1 integrin expression on keratinocytes. EMBO J. *19*, 3990–4003.

Casenghi, M., Barr, F.A., and Nigg, E.A. (2005). Phosphorylation of Nlp by Plk1 negatively regulates its dynein-dynactin-dependent targeting to the centrosome. J. Cell Sci. *118*, 5101–5108.

Chapman, G., Liu, L., Sahlgren, C., Dahlqvist, C., and Lendahl, U. (2006). High levels of Notch signaling down-regulate Numb and Numblike. J. Cell Biol. *175*, 535–540.

Chen, C.-H., Howng, S.-L., Cheng, T.-S., Chou, M.-H., Huang, C.-Y., and Hong, Y.-R. (2003). Molecular characterization of human ninein protein: two distinct subdomains required for centrosomal targeting and regulating signals in cell cycle. Biochem. Biophys. Res. Commun. *308*, 975–983.

Christian, M., Cermak, T., Doyle, E.L., Schmidt, C., Zhang, F., Hummel, A., Bogdanove, A.J., and Voytas, D.F. (2010). Targeting DNA Double-Strand Breaks with TAL Effector Nucleases. Genetics *186*, 757–761.

Clayton, E., Doupé, D.P., Klein, A.M., Winton, D.J., Simons, B.D., and Jones, P.H. (2007). A single type of progenitor cell maintains normal epidermis. Nature *446*, 185–189.

Colaluca, I.N., Tosoni, D., Nuciforo, P., Senic-Matuglia, F., Galimberti, V., Viale, G., Pece, S., and Di Fiore, P.P. (2008). NUMB controls p53 tumour suppressor activity. Nature *451*, 76–80.

Cong, L., Ran, F.A., Cox, D., Lin, S., Barretto, R., Habib, N., Hsu, P.D., Wu, X., Jiang, W., Marraffini, L.A., et al. (2013). Multiplex Genome Engineering Using CRISPR/Cas Systems. Science *339*, 819–823.

Cotsarelis, G., Cheng, S.Z., Dong, G., Sun, T.T., and Lavker, R.M. (1989). Existence of slow-cycling limbal epithelial basal cells that can be preferentially stimulated to proliferate: implications on epithelial stem cells. Cell *57*, 201–209.

Couturier, L., Mazouni, K., and Schweisguth, F. (2013). Numb localizes at endosomes and controls the endosomal sorting of notch after asymmetric division in Drosophila. Curr. Biol. CB *23*, 588–593.

Culurgioni, S., Alfieri, A., Pendolino, V., Laddomada, F., and Mapelli, M. (2011). Inscuteable and NuMA proteins bind competitively to Leu-Gly-Asn repeat-enriched protein (LGN) during asymmetric cell divisions. Proc. Natl. Acad. Sci. *108*, 20998–21003.

Davidson, G., Wu, W., Shen, J., Bilic, J., Fenger, U., Stannek, P., Glinka, A., and Niehrs, C. (2005). Casein kinase 1 γ couples Wnt receptor activation to cytoplasmic signal transduction. Nature *438*, 867–872.

Davidson, G., Shen, J., Huang, Y.-L., Su, Y., Karaulanov, E., Bartscherer, K., Hassler, C., Stannek, P., Boutros, M., and Niehrs, C. (2009). Cell cycle control of wnt receptor activation. Dev. Cell *17*, 788–799.

Dho, S.E., French, M.B., Woods, S.A., and McGlade, C.J. (1999). Characterization of four mammalian numb protein isoforms. Identification of cytoplasmic and membrane-associated variants of the phosphotyrosine binding domain. J. Biol. Chem. *274*, 33097–33104.

Du, Q., and Macara, I.G. (2004). Mammalian Pins is a conformational switch that links NuMA to heterotrimeric G proteins. Cell *119*, 503–516.

Du, Q., Stukenberg, P.T., and Macara, I.G. (2001). A mammalian Partner of inscuteable binds NuMA and regulates mitotic spindle organization. Nat. Cell Biol. *3*, 1069–1075.

El-Hashash, A.H., and Warburton, D. (2011). Cell polarity and spindle orientation in the distal epithelium of embryonic lung. Dev. Dyn. *240*, 441–445.

El-Hashash, A.H., Turcatel, G., Al Alam, D., Buckley, S., Tokumitsu, H., Bellusci, S., and Warburton, D. (2011). Eya1 controls cell polarity, spindle orientation, cell fate and Notch signaling in distal embryonic lung epithelium. Dev. Camb. Engl. *138*, 1395–1407.

Fodde, R., Kuipers, J., Rosenberg, C., Smits, R., Kielman, M., Gaspar, C., van Es, J.H., Breukel, C., Wiegant, J., Giles, R.H., et al. (2001). Mutations in the APC tumour suppressor gene cause chromosomal instability. Nat. Cell Biol. *3*, 433–438.

Fryer, C.J., White, J.B., and Jones, K.A. (2004). Mastermind recruits CycC:CDK8 to phosphorylate the Notch ICD and coordinate activation with turnover. Mol. Cell *16*, 509–520.

Fuchs, E. (1993). Epidermal differentiation and keratin gene expression. J. Cell Sci. Suppl. *17*, 197–208.

Fukunaga-Kalabis, M., Hristova, D.M., Wang, J.X., Li, L., Heppt, M.V., Wei, Z., Gyurdieva, A., Webster, M.R., Oka, M., Weeraratna, A.T., et al. (2015). UV-Induced Wnt7a in the Human Skin Microenvironment Specifies the Fate of Neural Crest–Like Cells via Suppression of Notch. J. Invest. Dermatol.

Ghazizadeh, S., and Taichman, L.B. (2005). Organization of Stem Cells and Their Progeny in Human Epidermis. J. Invest. Dermatol. *124*, 367–372.

Gönczy, P. (2008). Mechanisms of asymmetric cell division: flies and worms pave the way. Nat. Rev. Mol. Cell Biol. *9*, 355–366.

Graf, T., and Stadtfeld, M. (2008). Heterogeneity of embryonic and adult stem cells. Cell Stem Cell *3*, 480–483.

Green, H. (1977). Terminal differentiation of cultured human epidermal cells. Cell *11*, 405–416.

Gurley, L.R., Walters, R.A., and Tobey, R.A. (1973). Histone phosphorylation in late interphase and mitosis. Biochem. Biophys. Res. Commun. *50*, 744–750.

Habib, S.J., Chen, B.-C., Tsai, F.-C., Anastassiadis, K., Meyer, T., Betzig, E., and Nusse, R. (2013). A localized Wnt signal orients asymmetric stem cell division in vitro. Science *339*, 1445–1448.

Hadjihannas, M.V., Brückner, M., Jerchow, B., Birchmeier, W., Dietmaier, W., and Behrens, J. (2006). Aberrant Wnt/β-catenin signaling can induce chromosomal instability in colon cancer. Proc. Natl. Acad. Sci. *103*, 10747–10752.

Han, G., Li, F., Singh, T.P., Wolf, P., and Wang, X.-J. (2012). The Pro-inflammatory Role of TGFβ1: A Paradox? Int. J. Biol. Sci. *8*, 228–235.

Helfrich, I., Schmitz, A., Zigrino, P., Michels, C., Haase, I., Bivic, A. le, Leitges, M., and Niessen, C.M. (2006). Role of aPKC Isoforms and Their Binding Partners Par3 and Par6 in Epidermal Barrier Formation. J. Invest. Dermatol. *127*, 782–791.

Hendzel, M.J., Wei, Y., Mancini, M.A., Hooser, A.V., Ranalli, T., Brinkley, B.R., Bazett-Jones, D.P., and Allis, C.D. (1997). Mitosis-specific phosphorylation of histone H3 initiates primarily within pericentromeric heterochromatin during G2 and spreads in an ordered fashion coincident with mitotic chromosome condensation. Chromosoma *106*, 348–360.

Hsu, P.D., Scott, D.A., Weinstein, J.A., Ran, F.A., Konermann, S., Agarwala, V., Li, Y., Fine, E.J., Wu, X., Shalem, O., et al. (2013). DNA targeting specificity of RNA-guided Cas9 nucleases. Nat. Biotechnol. *31*, 827–832.

Hsu, Y.-C., Li, L., and Fuchs, E. (2014). Emerging interactions between skin stem cells and their niches. Nat. Med. *20*, 847–856.

Huang, P., Senga, T., and Hamaguchi, M. (2007). A novel role of phospho-beta-catenin in microtubule regrowth at centrosome. Oncogene *26*, 4357–4371.

Ito, M., Liu, Y., Yang, Z., Nguyen, J., Liang, F., Morris, R.J., and Cotsarelis, G. (2005). Stem cells in the hair follicle bulge contribute to wound repair but not to homeostasis of the epidermis. Nat. Med. *11*, 1351–1354.

Izaki, T., Kamakura, S., Kohjima, M., and Sumimoto, H. (2006). Two forms of human Inscuteable-related protein that links Par3 to the Pins homologues LGN and AGS3. Biochem. Biophys. Res. Commun. *341*, 1001–1006.

Izumi, Y., Ohta, N., Hisata, K., Raabe, T., and Matsuzaki, F. (2006). Drosophila Pins-binding protein Mud regulates spindle-polarity coupling and centrosome organization. Nat. Cell Biol. *8*, 586–593.

Jan, Y.N., and Jan, L.Y. (2001). Asymmetric cell division in the Drosophila nervous system. Nat. Rev. Neurosci. *2*, 772–779.

Jao, L.-E., Wente, S.R., and Chen, W. (2013). Efficient multiplex biallelic zebrafish genome editing using a CRISPR nuclease system. Proc. Natl. Acad. Sci. *110*, 13904–13909.

Jensen, K.B., Collins, C.A., Nascimento, E., Tan, D.W., Frye, M., Itami, S., and Watt, F.M. (2009). Lrig1 Expression Defines a Distinct Multipotent Stem Cell Population in Mammalian Epidermis. Cell Stem Cell *4*, 427–439.

Jensen, U.B., Lowell, S., and Watt, F.M. (1999). The spatial relationship between stem cells and their progeny in the basal layer of human epidermis: a new view based on whole-mount labelling and lineage analysis. Dev. Camb. Engl. *126*, 2409–2418.

Jinek, M., East, A., Cheng, A., Lin, S., Ma, E., and Doudna, J. (2013). RNA-programmed genome editing in human cells. eLife *2*, e00471.

Jones, P.H., and Watt, F.M. (1993). Separation of human epidermal stem cells from transit amplifying cells on the basis of differences in integrin function and expression. Cell *73*, 713–724.

Jones, P.H., Harper, S., and Watt, F.M. (1995). Stem cell patterning and fate in human epidermis. Cell *80*, 83–93.

Kalluri, R. (2003). Basement membranes: structure, assembly and role in tumour angiogenesis. Nat. Rev. Cancer *3*, 422–433.

Kanitakis, J. (2002). Anatomy, histology and immunohistochemistry of normal human skin. Eur. J. Dermatol. EJD *12*, 390–399; quiz 400–401.

Karaczyn, A., Bani-Yaghoub, M., Tremblay, R., Kubu, C., Cowling, R., Adams, T.L., Prudovsky, I., Spicer, D., Friesel, R., Vary, C., et al. (2010). Two novel human NUMB isoforms provide a potential link between development and cancer. Neural Develop. *5*, 31.

Kechad, A., Jolicoeur, C., Tufford, A., Mattar, P., Chow, R.W.Y., Harris, W.A., and Cayouette, M. (2012). Numb is required for the production of terminal asymmetric cell divisions in the developing mouse retina. J. Neurosci. Off. J. Soc. Neurosci. *32*, 17197–17210.

Kemphues, K. (2000). PARsing embryonic polarity. Cell *101*, 345–348.

Kern, F., Niault, T., and Baccarini, M. (2011). Ras and Raf pathways in epidermis development and carcinogenesis. Br. J. Cancer *104*, 229–234.

Kikuchi, K., Niikura, Y., Kitagawa, K., and Kikuchi, A. (2010). Dishevelled, a Wnt signalling component, is involved in mitotic progression in cooperation with Plk1. EMBO J. *29*, 3470–3483.

Kim, J.A., Cho, K., Shin, M.S., Lee, W.G., Jung, N., Chung, C., and Chang, J.K. (2008). A novel electroporation method using a capillary and wire-type electrode. Biosens. Bioelectron. *23*, 1353–1360.

Knoblich, J.A. (2008). Mechanisms of asymmetric stem cell division. Cell *132*, 583–597.

Konno, D., Shioi, G., Shitamukai, A., Mori, A., Kiyonari, H., Miyata, T., and Matsuzaki, F. (2008). Neuroepithelial progenitors undergo LGN-dependent planar divisions to maintain self-renewability during mammalian neurogenesis. Nat. Cell Biol. *10*, 93–101.

Koster, M.I., and Roop, D.R. (2005). Asymmetric Cell Division in Skin Development: A New Look at an Old Observation. Dev. Cell *9*, 444–446.

Koster, M.I., Kim, S., Mills, A.A., DeMayo, F.J., and Roop, D.R. (2004). p63 is the molecular switch for initiation of an epithelial stratification program. Genes Dev. *18*, 126–131.

Kraut, R., Chia, W., Jan, L.Y., Jan, Y.N., and Knoblich, J.A. (1996). Role of inscuteable in orienting asymmetric cell divisions in Drosophila. Nature *383*, 50–55.

Lapouge, G., Youssef, K.K., Vokaer, B., Achouri, Y., Michaux, C., Sotiropoulou, P.A., and Blanpain, C. (2011). Identifying the cellular origin of squamous skin tumors. Proc. Natl. Acad. Sci. U. S. A. *108*, 7431–7436.

Lavker, R.M., and Sun, T.T. (1983). Epidermal stem cells. J. Invest. Dermatol. *81*, 121s – 7s.

Lechler, T., and Fuchs, E. (2005). Asymmetric cell divisions promote stratification and differentiation of mammalian skin. Nature *437*, 275–280.

Legg, J., Jensen, U.B., Broad, S., Leigh, I., and Watt, F.M. (2003). Role of melanoma chondroitin sulphate proteoglycan in patterning stem cells in human interfollicular epidermis. Development *130*, 6049–6063.

Levy, V., Lindon, C., Harfe, B.D., and Morgan, B.A. (2005). Distinct stem cell populations regenerate the follicle and interfollicular epidermis. Dev. Cell *9*, 855–861.

Levy, V., Lindon, C., Zheng, Y., Harfe, B.D., and Morgan, B.A. (2007). Epidermal stem cells arise from the hair follicle after wounding. FASEB J. Off. Publ. Fed. Am. Soc. Exp. Biol. *21*, 1358–1366.

Li, H.S., Wang, D., Shen, Q., Schonemann, M.D., Gorski, J.A., Jones, K.R., Temple, S., Jan, L.Y., and Jan, Y.N. (2003). Inactivation of Numb and Numblike in embryonic dorsal forebrain impairs neurogenesis and disrupts cortical morphogenesis. Neuron *40*, 1105–1118.

Li, X., Upadhyay, A.K., Bullock, A.J., Dicolandrea, T., Xu, J., Binder, R.L., Robinson, M.K., Finlay, D.R., Mills, K.J., Bascom, C.C., et al. (2013). Skin Stem Cell Hypotheses and Long Term Clone Survival - Explored Using Agent-based Modelling. Sci. Rep. *3*, 1904.

Lim, X., Tan, S.H., Koh, W.L.C., Chau, R.M.W., Yan, K.S., Kuo, C.J., van Amerongen, R., Klein, A.M., and Nusse, R. (2013). Interfollicular epidermal stem cells self-renew via autocrine Wnt signaling. Science *342*, 1226–1230.

Liu, X.-F., Ishida, H., Raziuddin, R., and Miki, T. (2004). Nucleotide exchange factor ECT2 interacts with the polarity protein complex Par6/Par3/protein kinase Czeta (PKCzeta) and regulates PKCzeta activity. Mol. Cell. Biol. *24*, 6665–6675.

Löffler, G., Petrides, P.E., and Heinrich, P.C. (2007). Binde- und Stützgewebe. In Biochemie und Pathobiochemie (Heidelberg, Springer Medizin Verlag).

Mali, P., Esvelt, K.M., and Church, G.M. (2013). Cas9 as a versatile tool for engineering biology. Nat. Methods *10*, 957–963.

Mapelli, M., and Gonzalez, C. (2012). On the inscrutable role of Inscuteable: structural basis and functional implications for the competitive binding of NuMA and Inscuteable to LGN. Open Biol. *2*, 120102.

Mascré, G., Dekoninck, S., Drogat, B., Youssef, K.K., Brohée, S., Sotiropoulou, P.A., Simons, B.D., and Blanpain, C. (2012). Distinct contribution of stem and progenitor cells to epidermal maintenance. Nature.

McGill, M.A., and McGlade, C.J. (2003). Mammalian numb proteins promote Notch1 receptor ubiquitination and degradation of the Notch1 intracellular domain. J. Biol. Chem. *278*, 23196–23203.

McGrath, J.A., Eady, R. a. J., and Pope, F.M. (2004). Anatomy and Organization of Human Skin. In Rook's Textbook of Dermatology, T.B.M., BS, FRCP FRCP(Edin), S.B., MB, BChir, MD FRCP, N.C.Bs., MB, ChB, FRCP(Lond & Edin), and C.G.Bs., MD, FRCP FRCPath, eds. (Blackwell Publishing, Inc.), pp. 45–128.

McMillan, J.R., Akiyama, M., and Shimizu, H. (2003). Epidermal basement membrane zone components: ultrastructural distribution and molecular interactions. J. Dermatol. Sci. *31*, 169–177.

Merdes, A., and Cleveland, D.W. (1998). The role of NuMA in the interphase nucleus. J. Cell Sci. *111 (Pt 1)*, 71–79.

Merdes, A., Heald, R., Samejima, K., Earnshaw, W.C., and Cleveland, D.W. (2000). Formation of Spindle Poles by Dynein/Dynactin-Dependent Transport of Numa. J. Cell Biol. *149*, 851–862.

Meuten, D.J. (2008). Tumors in Domestic Animals (John Wiley & Sons).

Michel, M., Török, N., Godbout, M.J., Lussier, M., Gaudreau, P., Royal, A., and Germain, L. (1996). Keratin 19 as a biochemical marker of skin stem cells in vivo and in vitro: keratin 19 expressing cells are differentially localized in function of anatomic sites, and their number varies with donor age and culture stage. J. Cell Sci. *109 (Pt 5)*, 1017–1028.

Miller, J.C., Holmes, M.C., Wang, J., Guschin, D.Y., Lee, Y.-L., Rupniewski, I., Beausejour, C.M., Waite, A.J., Wang, N.S., Kim, K.A., et al. (2007). An improved zinc-finger nuclease architecture for highly specific genome editing. Nat. Biotechnol. *25*, 778–785.

Mogensen, M.M., Malik, A., Piel, M., Bouckson-Castaing, V., and Bornens, M. (2000). Microtubule minus-end anchorage at centrosomal and non-centrosomal sites: the role of ninein. J. Cell Sci. *113 (Pt 17)*, 3013–3023.

Moriyama, M., Durham, A.-D., Moriyama, H., Hasegawa, K., Nishikawa, S.-I., Radtke, F., and Osawa, M. (2008). Multiple Roles of Notch Signaling in the Regulation of Epidermal Development. Dev. Cell *14*, 594–604.

Morris, R.J., Liu, Y., Marles, L., Yang, Z., Trempus, C., Li, S., Lin, J.S., Sawicki, J.A., and Cotsarelis, G. (2004). Capturing and profiling adult hair follicle stem cells. Nat. Biotechnol. *22*, 411–417.

Muffler, S., Stark, H.-J., Amoros, M., Falkowska-Hansen, B., Boehnke, K., Bühring, H.-J., Marmé, A., Bickenbach, J.R., and Boukamp, P. (2008). A stable niche supports long-term

maintenance of human epidermal stem cells in organotypic cultures. Stem Cells Dayt. Ohio *26*, 2506–2515.

Niehrs, C., and Acebron, S.P. (2012). Mitotic and mitogenic Wnt signalling. EMBO J. *31*, 2705–2713.

Ohno, S. (2001). Intercellular junctions and cellular polarity: the PAR-aPKC complex, a conserved core cassette playing fundamental roles in cell polarity. Curr. Opin. Cell Biol. *13*, 641–648.

Ohyama, M. (2005). Characterization and isolation of stem cell-enriched human hair follicle bulge cells. J. Clin. Invest. *116*, 249–260.

Ohyama, M. (2007). Hair follicle bulge: A fascinating reservoir of epithelial stem cells. J. Dermatol. Sci. *46*, 81–89.

Packard, A., Georgas, K., Michos, O., Riccio, P., Cebrian, C., Combes, A.N., Ju, A., Ferrer-Vaquer, A., Hadjantonakis, A.-K., Zong, H., et al. (2013). Luminal Mitosis Drives Epithelial Cell Dispersal within the Branching Ureteric Bud. Dev. Cell.

Panousopoulou, E., and Green, J.B.A. (2014). Spindle orientation processes in epithelial growth and organisation. Semin. Cell Dev. Biol.

Paulson, J.R., and Taylor, S.S. (1982). Phosphorylation of histones 1 and 3 and nonhistone high mobility group 14 by an endogenous kinase in HeLa metaphase chromosomes. J. Biol. Chem. *257*, 6064–6072.

Pelletier, L., and Yamashita, Y.M. (2012). Centrosome asymmetry and inheritance during animal development. Curr. Opin. Cell Biol. *24*, 541–546.

Petersen, P.H., Zou, K., Hwang, J.K., Jan, Y.N., and Zhong, W. (2002). Progenitor cell maintenance requires numb and numblike during mouse neurogenesis. Nature *419*, 929–934.

Peyre, E., Jaouen, F., Saadaoui, M., Haren, L., Merdes, A., Durbec, P., and Morin, X. (2011). A lateral belt of cortical LGN and NuMA guides mitotic spindle movements and planar division in neuroepithelial cells. J. Cell Biol. *193*, 141–154.

Potten, C.S. (1974). The epidermal proliferative unit: the possible role of the central basal cell. Cell Tissue Kinet. *7*, 77–88.

Potten, C.S. (1981). Cell replacement in epidermis (keratopoiesis) via discrete units of proliferation. Int. Rev. Cytol. *69*, 271–318.

Potten, C.S., and Morris, R.J. (1988). Epithelial stem cells in vivo. J. Cell Sci. *1988*, 45–62.

Poulson, N.D., and Lechler, T. (2010). Robust control of mitotic spindle orientation in the developing epidermis. J. Cell Biol. *191*, 915–922.

Ran, F.A., Hsu, P.D., Wright, J., Agarwala, V., Scott, D.A., and Zhang, F. (2013). Genome engineering using the CRISPR-Cas9 system. Nat. Protoc. *8*, 2281–2308.

Rangarajan, A., Talora, C., Okuyama, R., Nicolas, M., Mammucari, C., Oh, H., Aster, J.C., Krishna, S., Metzger, D., Chambon, P., et al. (2001). Notch signaling is a direct determinant of keratinocyte growth arrest and entry into differentiation. EMBO J *20*, 3427–3436.

Rhyu, M.S., Jan, L.Y., and Jan, Y.N. (1994). Asymmetric distribution of numb protein during division of the sensory organ precursor cell confers distinct fates to daughter cells. Cell *76*, 477–491.

De Rosa, L., and De Luca, M. (2012). Cell biology: Dormant and restless skin stem cells. Nature *489*, 215–217.

Rose, L., and Gönczy, P. (2014). Polarity establishment, asymmetric division and segregation of fate determinants in early C. elegans embryos. WormBook Online Rev. C Elegans Biol. 1–43.

Rowden, G. (1975). Ultrastructural studies of keratinized epithelia of the mouse. III. Determination of the volumes of nuclei and cytoplasm of cells in murine epidermis. J. Invest. Dermatol. *64*, 1–3.

Salmon, J.K., Armstrong, C.A., and Ansel, J.C. (1994). The skin as an immune organ. West. J. Med. *160*, 146–152.

Santolini, E., Puri, C., Salcini, A.E., Gagliani, M.C., Pelicci, P.G., Tacchetti, C., and Di Fiore, P.P. (2000). Numb is an endocytic protein. J. Cell Biol. *151*, 1345–1352.

Schmit, T.L., Nihal, M., Ndiaye, M., Setaluri, V., Spiegelman, V.S., and Ahmad, N. (2012). Numb Regulates Stability and Localization of the Mitotic Kinase PLK1 and Is Required for Transit through Mitosis. Cancer Res. *72*, 3864–3872.

Schober, M., Schaefer, M., and Knoblich, J.A. (1999). Bazooka recruits Inscuteable to orient asymmetric cell divisions in Drosophila neuroblasts. Nature *402*, 548–551.

Seery, J.P., and Watt, F.M. (2000). Asymmetric stem-cell divisions define the architecture of human oesophageal epithelium. Curr. Biol. CB *10*, 1447–1450.

Shen, Q., Zhong, W., Jan, Y.N., and Temple, S. (2002). Asymmetric Numb distribution is critical for asymmetric cell division of mouse cerebral cortical stem cells and neuroblasts. Dev. Camb. Engl. *129*, 4843–4853.

Shitamukai, A., Konno, D., and Matsuzaki, F. (2011). Oblique Radial Glial Divisions in the Developing Mouse Neocortex Induce Self-Renewing Progenitors outside the Germinal Zone That Resemble Primate Outer Subventricular Zone Progenitors. J. Neurosci. *31*, 3683–3695.

Siller, K.H., Cabernard, C., and Doe, C.Q. (2006). The NuMA-related Mud protein binds Pins and regulates spindle orientation in Drosophila neuroblasts. Nat. Cell Biol. *8*, 594–600.

Smart, I.H. (1970a). Variation in the plane of cell cleavage during the process of stratification in the mouse epidermis. Br. J. Dermatol. *82*, 276–282.

Smart, I.H. (1970b). Changes in location and orientation of mitotic figures in mouse oesophageal epithelium during the development of stratification. J. Anat. *106*, 15–21.

Smith, C.A., Lau, K.M., Rahmani, Z., Dho, S.E., Brothers, G., She, Y.M., Berry, D.M., Bonneil, E., Thibault, P., Schweisguth, F., et al. (2007). aPKC-mediated phosphorylation regulates asymmetric membrane localization of the cell fate determinant Numb. EMBO J. *26*, 468–480.

Srinivasan, D.G., Fisk, R.M., Xu, H., and van den Heuvel, S. (2003). A complex of LIN-5 and GPR proteins regulates G protein signaling and spindle function in C elegans. Genes Dev. *17*, 1225–1239.

Stark, H.J., Baur, M., Breitkreutz, D., Mirancea, N., and Fusenig, N.E. (1999). Organotypic keratinocyte cocultures in defined medium with regular epidermal morphogenesis and differentiation. J. Invest. Dermatol. *112*, 681–691.

Stark, H.-J., Willhauck, M.J., Mirancea, N., Boehnke, K., Nord, I., Breitkreutz, D., Pavesio, A., Boukamp, P., and Fusenig, N.E. (2004). Authentic fibroblast matrix in dermal equivalents normalises epidermal histogenesis and dermoepidermal junction in organotypic co-culture. Eur. J. Cell Biol. *83*, 631–645.

Stojadinovic, O., Brem, H., Vouthounis, C., Lee, B., Fallon, J., Stallcup, M., Merchant, A., Galiano, R.D., and Tomic-Canic, M. (2005). Molecular pathogenesis of chronic wounds: the role of beta-catenin and c-myc in the inhibition of epithelialization and wound healing. Am. J. Pathol. *167*, 59–69.

Swensson, Langbein, Mcmillan, Stevens, Leigh, Mclean, Lane, and Eady (1998). Specialized keratin expression pattern in human ridged skin as an adaptation to high physical stress. Br. J. Dermatol. *139*, 767–775.

Terns, M.P., and Terns, R.M. (2011). CRISPR-based adaptive immune systems. Curr. Opin. Microbiol. *14*, 321–327.

Thiery, J.P., and Huang, R. (2005). Linking epithelial-mesenchymal transition to the well-known polarity protein Par6. Dev. Cell *8*, 456–458.

Tumbar, T., Guasch, G., Greco, V., Blanpain, C., Lowry, W.E., Rendl, M., and Fuchs, E. (2004). Defining the epithelial stem cell niche in skin. Science *303*, 359–363.

Uemura, T., Shepherd, S., Ackerman, L., Jan, L.Y., and Jan, Y.N. (1989). numb, a gene required in determination of cell fate during sensory organ formation in Drosophila embryos. Cell *58*, 349–360.

Urmacher, C. (1990). Histology of normal skin. Am. J. Surg. Pathol. *14*, 671–686.

Verdi, J.M., Schmandt, R., Bashirullah, A., Jacob, S., Salvino, R., Craig, C.G., Program, A.E., Lipshitz, H.D., and McGlade, C.J. (1996). Mammalian NUMB is an evolutionarily conserved signaling adapter protein that specifies cell fate. Curr. Biol. CB *6*, 1134–1145.

Verdi, J.M., Bashirullah, A., Goldhawk, D.E., Kubu, C.J., Jamali, M., Meakin, S.O., and Lipshitz, H.D. (1999). Distinct human NUMB isoforms regulate differentiation vs. proliferation in the neuronal lineage. Proc. Natl. Acad. Sci. U. S. A. *96*, 10472–10476.

Vorhagen, S., and Niessen, C.M. (2014). Mammalian aPKC/Par polarity complex mediated regulation of epithelial division orientation and cell fate. Exp. Cell Res. *328*, 296–302.

Wang, H., Yang, H., Shivalila, C.S., Dawlaty, M.M., Cheng, A.W., Zhang, F., and Jaenisch, R. (2013a). One-Step Generation of Mice Carrying Mutations in Multiple Genes by CRISPR/Cas-Mediated Genome Engineering. Cell *153*, 910–918.

Wang, S., Cha, S.-W., Zorn, A.M., and Wylie, C. (2013b). Par6b Regulates the Dynamics of Apicobasal Polarity during Development of the Stratified Xenopus Epidermis. PLoS ONE *8*, e76854.

Wang, X., Tsai, J.-W., Imai, J.H., Lian, W.-N., Vallee, R.B., and Shi, S.-H. (2009). Asymmetric centrosome inheritance maintains neural progenitors in the neocortex. Nature *461*, 947–955.

Watt, F.M. (2002). Role of integrins in regulating epidermal adhesion, growth and differentiation. EMBO J. *21*, 3919–3926.

Watt, F.M., and Green, H. (1982). Stratification and terminal differentiation of cultured epidermal cells. Nature *295*, 434–436.

Watt, F.M., Kubler, M.D., Hotchin, N.A., Nicholson, L.J., and Adams, J.C. (1993). Regulation of keratinocyte terminal differentiation by integrin-extracellular matrix interactions. J. Cell Sci. *106 (Pt 1)*, 175–182.

Watt, F.M., Estrach, S., and Ambler, C.A. (2008). Epidermal Notch signalling: differentiation, cancer and adhesion. Curr. Opin. Cell Biol. *20*, 171–179.

Webb, A., Li, A., and Kaur, P. (2004). Location and phenotype of human adult keratinocyte stem cells of the skin. Differ. Res. Biol. Divers. *72*, 387–395.

Wiedenheft, B., Sternberg, S.H., and Doudna, J.A. (2012). RNA-guided genetic silencing systems in bacteria and archaea. Nature *482*, 331–338.

Wilkes, G.L., Brown, I.A., and Wildnauer, R.H. (1973). The biomechanical properties of skin. CRC Crit. Rev. Bioeng. *1*, 453–495.

Williams, S.E., and Fuchs, E. (2013). Oriented divisions, fate decisions. Curr. Opin. Cell Biol.

Williams, S.E., Beronja, S., Pasolli, H.A., and Fuchs, E. (2011). Asymmetric cell divisions promote Notch-dependent epidermal differentiation. Nature *470*, 353–358.

Woo, W.-M., and Oro, A.E. (2011). SnapShot: Hair Follicle Stem Cells. Cell *146*, 334–334.e2.

Wood, A.J., Lo, T.-W., Zeitler, B., Pickle, C.S., Ralston, E.J., Lee, A.H., Amora, R., Miller, J.C., Leung, E., Meng, X., et al. (2011). Targeted Genome Editing Across Species Using ZFNs and TALENs. Science *333*, 307–307.

Yamashita, Y.M., Mahowald, A.P., Perlin, J.R., and Fuller, M.T. (2007). Asymmetric Inheritance of Mother Versus Daughter Centrosome in Stem Cell Division. Science *315*, 518–521.

Yasue, A., Mitsui, S.N., Watanabe, T., Sakuma, T., Oyadomari, S., Yamamoto, T., Noji, S., Mito, T., and Tanaka, E. (2014). Highly efficient targeted mutagenesis in one-cell mouse embryos mediated by the TALEN and CRISPR/Cas systems. Sci. Rep. *4*, 5705.

Zhong, W., Feder, J.N., Jiang, M.M., Jan, L.Y., and Jan, Y.N. (1996). Asymmetric localization of a mammalian numb homolog during mouse cortical neurogenesis. Neuron *17*, 43–53.

Zhong, W., Jiang, M.M., Weinmaster, G., Jan, L.Y., and Jan, Y.N. (1997). Differential expression of mammalian Numb, Numblike and Notch1 suggests distinct roles during mouse cortical neurogenesis. Dev. Camb. Engl. *124*, 1887–1897.

Zhong, W., Jiang, M.M., Schonemann, M.D., Meneses, J.J., Pedersen, R.A., Jan, L.Y., and Jan, Y.N. (2000). Mouse numb is an essential gene involved in cortical neurogenesis. Proc. Natl. Acad. Sci. U. S. A. *97*, 6844–6849.

Zhu, J., Wen, W., Zheng, Z., Shang, Y., Wei, Z., Xiao, Z., Pan, Z., Du, Q., Wang, W., and Zhang, M. (2011). LGN/mInsc and LGN/NuMA complex structures suggest distinct functions in asymmetric cell division for the Par3/mInsc/LGN and Gαi/LGN/NuMA pathways. Mol. Cell *43*, 418–431.

Zigman, M., Cayouette, M., Charalambous, C., Schleiffer, A., Hoeller, O., Dunican, D., McCudden, C.R., Firnberg, N., Barres, B.A., Siderovski, D.P., et al. (2005). Mammalian Inscuteable Regulates Spindle Orientation and Cell Fate in the Developing Retina. Neuron *48*, 539–545.

Zilian, O., Saner, C., Hagedorn, L., Lee, H.Y., Säuberli, E., Suter, U., Sommer, L., and Aguet, M. (2001). Multiple roles of mouse Numb in tuning developmental cell fates. Curr. Biol. CB *11*, 494–501.

Acknowledgements

First and foremost, I want to thank Prof. Dr. Petra Boukamp for providing the project for my thesis. Throughout my time as a PhD student in your lab, your door was always open for discussion and advice. Your kind and warm manner created a pleasant working atmosphere where I could freely pursue my research and develop into a “real” scientist. Your curious and enthusiastic view on scientific challenges inspired me to follow a career in science. Thank you!
I want to thank Prof. Dr. Harald Herrmann-Lerdon for supervising my thesis and being part of my TAC. Your calm and constructive manner guided and supported me.
Thanks to Prof. Oliver Gruss who was part of my TAC and whose practical advice often advanced my work.

For technical support I want to thank Iris and Katrin, who lovingly cared for my cell culture during holidays, and Angelika for special orders of paraffin sections. Special thanks to Damir for putting up with all microscopy-related matters and answering even the umpteenth question with patience and unmistakable humour and charme.
Many thanks to Mariana who during her summer stay performed innumerable stainings with unwavering enthusiasm and accurateness.

I want to thank my family, my parents and sisters for always supporting and encouraging me. You always gave me the feeling that I could do anything and be anything I wanted.

Lots of thanks to my friends, Sarah, Tinka, Anja and “the girls” Nathi, Jule, Claudi and Teresa for taking my mind off science and laughing about silly things every now and then!

But most of all I want to thank all Boukamps, past and present, for their good humour, loving care and positive spirit: Manuel Berning, Marius Tham, Iris Martin, Anja Bort, Lisa Schardt, Sabrina Bauer, Christine Leufke, Svenja Ewert, Katrin Schmidt, Hermann Stammer, Gaby Blaser, Philipp Scholz, Leonard Nevaril, Marco Nici, Hans-Jürgen Stark, Elke Laport and Elizabeth Pavez-Lorie. Thanks to you guys I enjoyed every single day in the lab! You made setbacks and hard times bearable and I will never forget the spontaneous parties, excursions and every day fun we had!
Elisa, what I got from you these past four years I cannot measure. Friendship beyond the lab, loyalty, a rock in difficult times and unparalleled fun! Thank you!